AMMONIA-FREE NOx CONTROL SYSTEM

Final Report

Prepared by

Song Wu
Zhen Fan
Andrew H. Seltzer
Foster Wheeler North America Corp.

And

Richard G. Herman
Lehigh University

June 2006

Work Performed Under Contract: DE-FC26-03NT41865

For

U.S. Department of Energy
National Energy Technology Laboratory
Morgantown, West Virginia

By

Foster Wheeler North America Corp.
12 Peach Tree Hill Road
Livingston, New Jersey 07039

Disclaimers

"This report was prepared as an account of work sponsored by an agency of the United States Government. Neither the United States Government nor any agency thereof, nor any of their employees, makes any warranty, express or implied, or assumes any legal liability or responsibility for the accuracy, completeness, or usefulness of any information, apparatus, product, or process disclosed, or represents that its use would not infringe upon privately owned rights. Reference herein to any specific commercial product, process, or service by trade name, trademark, manufacturer, or otherwise does not necessarily constitute or imply its endorsement by the United States Government or any agency thereof. The views and opinions of authors expressed herein do not necessarily state or reflect those of the United States Government or any agency thereof."

Neither the author, nor any affiliate, nor any of their employees, makes any warranty, express or implied, or assumes any legal liability or responsibility including, but not limited to, in regard to the accuracy, completeness, or usefulness of any information, apparatus, product, or process disclosed, or represents that its use would not infringe upon privately owned rights whether such liability or responsibility is of a direct, indirect, special, punitive, incidental, consequential, or other nature and whether arising in contract, warranty, tort including negligence, strict liability, or other legal theory. Utilization of this information is with the above understanding.

AMMONIA-FREE NOx CONTROL SYSTEM

Abstract

This report describes a novel NOx control system that has the potential to drastically reduce cost, and enhance performance, operation and safety of power plant NOx control. The new system optimizes the burner and the furnace to achieve very low NOx levels and to provide an adequate amount of CO, and uses the CO for reducing NO both in-furnace and over a downstream AF-SCR (*ammonia-free* selective catalytic reduction) reactor. The AF-SCR combines the advantages of the highly successful SCR technology for power plants and the TWC (three-way catalytic converter) widely used on automobiles. Like the SCR, it works in oxidizing environment of combustion flue gas and uses only base metal catalysts. Like the TWC, the AF-SCR removes NO and excess CO simultaneously without using any external reagent, such as ammonia. This new process has been studied in a development program jointed funded by the US Department of Energy and Foster Wheeler.

The report outlines the experimental catalyst work performed on a bench-scale reactor, including test procedure, operating conditions, and results of various catalyst formulations. Several candidate catalysts, prepared with readily available transition metal oxides and common substrate materials, have shown over 80-90% removal for both NO and CO in oxidizing gas mixtures and at elevated temperatures.

A detailed combustion study of a 400 MWe coal-fired boiler, applying computational fluid dynamics techniques to model boiler and burner design, has been carried out to investigate ways to optimize the combustion process for the lowest NOx formation and optimum CO/NO ratios. Results of this boiler and burner optimization work are reported. The paper further discusses catalyst scale-up considerations and the conceptual design of a 400 MWe size AF-SCR reactor, as well as economics analysis indicating large cost savings of the ammonia-free NOx control process over the current SCR technology.

Table of Contents

1.0 INTRODUCTION 1
1.1 Project Background 1
1.2 NOx and CO Interrelation 3
1.3 Review of DeNOx Catalysts 4

2.0 EXPERIMENTAL 11
2.1 Test Rig 11
2.2 Catalyst Preparation 12
2.3 Catalyst Test Procedure 13

3.0 CATLYST DEVELOPMENT 17
3.1 Activated Carbon Based Catalysts 17
3.2 Activated Alumina Based Catalysts 43

4.0 FURNACE OPTIMIZATION 52
4.1 Computer Program Description 52
4.2 Furnace Model 52
4.3 HRA Model 60
4.4 Baseline Simulation Results 64
4.5 Parametric Cases Simulation Results 64
4.6 Further Optimization 72

5.0 CATALYTIC REACTOR SCALE-UP AND DESIGN 73
5.1 Honeycomb Reactor versus Packed Bed of Granular Catalysts 73
5.2 Transport Phenomena and Limiting Factors of Catalyst Performance 73
5.3 External Mass Transfer 74
5.4 Distribution of Active Species in Granular Catalysts 74
5.5 Catalysts Reaction and Scale-Up Model 75
5.6 Reaction Order and Activation Energy 77
5.7 Catalyst Effectiveness Factor 79
5.8 Reactor Conceptual Design 81

6.0 COST ANALYSIS 84
6.1 Basis for Cost Analysis 84
6.2 Cost of Catalyst 84
6.3 Cost of Ammonia 85
6.4 Cost Evaluation of Ammonia-Free NOx Reduction System 85

7.0 CONCLUSIONS and FUTURE RESEARCH WORKS 89

8.0 REFERENCES 92

List of Figures

Figure 1-1. Typical Boiler Plant with SCR 1
Figure 1-2. Plant with AF-SCR NOx Control System 2
Figure 1-3. Effect of Furnace Excess Air on NO and CO Emissions 4

Figure 2-1. Bench Scale NOx Testing System 11
Figure 2-2. Photo of Test Rig 12

Figure 3-1. Typical Transient Test Data 17
Figure 3-2. Conversion of NO, CO, and O_2 and N_2 Product Selectivity Over the 40% Fe/30% Cu AC Catalyst 18
Figure 3-3. Baseline Test with Unpromoted AC (Catalyst-I) 19
Figure 3-4. As Received vs Aqueous Treated AC 19
Figure 3-5. Fe Effect on Catalysts without Cu 21
Figure 3-6. Fe Effect on Catalysts with 10% Cu 21
Figure 3-7. Fe Effect on Catalysts with 30% Cu 22
Figure 3-8. Cu Effect on Catalysts with 40% Fe 23
Figure 3-9. CO Concentrations for Different Catalysts 24
Figure 3-10. Effect of Ce on Catalyst Performance 25
Figure 3-11. NO Conversion Performance for Various Catalysts 23
Figure 3-12. Effect of Total Loading on Reactivity Index T50 26
Figure 3-13. NO to N_2O conversion 27
Figure 3-14 CO and O_2 Conversions for Catalyst F 28
Figure 3-15. Relationship between CO and O_2 Conversions 29
Figure 3-16. Effect of Catalyst Type on O_2 Conversion 29
Figure 3-17. Long Duration Test at Constant Conditions 30
Figure 3-18. NO, CO, O_2, and SO_2 Conversion Over the 40% Fe/30% Cu/AC Catalyst at Approximate 257°C (M-3) 31
Figure 3-19. Conversions of NO, CO, O_2, and SO_2 Over the 40% Fe/30% Cu/20% Ce/AC Catalyst at 239°C 32
Figure 3-20. NO, O_2, and SO_2 Conversion Over the Cu-free 40% Fe/AC Catalyst in the Presence of Moisture and SO2 at 321ºC 34
Figure 3-21. NO, CO, and O_2 Conversions Over the 40% Fe/30% Cu/20% K/AC Catalyst Before, During, and After Moisture Injection at 235ºC 36
Figure 3-22. Conversions of NO, CO, O_2, and SO_2 Over the 40% Fe/30% Cu/20% K/AC Catalyst at 232ºC 36
Figure 3-23. Comparisons of K- and Ce-Containing Catalysts 37
Figure 3-24. Conversion of O_2 vs NO under Dry Conditions 38
Figure 3-25. Comparisons of CO vs NO Conversions 39
Figure 3-26. Conversion / Generation of CO vs Temperature 39
Figure 3-27. Effect of SO_2 Exposure on NO Conversion 40
Figure 3-28. Effect of SO_2 Exposure on CO Conversion 40
Figure 3-29. Restoration of NO Activity After SO_2 Exposure for Catalyst M (H) 41
Figure 3-30. Restoration of NO Activity After SO_2 Exposure for Catalyst J 41
Figure 3-31. NO, CO and O_2 Conversions over 40% Fe/30% Cu / AA Catalyst N 44
Figure 3-32. Conversion of NO, CO, and O_2 over 40% Fe/30% Cu / AC Catalyst 44

Figure 3-33. Historical Data of Catalyst N upon Exposure to H_2O/SO_2 45
Figure 3-34. Transient NO Concentrations before and after the Start of Water Addition..... 46
Figure 3-35. Historical Data of Type O Catalyst upon Exposure to H_2O/SO_2 47
Figure 3-36. NO Conversion for N and O Catalysts..... 48
Figure 3-37. NO to N_2O Conversion for AC and AA Catalysts 49
Figure 3-38. Effect of Space Velocity on NO Conversion for AC and AA Catalysts..... 50
Figure 3-39. NO, CO and O_2 Conversions over Previously Tested (P) and Fresh (Q) 40% Fe / 30% Cu /AA Catalyst with GHSV = 5250 hr-1 51

Figure 4-1. Computational Model of Furnace (with right side wall removed)..... 54
Figure 4-2. Furnace Gas Temperature 55
Figure 4-3. Furnace O_2 Mole Fraction..... 56
Figure 4-4. Furnace CO Concentration..... 57
Figure 4-5. Furnace Gas Velocity..... 58
Figure 4-6. Furnace NOx Concentration 59
Figure 4-7. Flue Gas Temperature Vs. Height at Furnace Outlet & HRA Inlet, Baseline Case . 61
Figure 4-8. 400 MWe Boiler Design 62
Figure 4-9. Ratio of CO/CO inlet Vs. Residence Time and Temperature 63
Figure 4-10. CO Concentration at HRA Inlet Vs. Height 63
Figure 4-11. Flue Gas Velocity Distribution in HRA, Baseline Case 65
Figure 4-12. Flue Gas Temperature Distribution in HRA, Baseline Case..... 66
Figure 4-13. CO Distribution in HRA, Baseline Case..... 67
Figure 4-14. NOx Distribution in HRA, Baseline Case 68
Figure 4-15. CO/NO Distribution in HRA, Baseline Case 69
Figure 4-16. CO/NO Distribution in HRA, 40% OFA, 3% O2 70
Figure 4-17. HRA Outlet CO and NO Concentration Versus Outlet O2..... 71
Figure 4-18. HRA Outlet CO and NO Concentration Versus OFA Flow 71
Figure 4-19. Fuel Burnout Versus Outlet O2..... 72
Figure 4-20. Fuel Burnout Versus OFA Flow 72

Figure 5-1. Cross Section of a Fresh Catalyst Particle 75
Figure 5-2. SEM EDX Image of Fresh Catalyst Cross Section..... 75
Figure 5-3. Effectiveness Factor as a Function of Thiele Modulus 77
Figure 5-4. Test Data and Model Prediction with First Order Assumption..... 78
Figure 5-5. Observed Activation Energy of Test Data 78
Figure 5-6. Reactant Distribution Profile for Lab and Honeycomb Catalysts..... 80
Figure 5-7. 400 MWe AF-SCR System General Arrangement 83

Figure 6.1. Price Trend of Anhydrous Ammonia 85

List of Tables

Table 2-1. Catalyst Samples Tested* 16
Table 3-1. Impact of Cu Loading on T50 23

Table 3-2. Conversions and N_2O Selectivity over the 40% Fe/30% Cu/20% Ce/AC Catalyst J at 239 ± 1oC. 33

Table 3-3. BET Surface Area (m^2/g) of Type N and O Catalysts 47
Table 5-1. External Mass Transfer Data 74

Table 5-2. Pore Diffusion and Effectiveness Factor Calculation 79
Table 5-3. 400 MWe AF-SCR Performance and Catalyst Geometry 82
Table 6-1. Estimation of AF-SCR Catalyst Cost 84
Table 6-2. NOx Control Performance and Cost Summary 87
Table 6-3. Financial Analysis for NOx Control 88

EXECUTIVE SUMMARY

State-of-the-art NOx control technology for coal-fired power plants involves a combination of low NOx combustion and selective catalytic reduction (SCR) technologies. These systems have reached maturity and further improvements will likely be incremental. To advance NOx control technology to the next level, new concepts must be considered.

Today's low NOx combustion technology emphasizes the precise control of local combustion stoichiometry and temperature within the primary combustion zone. The design strategy has been focused on delaying mixing of oxygen and fuel in the primary combustion zone to minimize NOx formation while at the same time maintaining acceptable combustion performance in terms of low unburned carbon and CO emissions.

In the new NOx control system, an increased CO concentration in the furnace is actually desirable, since the presence of CO reduces NOx in the furnace and also in a downstream catalytic reactor, called AF-SCR (ammonia-free selective catalytic reduction). Unlike the ammonia-based SCR system, the new system does not need any added reagent. The excess CO not consumed to reduce NO is oxidized to CO_2 by the same catalyst. Figures E1 and E2 depict boiler plants with a conventional SCR system and with the ammonia-free SCR system.

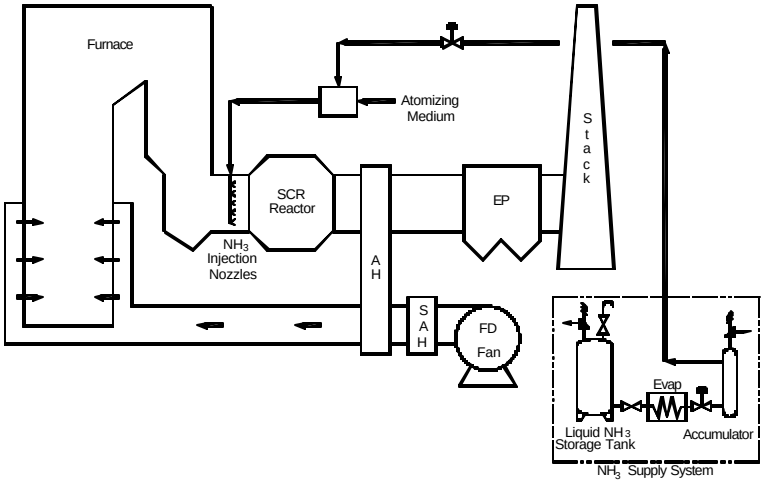

Figure E1 Typical Boiler Plant with SCR

This new concept breaks the constraining relationship between furnace NOx and CO emissions. By reducing combustion excess air and other furnace / burner modifications, lower furnace outlet NOx and higher back-end catalytic NOx reduction can be achieved. The integrated system including the optimized furnace and the AF-SCR has the potential to achieve lower overall NOx emissions than the current LNB/SCR technologies. It will also

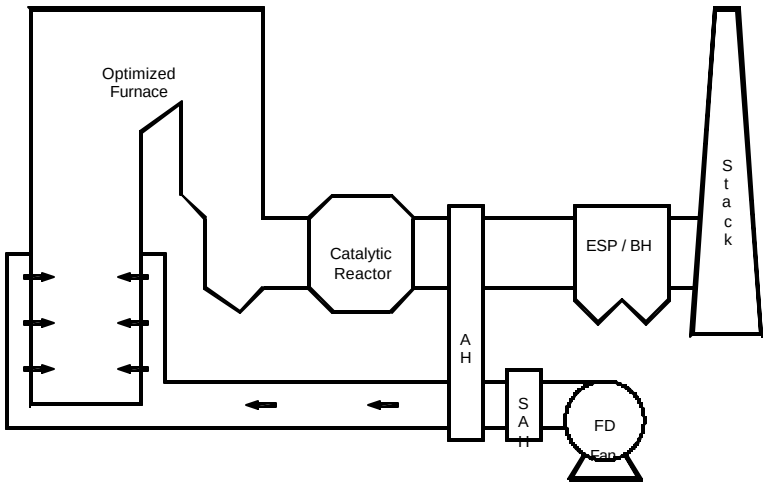

Figure E2 Plant with AF-SCR NOx Control System

drastically reduce the NOx control cost by avoiding the large capital and operating expenses for the reagent system, because the reductant CO is inherently generated during the boiler combustion process at no additional cost and without external handling. All other ammonia related plant issues, such as NH_3 slip, air heater fouling, safety and permitting, etc, are eliminated.

This development project attempts to answer three key questions: First, can NO be further reduced in the furnace and adequate CO / NO ratio be obtained entering the AF-SCR? Second, can simultaneous reduction of NO and oxidation of CO be achieved over catalysts, in oxidizing combustion flue gas atmosphere? Third, will the new NOx control system be competitive in both performance and cost with existing technologies? The study has led to the following conclusions:

- Furnace outlet NO level can be reduced and adequate CO/NO ratios can be obtained by modifying furnace operating conditions, such as reducing the overall excess air level or increasing the over fire air portion of total combustion air, without physical changes to the burner and boiler equipment. CFD study predicts that the effects by these adjustments on boiler efficiency, unburned carbon in flyash, and furnace exit gas temperature are relatively small and within the range seen in normal power plant operations.

- The base metal catalysts prepared and tested in this study exhibited very promising NO conversion under simulated flue gas conditions, including 3% oxygen. NO reduction in the range of 80-90% (outlet NO about 25-50 ppmv) has been achieved with operating temperatures ranging from 230-350^{o}C. The catalysts also oxidized over 80-90% of the CO in the gas mixture in a wide temperature range. All tested catalysts showed strong selectivity toward N_2 rather than N_2O as final product.

- Detailed analysis of the test data and catalyst reaction modeling indicate that catalyst effectiveness ç is close to 1.0 for the tested samples. Bulk mass transfer and pore diffusion were not significant limiting factors for catalyst performance during laboratory tests; they will not be rating limiting for the commercial scale catalysts. Preliminary scale-up correlations have been obtained to design honeycomb type commercial catalysts with high activity and effectiveness.

- Based on the conceptual design and predicted performance data of the ammonia-free selective catalytic reactor (AF-SCR) for a 400 MWe size coal-fired power plant, economic evaluation has been performed for NOx reduction with the AF-SCR system. By eliminating ammonia as reagent and using of low cost catalyst, the AF-SCR system will have significant cost advantages. Compared to the state-of-the-art SCR system, the AF-SCR system is projected to be 17% lower in capital investment, and almost 30% lower in cost of per ton NOx removed.

1.0 INTRODUCTION

1.1 Project Background

NOx is a precursor for ground level ozone formation, and a contributor to fine particulates ($PM_{2.5}$). Nearly 30% of the US population currently resides in counties with ozone levels above the National Ambient Air Quality Standards (NAAQS). Coal-fired power plants are among the largest single point emitters of NOx. New, stringent emission regulations are being proposed or implemented to deal with this environmental issue, as exemplified by the recent EPA Interstate Air Quality Rule, which calls for 53% reduction by 2009 and 61% reduction by 2015 of total power plant NOx emissions from 2003 levels. To achieve these ambitious goals, while maintaining reliable and affordable electricity supply, advancements in NOx control technologies are needed.

Existing NOx reduction technologies for coal-fired power plants fall within two categories: (1) combustion controls such as low NOx burners (LNB) and over fire air (OFA) to minimize NOx formation, and (2) post-combustion NOx reduction technologies, such as SCR (selective catalytic reduction) and SNCR (selective non-catalytic reduction), to destroy NOx once it has formed. The state-of-the-art new coal-fired utility boilers can typically achieve NOx emissions in the range of 0.06 – 0.10 lb/MMBtu (about one tenth of the emissions from old uncontrolled PC boilers), by using a combination of SCR with a LNB/OFA system. For the existing coal-fired power plants, US DOE / NETL has proposed the NOx R&D performance targets of 0.15 lb/MMBtu by 2006 and 0.10 lb/MMBtu by 2010, while achieving a levelized cost savings of at least 25% compared to the state-of-the-art SCR control technology (Lani et al 2005).

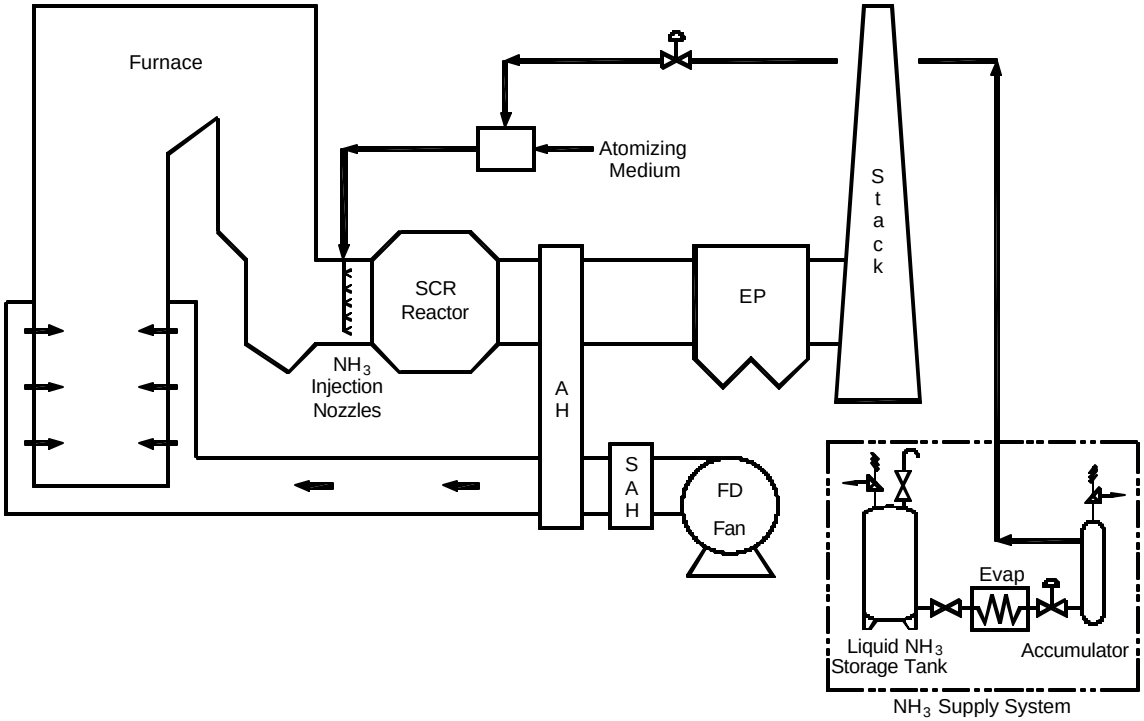

Figure 1-1. Typical Boiler Plant with SCR

Today's low NOx combustion technology emphasizes the precise control of local combustion stoichiometry and temperature within the primary combustion zone. The design strategy has been focused on delaying mixing of oxygen and fuel in the primary combustion zone to minimize NOx formation while at the same time maintaining acceptable combustion performance in terms of low unburned carbon and CO emissions.

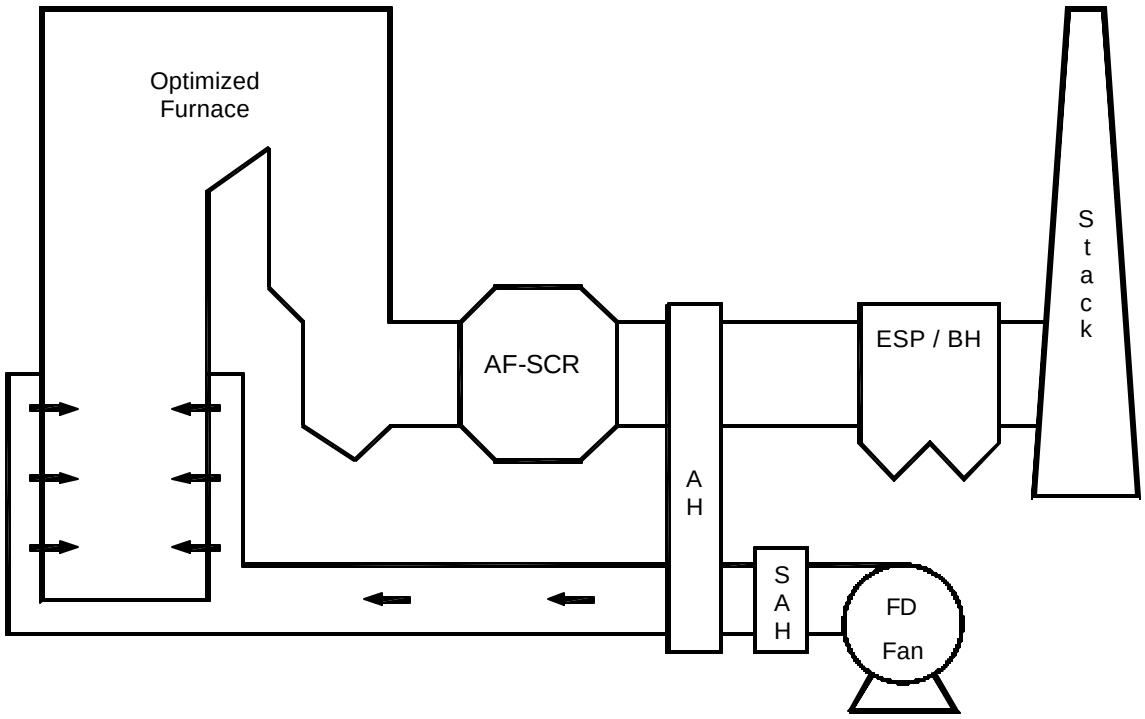

Figure 1-2. Plant with AF-SCR NOx Control System

In the new NOx control system, an increased CO concentration in the furnace is actually desirable, since the presence of CO reduces NO in the furnace and also in a downstream catalytic reactor, called AF-SCR (ammonia-free selective catalytic reduction). The new system does not need any added reagent. The excess CO not consumed to reduce NO is oxidized to CO_2 on the same catalyst. Figures 1-1 and 1-2 depict boiler plants with a conventional SCR system and with the ammonia-free SCR system, respectively.

This new concept breaks the constraining relationship between furnace NOx and CO emissions. By reducing combustion excess air and with other furnace / burner modifications, lower furnace outlet NOx levels and higher downstream catalytic NOx reduction can be achieved. The integrated system including the optimized furnace and the AF-SCR has the potential to achieve lower overall NOx emissions than the current LNB/SCR technologies. It will also drastically reduce the NOx control cost by avoiding the capital and operating expenses for the reagent system, because the reductant CO is inherently generated during the boiler combustion process at no additional cost and without external handling. All other ammonia-related plant issues, such as NH_3 slip, air heater fouling, safety and permitting, etc., are eliminated.

This study attempts to answer three key questions. First, can NO be further reduced in the furnace and an adequate CO / NO ratio be obtained entering the AF-SCR? Second, can simultaneous reduction of NO and oxidation of CO be achieved over catalysts, in an oxidizing combustion flue gas atmosphere? Third, will the new NOx control system be competitive in both performance and cost with existing technologies?

The project starts with a review and evaluation of commercial and developmental catalysts for NOx reduction and CO oxidation for their potential use in PC power plants. This knowledge combined with prior catalyst research experience allows the project team to develop and test catalyst formulations robust enough for the oxidizing flue gas environment in power plants, and capable of achieving competitive NOx reduction performance and economic targets.

A detailed PC combustion study, applying computational fluid dynamics simulation program to perform boiler and burner design modeling, complements the catalyst development effort by investigating ways to optimize the combustion process for the lowest NOx formation while generating sufficient levels of CO needed by the downstream catalytic NOx reduction process. Furnace configuration, air staging, and burner design are evaluated in this process.

The study then focuses on the comparative evaluation of a conceptual NOx control system for a 400 MWe, coal-fired power plant, utilizing this novel NOx control concept. For this evaluation, the concept system with the AF-SCR will be compared to a traditional PC boiler plant configured with current low NOx combustion technology and an ammonia-based SCR system. The comparison will involve conceptual level design of the AF-SCR to obtain equipment pricing, operational costs, performance data as well as qualitative reliability information.

1.2 NOx and CO Interrelation

NOx in coal-fired boilers comes from two main sources, thermal NOx due to oxidation of air nitrogen and fuel NOx due to oxidation of fuel nitrogen. In today's boilers with advanced combustion systems, thermal NOx is minimal; NOx is mainly formed from a small fraction of fuel nitrogen. The NOx emission level from a given fuel/combustor combination is a balance between formation reactions and reduction reactions, determined primarily by the following factors,

1. Primary combustion zone stoichiometry;
2. Primary combustion zone temperature;
3. Total stoichiometry (excess air);
4. Concentration of suspended solids including char;
5. CO levels in furnace.

CO and char together play a key role in NO reduction inside the furnace,

$$2NO + 2CO \rightarrow N_2 + 2CO_2 \quad \text{(over char surface)} \qquad (1\text{-}1)$$

The current low NOx combustion technologies (LNB and FBC) address the factors 1 and 2 above; however, they are unable to fully take advantage of excess air optimization and the NO

reduction effect of CO and char, due to CO emission concerns. In the proposed system, the furnace will be operated with a high CO concentration to achieve substantially reduced furnace exit NO levels. The NO in flue gas is further reduced across the catalyst section located in the boiler back pass, resulting in ultra low NOx emissions at the stack. The most direct means to achieve appropriate furnace outlet CO/NO ratios is by reducing overall excess air level. The impact of furnace overall excess air on NO and CO concentrations is qualitatively shown in Figure 1-3. The CO/NO ratio can also be controlled with other design and operational modifications, such as combustor average or local temperatures, primary combustion zone / burner operating condition changes and design modifications.

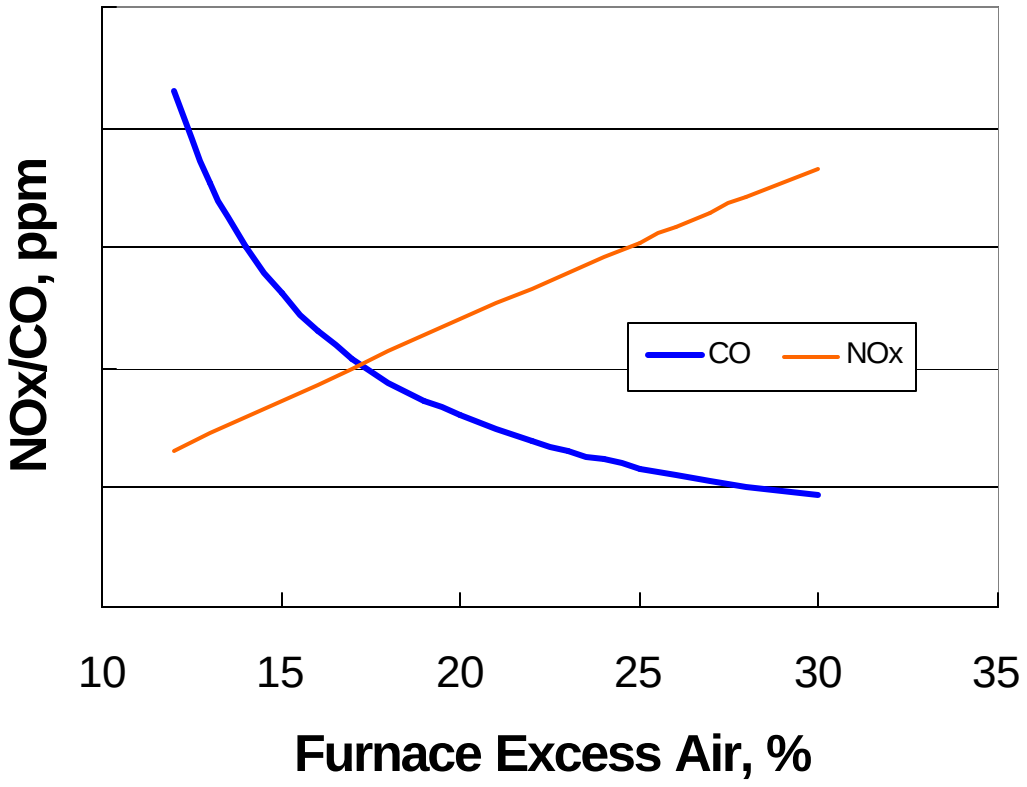

Figure 1-3. Effect of Furnace Excess Air on NO and CO Emissions

1.3 Review of DeNOx Catalysts

Theoretically, there are two ways NOx can be reduced to nitrogen. The first is direct decomposition of NO to N_2 and O_2. Catalysts including platinum group metals, transition metal exchanged zeolites, and base metal oxides have been considered for this process (White et al 1999). Due to the slow reaction rate and the interference with oxygen and moisture in the flue gas, direct reduction studies have only limited success.

The second method is NOx reduction by reagent addition. Ammonia is widely used in commercial SNCR and SCR processes. Other reductants such as CO, H_2 and hydrocarbons have

been successfully used in the automobile industry since the late 1970s, with the so-called "Three-way Converter" (TWC) that simultaneously reduces NOx, CO and HC emissions. Today all passenger cars with conventional gasoline engines sold in the US are equipped with TWC (Mooney 2001). The catalyst used in a TWC is based on platinum or palladium and rhodium on ceramic or metal substrate. CO functions as the NO reductant over the rhodium surface according to the following reaction:

$$2NO + 2CO \rightarrow N_2 + 2CO_2 \quad \text{(over metal catalyst)} \qquad (1\text{-}2)$$

The excess CO and hydrocarbons are oxidized over the platinum/palladium surfaces. The TWC usually works in the 200 ℃ to 500 ℃ temperature range. Note that the reaction (1-2) is the same reaction as (1-1), except that a different catalyst is needed at the low temperature range. High NOx conversion up to 90-99% is achievable with TWC. Conventional gasoline engines run at near stoichiometric conditions, controlled by fuel injection. Thus the exhaust gas oscillates between slightly oxidizing and slightly reducing conditions at high frequency (usually one cycle in less than a second). Since continuous oxygen supply is needed for the CO and HC conversions, cerium oxides, by the REDOX reaction between Ce_2O_3 and CeO_2, have been applied on TWC catalysts to regulate oxygen availability.

The automotive application shows that NOx control with CO as the reductant is effective. However, the TWC catalysts cannot be directly used in the combustion power plants. First, the precious metal-based catalysts would be cost-prohibitive for large-scale power plant applications. Secondly, these catalysts are inhibited by the high oxygen content found in the flue gas from combustion power plants where excess air (oxygen) must be maintained for fuel burnout and for operation safety.

Therefore the first task of the current study is to find a low cost catalyst that will work in the oxidizing environment. Various mixed oxide catalysts have been considered for the *in situ* reduction of NO by CO, principally as replacement for the noble metal based catalysts used in TWC. The following groups of metal oxides are of particular interest to this project and have been reviewed in detail:

- Perovskite type minerals
- Copper oxide catalysts, and cerium-promoted copper oxide catalysts
- Hydrotalcite-based catalysts
- Carbon / char-based catalysts

1.3.1 Perovskite-type Catalysts

Perovskite oxide catalysts are a large family of crystalline ceramics that derive their name from a specific mineral known as perovskite, $CaTiO_3$. Perovskites are among the most abundant minerals on earth. The generic formula for perovskite is ABO_3 or $A_{1-x}C_xBO_3$, where the elements A, B, and C can be a large variety of different elements. Perovskite oxide catalysts exhibit high thermal stability but low surface areas. Perovskite materials can be active catalysts, especially if they are synthesized with additional components that enhance the redox properties of the A_{1-}

$_xC_xBO_3$ materials. The activity of the catalysts will then be strongly dependent on the reducing or oxidizing environment of the catalytic reaction of interest. The redox properties of the B cation are important and can determine the lability of the structural oxygen atoms. Since perovskites are relatively low-cost materials and can be both oxidation and reduction catalysts, they were proposed as automotive exhaust treatment catalysts.

Model studies have demonstrated that particular perovskites are active for the NO + CO reaction at moderate temperatures, e.g. as low as 300°C under some conditions, and exhibit high selectivity for N_2 product formation at temperatures of 400°C and higher. Most research on the reduction of NO with CO over perovskites has focused on the need to control NO and CO emissions from motor vehicles. A successful catalyst must be designed to inhibit the promotion of N_2O, a greenhouse gas, while having an optimum concentration of adsorbed oxygen on the surface of the catalyst. Successful catalysts for this emission control reaction would preferably have high surfaces and maintain high activity and selectivity at low concentrations of NO and CO (ppm levels) in exhaust gases.

In general, the perovskite catalysts studied in the literature provide a wide temperature window for the reduction of NO. Experimental evidence indicates that the catalyst surface is first reduced by CO to create an oxygen vacancy, and then NO adsorption and dissociation occurs. The latter process takes place at a catalytic site consisting of a redox cation adjacent to the oxygen vacancy. The rate-determining step can be the removal of the surface oxygen or the adsorption and dissociation of the NO reactant. Gas-phase components such as O_2, CO_2, and H_2O can inhibit the overall CO + NO reaction by retarding the oxygen removal and by competitive adsorption on the catalyst surface. After dissociation of the NO molecule, rapid mobility and removal of the oxygen is required for high, stable catalytic activity, which again is promoted by cations that readily undergo redox reactions and can function as oxygen transfer / storage components. Examples of the latter active cations in the perovskite structure are Fe and Ce. At low reaction temperatures, N_2O is a dominant product formed from NO, while at high reaction temperatures, e.g. >350°C, N_2 is the dominant or only nitrogen-containing product formed.

1.3.2 Copper Oxide Catalysts

Supported copper-based catalysts have been shown to exhibit relatively high NO conversion and N_2 selectivity under model laboratory conditions. It has been proposed that the high reactivity is correlated with the redox chemistry related to the Cu active site, although there is still controversy as to the oxidation state of the copper involved in the catalysis. Most of the studies indicate that the NO reduction reaction is produced by cations that readily undergo redox reactions. Additions of dopants that also can undergo redox reactions, e.g. Ce and Fe, have been shown to enhance the NO conversion and N_2 selectivity.

The product selectivity is at least in part determined by the reaction temperature, where low reaction temperatures tend to favor N_2O formation relative to the desired N_2 product. Gas-phase components such as O_2, CO_2, and H_2O can inhibit the overall CO + NO reaction by competitive adsorption on the catalyst surface and by retarding oxygen removal from the surface of the catalyst. The presence of moisture inhibited the reaction by reversible competitive adsorption,

while CO_2 did not, and the presence of oxygen completely inhibited the reduction of NO. The reduction of NO only took place after all oxygen has been converted to CO_2, and therefore the NO reaction when oxygen was present required higher reaction temperatures, which also favored selectivity toward N_2 and away from N_2O. However, depletion of CO in the reactant stream resulted in oxidation of the carbon support if excess oxygen were present, and NO was also reduced by the carbon support, which was oxidized, at temperatures >327°C. It was also found that highly dispersed Cu2+ species on Al_2O_3 were the active sites for selective reduction of NO to N_2, while aggregated Cu species preferentially oxidize CO without reducing NO. Upon increasing the Cu content of the catalysts, it was shown that the increasing presence of aggregated Cu species drastically reduced the NO conversion and N_2 formation capability, while reducing the reaction temperature at which N_2O was formed and CO was oxidized.

1.3.3 Cerium Promoted Catalysts and Hydrotalcite Group

Supported copper-based oxide catalysts have been shown to exhibit high NO conversion and N_2 selectivity under model laboratory conditions. It has also been demonstrated that adding Ce to Cu-based catalysts can enhance the NO reduction activity and/or N_2 selectivity. The Ce promoter also provides a synergetic effect with the Cu in providing tolerance of the catalyst for the presence of O_2, H_2O, and SO_2 in the NO + CO reactant stream. Thus, the Ce/Cu couple inhibits deactivation induced by poisons. It has been proposed that effect results from enhancing redox couples so that redox reactions involving Cu and Ce are promoted and occur more easily and at lower temperatures. At the same time, selectivity to the N_2 is promoted, which is important since the formation of undesirable N_2O as a reaction product tends to be favored by low reaction temperatures. High dispersions of the active sites are required, and it has been reported that formation of ternary oxide catalysts through a hydrotalcite-type intermediate, based on the structure found in nature for $Mg_6Al_2(OH)_{16}(CO_3)\cdot 4H_2O$, provides high dispersions of active components.

It is well established that cerium oxide is a beneficial additive to three-way automotive catalysts. Its attributes include stabilization of alumina supports against sintering, increased dispersion of noble metals, promotion of the water gas shift reaction. To study the synergism between Cu and Ce in oxides, catalysts consisting of (a) CuMgAlO, (b) CeMgAlO, and (c) CuCeMgAlO were synthesized by a co-precipitation method. The presence of both Cu and Ce in the catalyst resulted in a highly dispersed, active, stable, and poison-resistant catalyst for the reduction of NO by CO. It was proposed that Cu and Ce together gives a high concentration of Cu^{1+} species and oxygen vacancies that function as adsorption sites and promotes the water gas shift reaction, as well as the NO reduction reaction. The SO_2 tolerance of the (c) CuCeMgAlO catalyst was the most interesting result.

It has been shown that ternary component catalysts, e.g. Cu/Zn/Al and Cu/Zn/Cr used for methanol synthesis from syngas, one of the largest industrial processes today, catalysts with the "proper" composition and formed *via* a hydrotalcite-type intermediate appears to yield the most active and highly dispersed catalysts. A variety of hydrotalcite-type materials, including Cu/Co/Al and Cu/Mg/Al, have been prepared as catalysts for the reduction of NO by CO. Catalysts prepared through a hydrotalcite-type precursor were more active for NO reduction than catalysts prepared by stoichiometrically co-precipitated samples and materials prepared by

mechanically mixing the metal oxides prior to calcination. It was shown that calcinations at 350-400°C gave more active catalysts than calcinations at 600 or 800°C. It was noted that the most reducible catalyst, Cu/Co/Al, was the best catalyst for reduction of NO by CO. It is clear that once again, surface redox chemistry is crucial to the performance of the catalyst and that oxygen transfer and removal from the surface of the catalyst can be the limiting reaction step.

1.3.4 Carbon Based Catalysts

Activated carbon and other carbons have been investigated as direct reducing agents, as well as providing high surface area supports for alkali and transition metal catalysts for NO reduction. Carbons do directly reduce NO, and different reactions are dominant in different temperature regimes. Under some reaction conditions, the presence of O_2 in the reactant mixture promotes NO reduction, while the presence of moisture tends to inhibit the reaction, particularly by competitive adsorption at lower reaction temperatures.

Highly activated materials that have been pyrolyzed usually require appreciably higher temperatures for NO reduction, even when catalysts are impregnated into the carbons. However, dispersed metal catalysts tend to enhance higher NO reduction at lower temperatures over most carbons, as well as higher carbon burn-off. High dispersions of the active sites are required, preferably on the surface of high surface area carbons. The presence of CO in the reactant gas mixture aids in the reduction of NO, again in a temperature dependent manner. The simultaneous presence of catalysts on carbon supports and CO in the reactant gas mixture can greatly promote the reduction of NO in a gas stream.

Carbon Reduction of NO: Various carbons have been investigated as a reducing medium for NO conversion to N_2. The carbon is the reducing agent and is consumed in the reduction of NO. Carbons and chars can naturally contain other moieties such as alkali/alkaline earth metals and transition metals usually in an oxidized or sulfided state. It is sometimes difficult to separate the effects of carbons in reducing NO from the effects of catalysts. It was observed that the presence of CO enhances the reduction of NO. The CO might fulfill two roles in NO reduction; (A) removing surface oxides from the carbon surface, C(O), to expose free reactive carbon sites, C*, and (B) direct reduction of the NO by reaction, i.e.

(A) $CO + C(O) \rightarrow CO_2 + C^*$

(B) $2CO + 2NO \rightarrow 2CO_2 + N_2$.

With respect to other gases in the reactant stream, it has been reported that the NO-carbon reaction is inhibited by the presence of water vapor. On the other hand, the presence of oxygen enhances the rate of NO reduction, especially in the presence of catalysts in the carbons.

Reduction of NO by Catalyst-Promoted Activated Carbons: A large amount of studies was related to catalyst-promoted activated carbons. Example of doping the coal-derived carbon with K^+, *via* CH_3COOK, or KOH, by ion exchange or by impregnation, promotion of significant reduction of NO was found to occur at considerably lower temperatures. Three characteristic reactivity regions were found. Potassium was found to be very active in dissociating NO, even at temperatures as low as 60°C. It was proposed that this is due to K^+ being reduced by the carbon substrate and promotion of surface redox reactions. The effects of K^+ on NO reduction over five coal-derived chars were examined, where the chars were obtained from two lignites, two

subbituminous, and one hvA bituminous coals. The most active coal chars for NO reduction were obtained by pyrolysis at 900°C followed by treatment with aqueous KOH using a KOH/coal wt ratio of 0.5/1.0.

A study of monometallic K, Fe, Co, Ni, and Cu catalysts on activated carbon was subsequently carried out. The activated carbon was prepared from a hvA bituminous coal and impregnated with aqueous KOH. It was reported that the metal catalysts were ineffective at temperatures lower than about 200°C. However, at higher temperatures all of the metals catalyzed the NO reduction reaction, and the total activity was the result of two factors, the tendency of the metal to be oxidized by NO and the easiness of the resulting oxide to be reduced by carbon. The Cu and Co catalysts exhibited the highest NO conversion at 300°C and the lowest temperatures for significant NO reduction to be observed. However, these two catalysts exhibited the highest burnoff of carbon at 300°C, some 2-3 times higher than observed for the Ni, Fe, and K catalysts. However, the latter three catalysts exhibited lower NO reduction levels than the Cu and Co catalysts. The effect of Fe, as well as Na and Ca, on coal chars was studied too.

Portions of the same coal-derived activated carbon were also impregnated with excess aqueous solutions of Cr, Fe, Co, Ni, and Cu nitrates. All of the transition metals catalyzed the NO-carbon reaction (studied in the absence of O_2), causing a decrease in the activation energy and substantial shifts of the NO reduction curves toward lower temperatures. The TPR curves support a redox mechanism involving different oxidation states of the metals and the carbon matrix. At low reaction temperatures (<400°C), Fe, Co, and Ni are the most effective catalysts, which is consistent with their abilities to chemisorb NO dissociatively. At high reaction temperatures (500°C), Cu, Co, and Ni exhibit the highest activities. These observations indicate that at low temperatures, the controlling step in the process is NO chemisorption, whereas at high temperatures reduction of the intermediate oxidized metal species is the rate-limiting step in the reaction sequence. At low reaction temperatures, all of the transition metals were much less active in promoting the NO-carbon reaction than was K (in terms of mol NO reduced/mol of metal/sec). However, at 500°C the Cu catalyst was more reactive than the K catalyst, and Co and Ni were approaching the activity of the K promoter. It was pointed out that the K catalyst showed a high NO removal capability at about 200°C and achieved 100% NO reduction at 500°C. The transition metal catalysts exhibit differing behaviors because of their difference redox properties. At low temperatures, catalyst deactivation is observed because of oxygen accumulation on the surface. For the catalysts, the transfer of oxygen from the oxidized catalytic site to the carbon is proposed to be crucial for maintaining high steady-state catalytic activity.

More recently, deposition of bimetallic catalysts on carbon supports and model studies of NO reduction by the carbon have been carried out. It was found that all of the transition metals promoted the K-carbon system and exhibited a synergetic effect, in particular the temperature for NO reduction was reduced, i.e. to the 200-250°C range, and the N_2 selectivity was nearly 100%. Among the metals analyzed, it was stated that the K-Ni catalyst was the most interesting because it combined a high NO reduction activity at low temperatures with the lowest loss of carbon by combustion. The bimetallic catalysts, K-Ni, Ni-Co, and Ni-Cu, promoted NO reduction too. The Ni-Cu catalyst was reported to yield the best performance at 250°C by showing a high NO conversion and selectivity, and absence of N_2O and CO in the reaction products.

As a summary, carbons are active support materials for the reduction of NO in gas streams. Without the presence of catalysts, operation temperatures are higher than 500^{o}C. However, supporting base metal catalysts and/or redox transition metal catalysts in mono, bi or ternary metal forms on the carbon supports reduced the temperature required for NO reduction. The thermal treatment in obtaining the activated carbon or char can greatly affect the temperature that is needed to obtain significantly high levels of NO reduction. The presence of CO and O_2 in the reactant stream both promotes the reduction of NO. In addition, the simultaneous presence of catalysts on carbon supports and CO in the reactant gas mixture can greatly promote the reduction of NO in a gas stream.

2.0 EXPERIMENTAL

2.1 Test Rig

A fixed bed reactor at Lehigh University was the main experimental tool employed in this study. The catalyst testing system features a vertical down flow quartz tube reactor (10.5 mm ID x 13 mm OD). Temperature in the reactor was monitored by an axial thermocouple located in the catalyst bed. The tip of the thermocouple was usually positioned 2.5 to 5.5 cm below the top of the catalyst bed. Heating was accomplished with a vertical split-tube furnace surrounding the reactor. The gas stream inlet and outlet 316 stainless steel sections were wrapped with heating tapes and insulation and heating was controlled by two Variacs. Temperatures of the inlet and outlet lines were monitored by six thermocouples and maintained above 100°C.

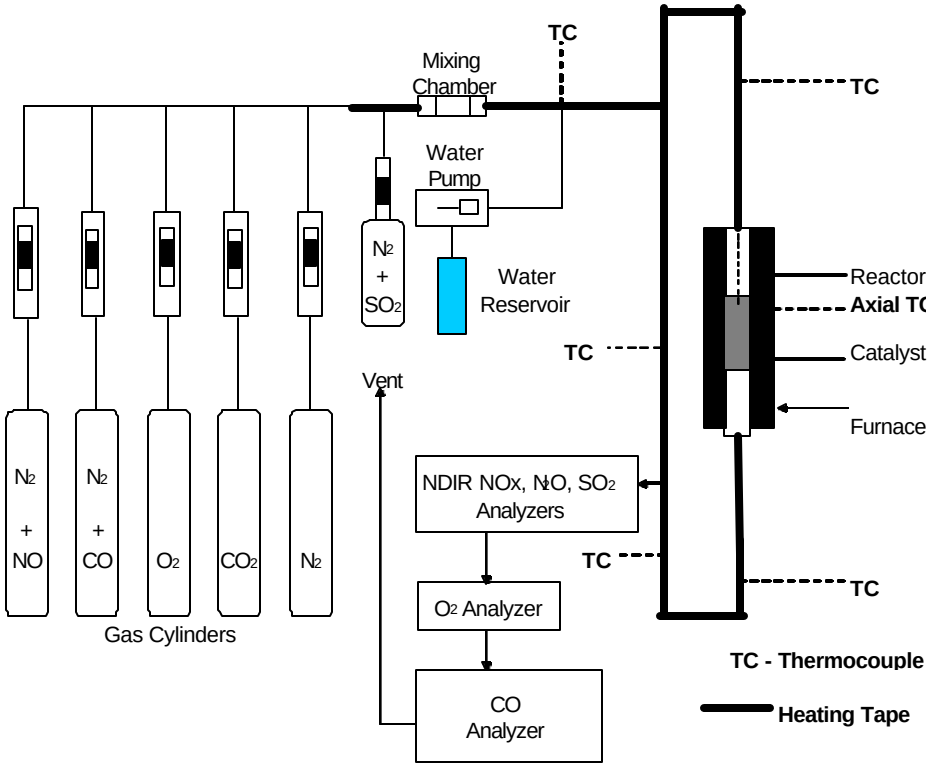

Figure 2-1. Bench Scale NOx Testing System

A process flow diagram of the NO reduction test rig is shown in Figure 2-1. Figure 2-2 shows the rig with the furnace open with a quartz tube reactor inside. Approximately 20 ml of weighed catalyst sample was placed in the reactor and supported by a quartz wool plug. Based on literature survey, the CO-NO reaction under study is not catalyzed by the quartz reactor tube at temperatures below 1000°C. Individual gas flow meters were used to regulate flow rates from

gas cylinders containing NO/N_2, CO/N_2, O_2, CO_2, N_2, and SO_2/N_2 to simulate flue gas from coal-fired power plants. A cylinder pump was used to inject desired amount of distilled water through a vaporizing pipe section into the heated inlet gas line to the reactor. The outlet test gas goes through a chiller before entering the gas analyzers. A bypass valve can be used to connect the inlet gas stream directly to the analyzers to check and confirm the inlet concentrations of NO and other gases. A bubble flow meter was used to calibrate the rotameters for individual gas streams.

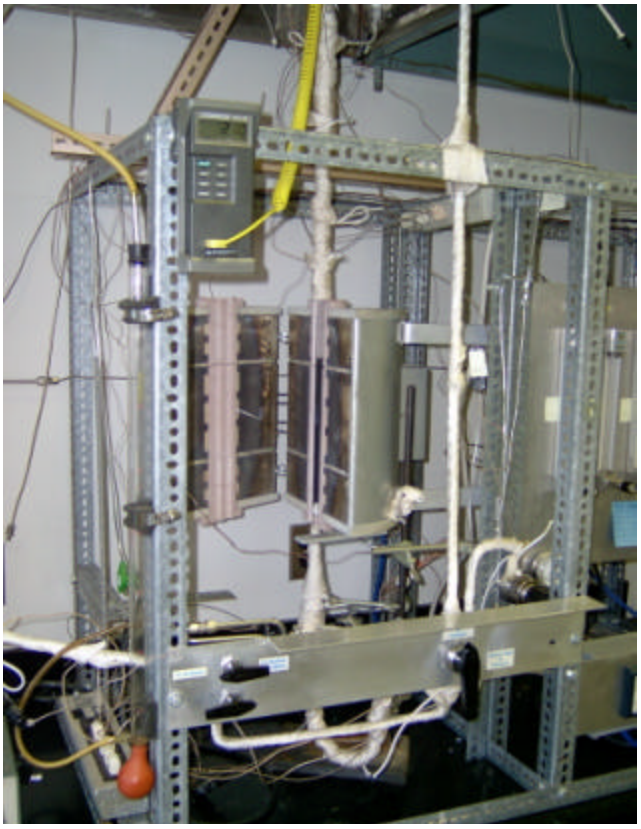

Figure 2-2. Photo of Test Rig

Analysis of the NO, N_2O, and SO_2 concentrations in the gas stream were achieved with a Siemens Ultramat 6 non-dispersive infrared (NDIR) analyzer, while O_2 was analyzed by a Siemens Oxymat 6 Paramagnetic analyzer. CO was determined by a Testo 325-3 digital CO analyzer. Monitoring of these gases in the reactor inlet and outlet streams was carried out to determine if these components of the gas mixture were being generated or consumed. Moisture, CO_2, and N_2 concentrations were calculated based on their flow rates into the reactor.

2.2 Catalyst Preparation

The activated carbon (AC) used in this study was a 12-20 mesh size product purchased from Aldrich. It was lignite-derived, designated as Darco Activated Carbon and manufactured by American Norit Co. Due to its relatively low cost, lignite-based activated carbon has been widely

used in the waste to energy industry for trace pollutant removal, and is currently being demonstrated to capture mercury for coal fired utility plants. The BET surface area of an "as received" AC sample was determined (6-point analysis) by nitrogen adsorption at -196°C using a Micromeritics Gemini 2360 V1.03 instrument. Before analysis, the sample was purged with flowing N_2 while heating from 60°C to 200°C over a period of 55 min. The sample was then maintained at 200°C for 2 hr and cooled to ambient temperature. During this thermal treatment, the sample exhibited a 1.5 wt% loss of weight. The determined surface area of the activated carbon was 525 m^2/g. After loading of the catalytic components the surface area for catalyst Type B became 468 m^2/g, which is very close to that of the as received AC.

Another catalyst substrate used was activated alumina (AA). An 8-14 mesh size activated alumina (AA) product was obtained from Fisher Scientific. It was designated as A-505 adsorption grade alumina. The alumina was utilized either *as received*, or *after calcining*. The as received sample was simply purged with N_2 and stored in a N_2-filled glove bag containing a beaker of Drierite to maintain a dry atmosphere before catalyst preparation. To obtain a calcined sample, a portion of the alumina was placed in a porcelain evaporation dish and placed in a furnace at 180°C. The temperature was increased to 500°C, and the sample was held at this temperature overnight. It was then removed from the furnace, cooled, and placed in a N_2-filled glove bag containing a beaker of Drierite to maintain a dry atmosphere. A small portion of the activated alumina in a separate dish with the same calcination treatment exhibited a 14.4 % wt loss. The BET surface areas of the alumina samples used as substrate are given later in Table 3-3.

The catalysts were prepared by an aqueous impregnation method. Reagent grade chemicals of metal nitrates from Fisher Scientific or Strem Chemcials were dissolved in distilled water and heated to 60°C. To the solution was added AC or AA while maintaining constant stirring. The solution was then evaporated over a period of a few hours, and when the solid was dry to the touch, it was placed in a plastic bottle. The open plastic bottle was placed in an N_2-filled glove bag containing a beaker of Drierite desiccant for further drying.

Activation of catalysts was carried out by decomposition of metal salts. The impregnated multi-metal nitrate salts were decomposed by heating under established flow rates of the simulated gas mixture containing approximately 3.0% O_2, 14% CO_2, 520 ppm CO, and balance N_2. The gas hourly space velocity (GHSV) used for the decomposition treatment was about 930 hr^{-1}. The inlet and exit lines as well as the furnace were then heated. Usually, the catalyst was slowly heated to about 270°C over a period of 3-6 hr and maintained at this temperature for 0.5-3 hr until the emitted NO achieved low levels.

During this treatment, a large amount of NO was released from the catalyst, as a result of nitrate salt decomposition, which peaked in the temperature range of 100-200°C and then decreased with further increase of temperature and time of equilibration. CO, O_2, and N_2O were also measured during decomposition/activation at increased temperatures. After the decomposition treatment, the furnace controller was turned off and only the flow of N_2 was maintained overnight as the furnace cooled to ambient temperature.

2.3 Catalyst Test Procedure

For NO reduction activity determination, the flow rates of the gas mixture components were reestablished and the flow rates were measured/confirmed by means of a bubble meter. The reactor was then heated and the NO/N_2 flow was turned on. The temperature of the catalyst bed was then sequentially changed to obtain a conversion-temperature profile both in steady state and in transient conditions. To screen the performance of different catalysts, a constant GHSV of 1050 hr^{-1} at ambient temperature and pressure and the inlet gas composition was used. The established dry reactant gas mixture consisted of the following for most of the tests:

NO	CO	O_2	CO_2	N_2
260 ppm	520 ppm	3.0 %	14.0%	83%.

This gas mixture gives a CO/NO molar ratio of 2.0, with enough excess reductant for the NO reduction reaction. To study the catalyst reactivity for NO reduction without the interference of poisoning or inhibition, the initial catalyst evaluation tests were carried in the absence of SO_2 and moisture. After the initial tests, selected catalysts were exposed to the reactant gas stream containing moisture and SO_2 to determine inhibition and poisoning effects.

For experiments with moisture added to the gas stream, water was injected and vaporized to give the following reactant gas mixture with an overall GHSV of 1140 hr^{-1}:

NO	CO	O_2	H_2O	CO_2	N_2
240 ppm	480 ppm	2.8 %	8.0%	12.9%	76.3%.

When the reactant stream contained SO_2, a 5727 ppm SO_2/N_2 mixture was utilized and its flow rate was compensated by decreasing the N_2 flow rate accordingly to maintain the overall GHSV at 1140 hr^{-1}. The resultant reactant gas mixture consisted of:

NO	CO	SO_2	O_2	H_2O	CO_2	N_2
240 ppm	480 ppm	200 ppm	2.8 %	8.0%	12.9%	76.3%.

Catalytic reactivity is expressed by conversions, where the calculated conversions are multiplied by 100 to obtain % Conversion, i.e.

NO	Conversion = $1 - (NO)_{out} / (NO)_{in}$
N_2O	Conversion = $2(N_2O)_{out} / (NO)_{in}$
CO	Conversion = $1 - (CO)_{out} / (CO)_{in}$
O_2	Conversion = $1 - (O_2)_{out} / (O_2)_{in}$
SO_2	Conversion = $1 - (SO_2)_{out} / (SO_2)_{in}$

It was assumed that there was no significant difference between gas inlet and outlet in its molar flow rates, considering that about 97% of the dry feed gas is N_2 or CO_2, neither of which are expected to participate in any of the reactions under study here. The NO reduction levels were determined following attainment of steady state. As a post-combustion NO control process, a

low NO level of 260 ppm was used in this test, assuming some form of low NOx combustion technology is already being used.

The temperature of the catalyst bed was changed and the NO conversion was determined as it approached to a steady state at each set point. The set point temperatures were selected to achieve the maximum NO reduction for each catalyst. The NOx conversion as a function of temperature and time were recorded. The other gases, such as O_2, CO, SO_2, and N_2O, were also recorded. They were used to analyze catalytic selectivity, NOx reduction pathways, and possible side reactions, especially the relations among NOx reduction, CO depletion, and O_2 consumption. The reactivity profile of NOx reduction *vs*. temperature can then be plotted to compare the performance from different catalysts.

After a test, the test sample was cooled down and preserved in an N_2 environment for subsequent characterization. Most of the tested catalysts were subjected to repeat test(s) under identical conditions as used for the first day test. The multi-day tests ensure data/procedure repeatability and provide clues to any deactivation over time on stream.

Tests on various combinations of Fe, Cu, Ce, and K on the AC and AA supports have been conducted. To date, 13 catalysts have been prepared and evaluated.

Table 2-1 describes the various catalyst samples tested. The amount of each metal impregnated on the AC or AA support is expressed as the percentage of a reference total metal loading. The test runs in this report are reported as a combination of letters and numbers, such as A-1, B-2, where the letter indicates the catalyst type tested and the number indicates the order of the test run, for example, 1 for first run (e.g. Day 1). Duplicate samples of some of the catalysts were tested under different conditions and designated with different names for convenience of reference. For instance, P is a sample of the remaining O catalysts after eight tests at a GHSV of 1050 1/hr. It is used for high GHSV testing at 5250 1/hr.

Table 2-1. Catalyst Samples Tested*

Catalyst Name	First Test Date	Catalyst Formula	GHSV, l/hr	Substrate
A	4/07	As-received AC	1050	AC
B	4/09	10% Fe/10% Cu	1050	AC
C	4/21	40% Fe/10% Cu	1050	AC
D	4/30	10% Fe/30% Cu	1050	AC
E	5/21	40% Fe/0% Cu	1050	AC
F	5/26	7% Fe/7% Cu	840	AC
G	5/29	40% Fe/10% Cu	1050	AC
H	6/09	40% Fe/30% Cu	1050	AC
I	6/22	Aqueous-treated AC	1050	AC
J	6/29	40%Fe/30%Cu/20% Ce	1050	AC
K	7/22	40% Fe/30% Cu/20% K	1050	AC
L (duplicate of E)	8/13	40% Fe/0% Cu	1050	AC
M (duplicate of H)	9/02	40% Fe/30% Cu	1050	AC
N	10/04	40% Fe/30% Cu	1050	AA
O	11/05	40% Fe/30% Cu	1050	AA (calcined)
P (previously tested O)	12/09	40% Fe/30% Cu	5250	AA (calcined)
Q (duplicate of O)	12/16	40% Fe/30% Cu	5250	AA (calcined)
R (duplicate of H)	01/07	40% Fe/30% Cu	5250	AC (calcined)

* Percentage in catalyst formula refers to a reference total loading.

3.0 CATLYST DEVELOPMENT

3.1 Activated Carbon Based Catalysts

3.1.1 Catalyst Tests Overview and Data Reproducibility

Figure 3-1 is an example of a typical catalyst test history. At the beginning of a test when the catalyst bed is cold, the activated carbon can adsorb approximately 85-90% of NO. When the catalyst bed reaches a temperature of about 120°C, only a slight adsorption of NO still occurs. Therefore, for most of the tests, NO was added to test gas stream only when the bed temperature reaches 150°C. Multi-day tests were carried out for most of the catalyst samples. Excellent repeatability was obtained.

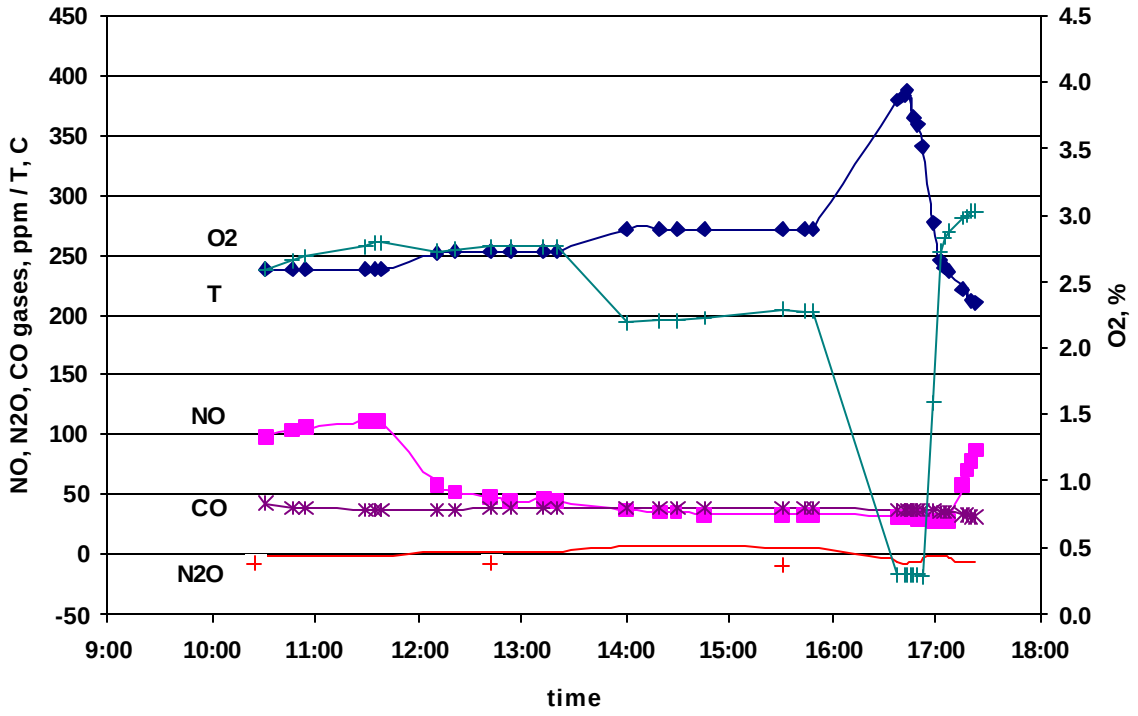

Figure 3-1. Typical Transient Test Data

Figure 3-2 shows the conversion data for CO, NO, O_2 and N_2 selectivity for the 40% Fe/30% Cu/AC catalysts Type H (Test 1) and Type M (Test 2). The NO conversion displayed a typical S-type curve where the catalyst reactivity rapidly increased at a rather sharp "light-off" temperature. When temperature increased further, the NO conversion reached a maximum of about 80-90% NO conversion and then leveled off.

Test 2 utilized a fresh 20 ml portion of the same catalyst as used in Test 1 earlier. The two tests were three months apart, during which time the as-prepared catalyst had been stored under a N_2 environment. Comparisons of the activities and selectivity observed during the tests with the dry

reactant gas mixture as shown in Figure 3-2 clearly demonstrated that the testing procedure had generated reproducible behavior of the catalyst.

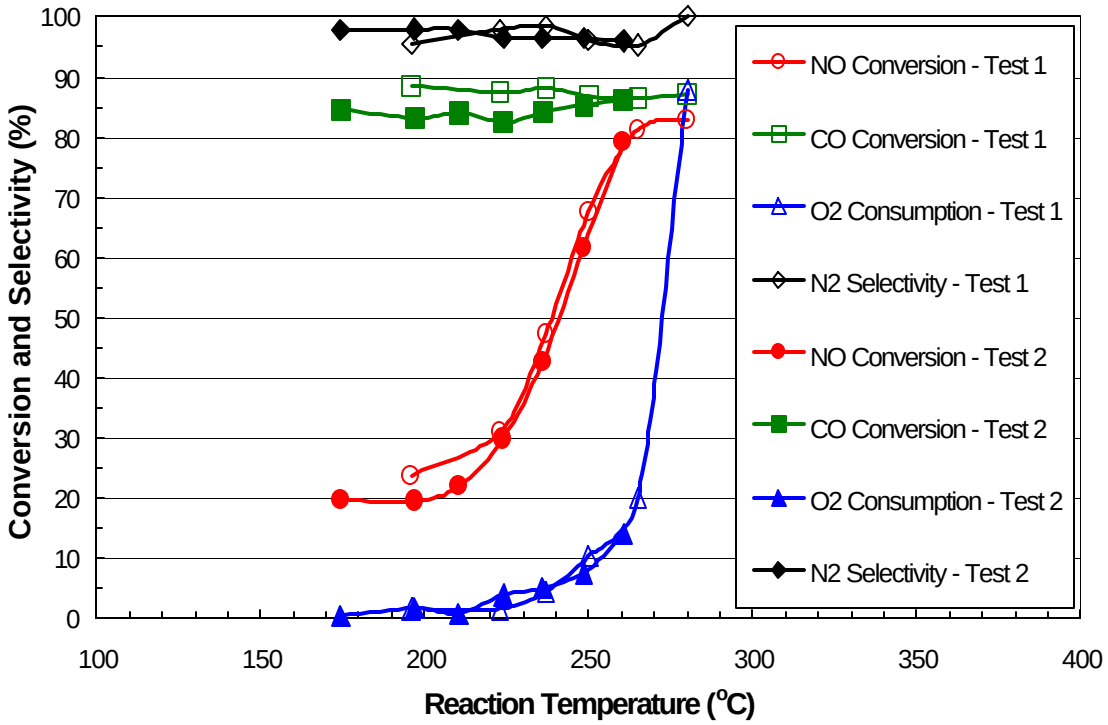

Figure 3-2. Conversion of NO, CO, and O_2 and N_2 Product Selectivity Over the 40% Fe/30% Cu AC Catalyst

3.1.2 Base Line Tests with Activated Carbon

Active carbon has been reported to catalyze the NO reduction. For reference purpose, two un-promoted AC samples were tested. The first is the as-received AC. To determine the impact of our catalyst preparation procedure, a sample of the AC was aqueous-treated using the same procedure as used for the catalysts, except for using only distilled water without salts. The aqueous-treated AC was activated then in the same way as the other catalysts. The same operation conditions for testing catalyst were used, such as the GHSV and feed gas composition.

As shown in Figure 3-3, the AC itself reduced very little NO at temperatures below 300°C. Similarly, little O_2 was consumed by reaction with carbon. As the temperature increased, CO was generated over the AC. At about 340°C, the CO in gas had doubled over inlet concentration, and the NO conversion increased too. Meanwhile, the O_2 consumption started to rise, indicating the AC direct combustion or partial combustion had occurred. The data shows that there is a link between the NO reduction and carbon partial combustion (oxidation), which is consistent with the so-called low temperature regime of NO carbon reaction in the literature (Aarna and Suuberg, 1997, Jurczyk and Drago, 1988).

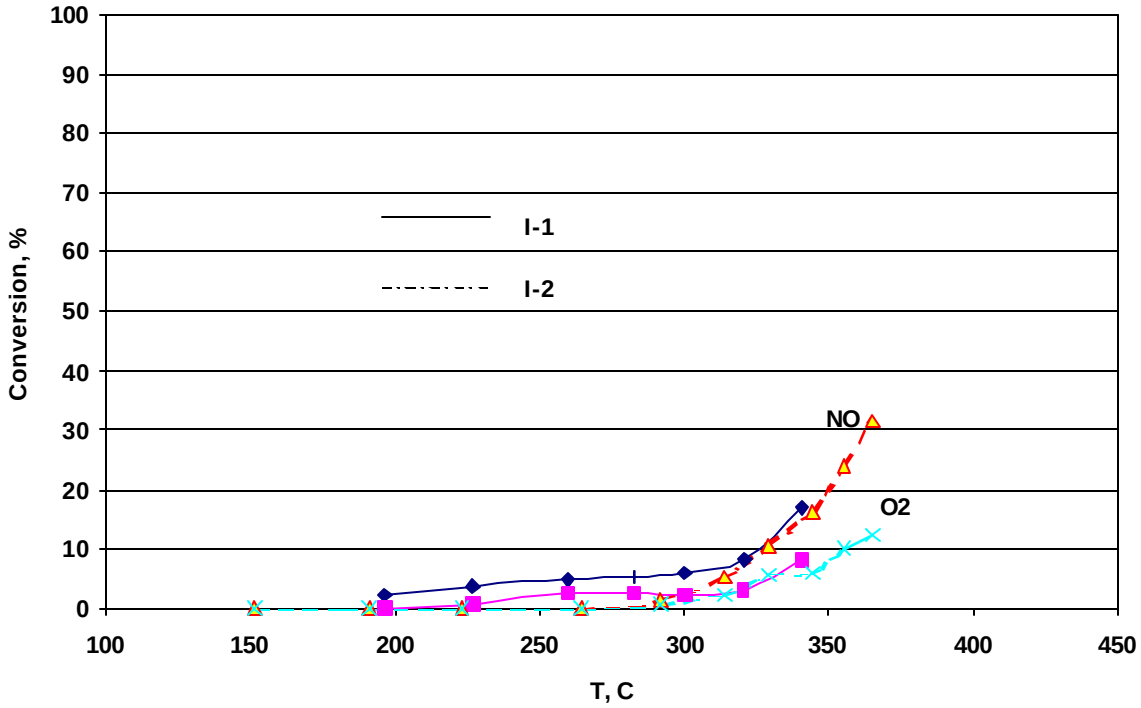

Figure 3-3. Baseline Test with Unpromoted AC (Catalyst-I)

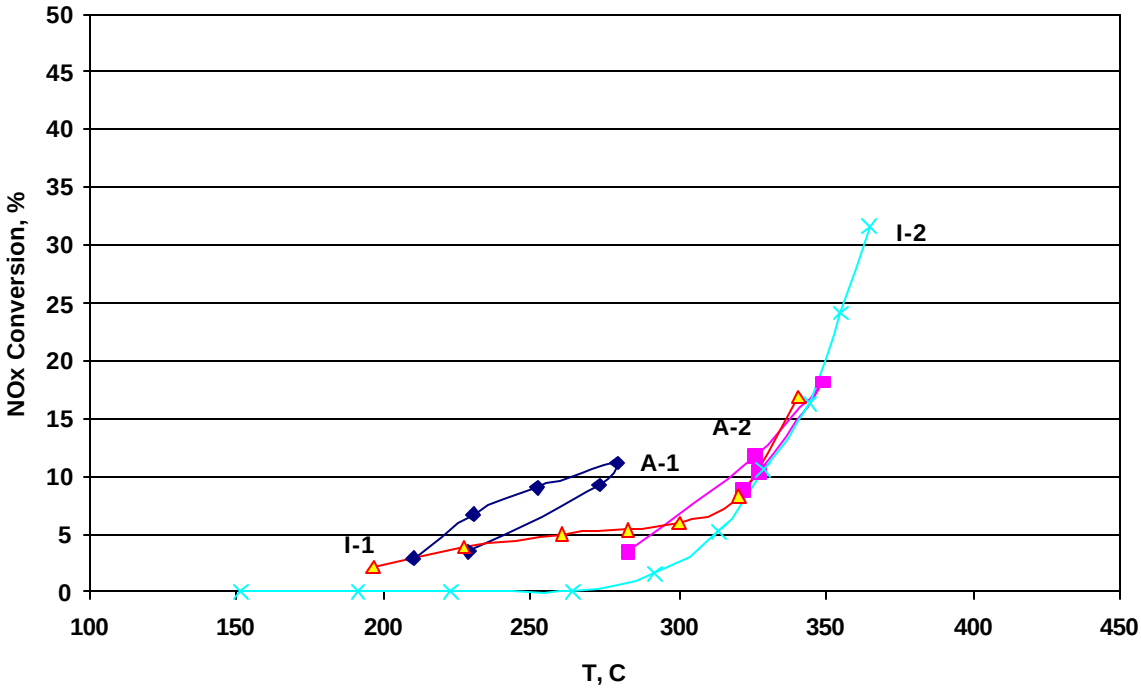

Figure 3-4. As Received vs Aqueous Treated AC

The NO conversion data for aqueous–treated and as-received AC are plotted in Figure 3-4. There was no significant difference between the as-received AC and the aqueous-treated AC. For

NO reduction by AC, there was some difference between day one and day two tests (A-1 and A-2) for the as- received AC, but A-2, and I-1 and I-2 were very similar. The reference AC samples (as-received AC, and aqueous-treated AC) had similar behavior during the testing.

The NO-carbon reaction can be boosted with presence of catalysts. The tested AC was made from lignite, and washed by acid to remove minerals. According to the product catalog, it contains less than 100 ppm Fe, indicating that little coal ash from the original lignite remained. Carbon burnout at the high temperatures needed for significant NO conversion and associated temperature runaway may limit the direct use of untreated AC for NOx reduction. However, if and where the carbon consumption is permitted, the direct NO-carbon reaction and reaction of NO with CO generated from AC can be beneficially utilized as part of the overall NO control process.

Another significant observation is that there was no CO reduction by the reference AC samples, as confirmed by repeated tests with both AC samples. No N_2O was formed for the reference AC test shown in Figures 3-3 and 3-4.

3.1.3 Fe Effect

Iron's potential as a NO reduction catalyst stems from its effectiveness as a catalyst for carbon gasification and combustion. It enhances the carbon reaction through different reaction pathways (Illan-Gomez et al 1995, Randall et al 1998). The enhancement lowers the reaction activation energy, reaction temperature and NOx generation. It is of interest to analyze the contribution of the catalytic effect by Fe in a group of Fe/Cu/AC catalysts. The tests for Fe loading effect, therefore, were carried out with different Cu levels.

The first effect, as shown in Figure 3-5, is that the addition of Fe on AC improved catalyst reactivity. The NO reduction reached over 70% as the temperature was increased to about 330°C. It shifted the catalyst bed temperature required for 50% NOx reduction (hereafter referred to as T_{50}) from 380°C for AC only (extrapolated from tested data range) to 320°C for the case with 40 % Fe loading. However, it was noted that even with Fe loading as high as 40%, there was no CO reduction for the Fe only cases. As the bed temperature increased, the CO generation started at about 270°C, and increased rapidly at about 330°C. O_2 was consumed as CO concentration increased. Thus, a large surplus of CO relative to needed amount for NO reduction resulted. It was also noted that the O_2 consumption was much higher than the stoichiometric amount required for CO generation, indicating the dominant combustion product was CO_2. The significant release of both CO and CO_2 as a consequence of carbon partial combustion verifies that although Fe is a good catalyst for the carbon gasification and combustion, it does not have any catalytic function for the CO reduction. The NOx reduction here is through NO - char reaction enhanced by Fe as catalyst. Further discussions on the effect of Fe on partial combustion and CO generation are included in section 3.1.4 – Cu Effect.

In comparing with other supports, such as TiO_2, ZrO_2, Al_2O_3, and SiO_2, as reported in literature for iron oxide catalyst, where the N_2O is favored at low temperatures, the present AC supported iron oxide catalyst shows very good selectivity with little N_2O formation.

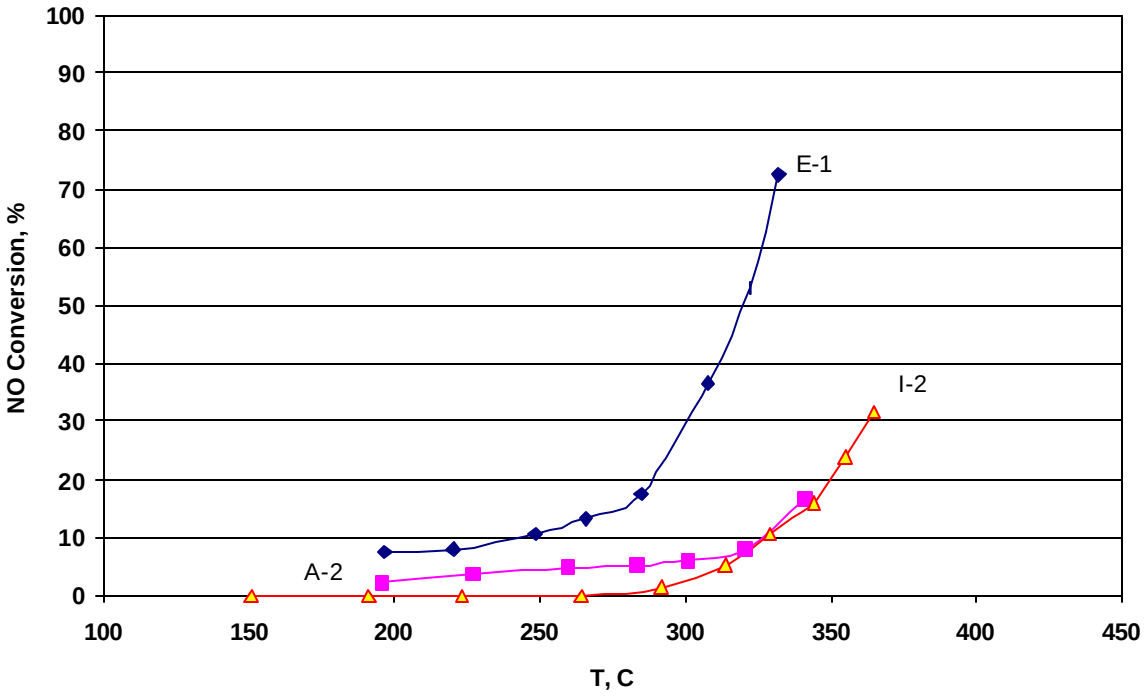

Figure 3-5. Fe Effect on Catalysts without Cu

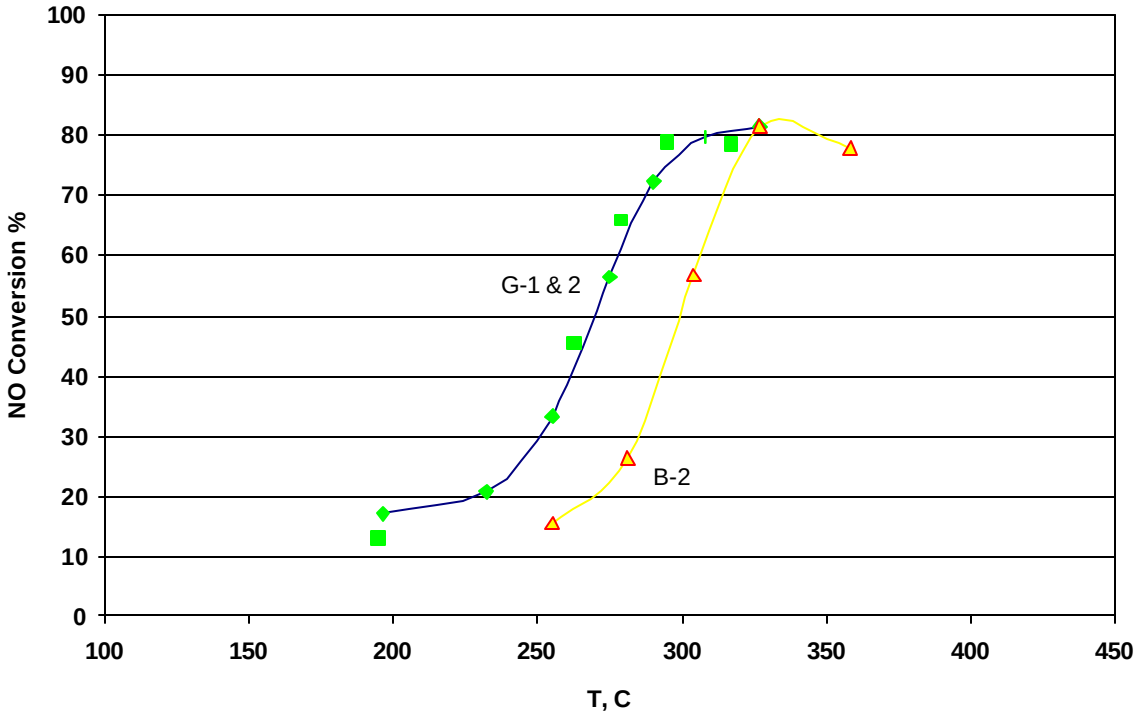

Figure 3-6. Fe Effect on Catalysts with 10% Cu

Figure 3-6 shows the test data of Type B (10%Fe/10%Cu/AC) and Type G (40%Fe/10%Cu/AC). The index temperature T_{50} was again shifted lower, from 300°C to 270°C, when Fe is increased from 10% - 40% with copper constant at 10% compared to a shift from 380°C to 320°C when 10% Fe is added to the activated carbon. The maximum NO conversion also increased as Fe increased at given Cu=10% condition. A notable CO depletion was observed for both 10%Fe/10%Cu and 40%Fe/10% Cu cases.

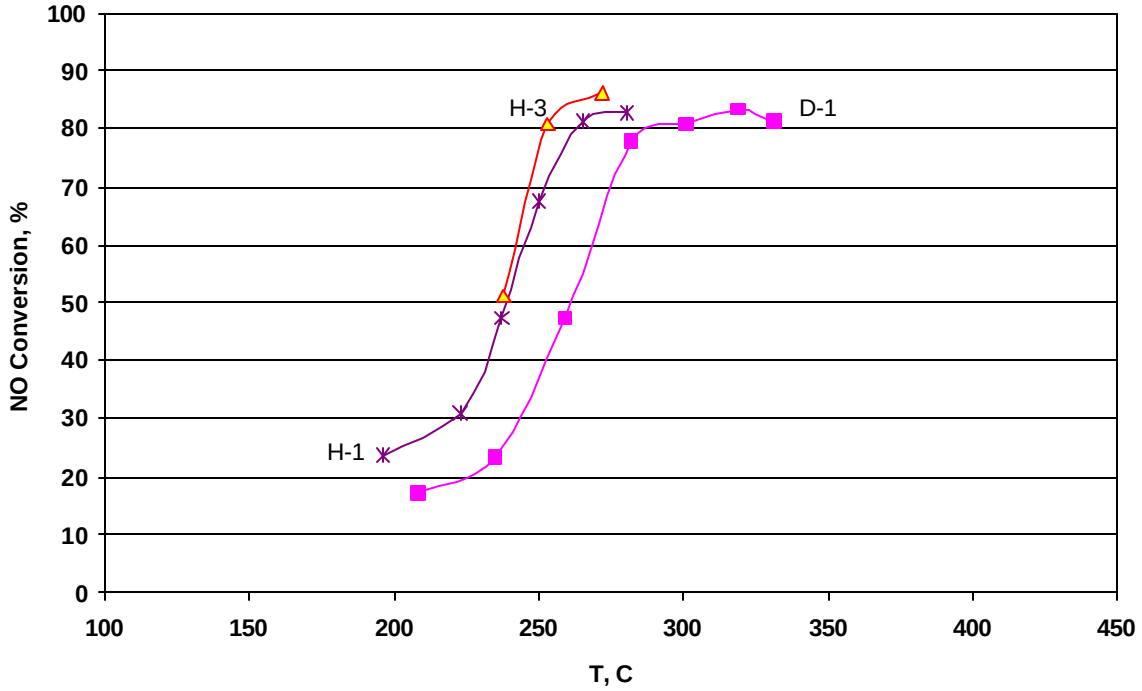

Figure 3-7. Fe Effect on Catalysts with 30% Cu

To explore the effect of Fe on catalyst performance under high Cu loading, the Cu loading was increased from 10% to 30%, a further reduction in NO was obtained. The index temperature was shifted down further to 270°C for Type H (40%Fe/30%Cu/AC) and 240°C for Type D (10%Fe/30%Cu/AC) (Figure 3-7). Again, for a given Cu loading, the increase of Fe loading enhanced catalyst reactivity, both in lowering T_{50} and in increasing the maximum NOx reduction. It is also very interesting that the CO was depleted this time at Cu=30% conditions for a wide range of temperatures. This effect on CO will be further discussed in the next section.

A high temperature excursion during test D-1 shown that the level of NO reduction hardly changed in the 308-365°C range, remaining relatively constant at above 80%. However the high temperature led to high CO generation. It apparently caused the formation of some reddish iron oxide on the catalyst, but no deactivation of the catalyst was observed.

As discussed so far in this section, the catalyst reactivity increased and T_{50} decreased as combined catalyst loading of Cu and Fe increased. However the benefit diminished as more metals were loaded. This total loading effect will be further discussed in a later section.

3.1.4 Cu Effect

Commercially, Cu has been used as catalytic agent for synthesis of CH_3OH from syngas, $CO+H_2$. Copper chloride solution has been used as chemical solvent for the CO removal from H_2 gas in ammonia plant. Cu salts supported on AC were found to be more reactive than on other supports at low temperatures.

As discussed in the previous section, the addition of Cu changes the reaction pathways. Without Cu, apparently, the CO could not react with NO even with the presence of Fe.

The loading effect of Cu on catalyst performance was further investigated. Three catalysts with different Cu loadings, (Cu=0%, Cu=10% and Cu=30%) were made for a constant Fe=40%. As expected, the test results showed that the catalyst reactivity increased as the loading of Cu increased (Figure 3-8 and Table 3-1):

Table 3-1 Impact of Cu Loading on T_{50}

Cu, Loading ,%	0	10	30
$T_{50,}$ °C	320	270	240

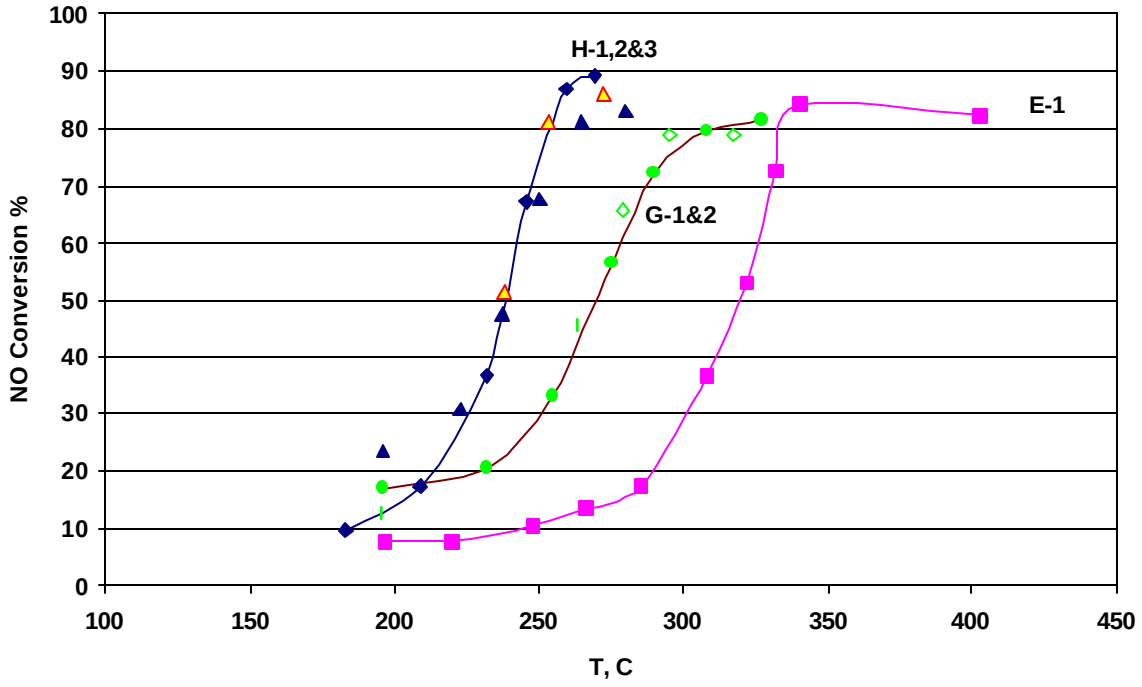

Figure 3-8. Cu Effect on Catalysts with 40% Fe

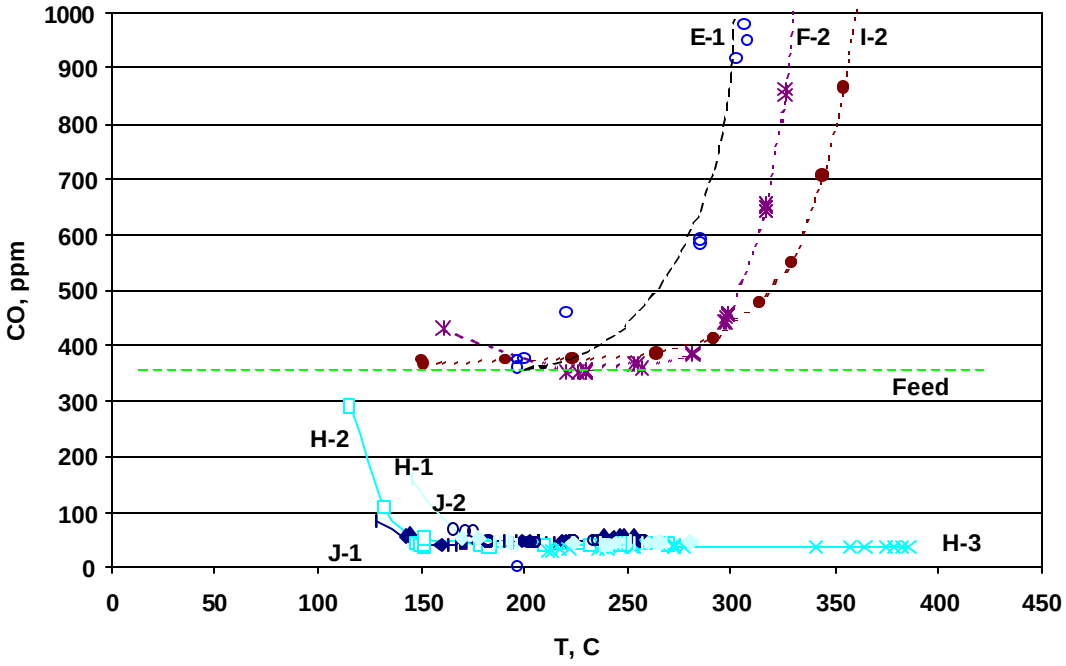

Figure 3-9. CO Concentrations for Different Catalysts

As mentioned earlier, Cu plays an important role in CO reduction. The NO reduction by CO involved a surface reaction between Cu and the adsorbed CO. As shown in Figure 3-9, for catalyst-H with a high Cu loading (30%), CO reduction was as high as 87 to 90% for the entire test temperature range up to 390°C. However, the catalysts E & F, with no Cu or very low Cu, behaved the same way as the AC only cases, with little CO depletion even at very low temperatures.

There are two competing reactions between CO generation promoted by Fe, and CO reduction promoted by Cu. This competition is affected by bed temperature. High bed temperature enhances the catalytic conversion of carbon to generate more CO and CO_2, while the high Cu loading enhances the CO depletion. The optimum composition of catalyst should address both reaction pathways. For operation at increased temperatures, the Cu loading needs to be increased. To ensure low levels of CO emissions, a low operation temperature and a relative high loading of Cu are necessary.

3.1.5 Ce Effect

In general, the literature (as reviewed by Aarna and Suuberg, 1997) shows that the Fe and Cu are the most effective catalyst components for NO reduction by carbon or by CO. Cerium had been reported to enhance catalytic redox processes. It is widely used in automobile three-way catalyst as an oxygen-transferring agent due to its redox behavior.

The test data plotted in Figure 3-10 shows that the addition of 20% Ce (catalyst-J) increased the catalyst reactivity, compared with catalyst-H. T_{50} was lowered further to 210-220°C. It was also noted that the O_2 consumption "light off" temperature was reduced by 15 to 20 °C. There were

no changes in CO depletion by adding Ce to the Fe/Cu/AC group. Because the addition of Ce increased the total loading, it shows the similar reactivity trend as catalyst loading of other metals (Fe and Cu) increased. It appears that the Ce boosted the reactivity more on the low temperature side. Appreciable NO conversion was observed at reaction temperatures below 200°C. This high loading catalyst results in a very low operation temperature, and therefore it greatly suppresses the CO generation. However, the O_2 consumption data of catalyst J appears to indicate predominately CO_2 generation at low temperatures and the lack of significant CO generation may be due to the high Cu loading, and possibly the Ce application.

No special characteristics were found at this time from Ce addition except that it enhances the catalyst reactivity in a similar way as Cu and Fe. The literature has reported that the addition of Ce improved the selectivity to N_2 during NO reduction. However, the present test data showed that a very good selectivity to N_2 was achieved even without Ce. Therefore, Ce does not bring distinct benefits to the catalysts tested so far, especially considering its price is higher than Cu and Fe.

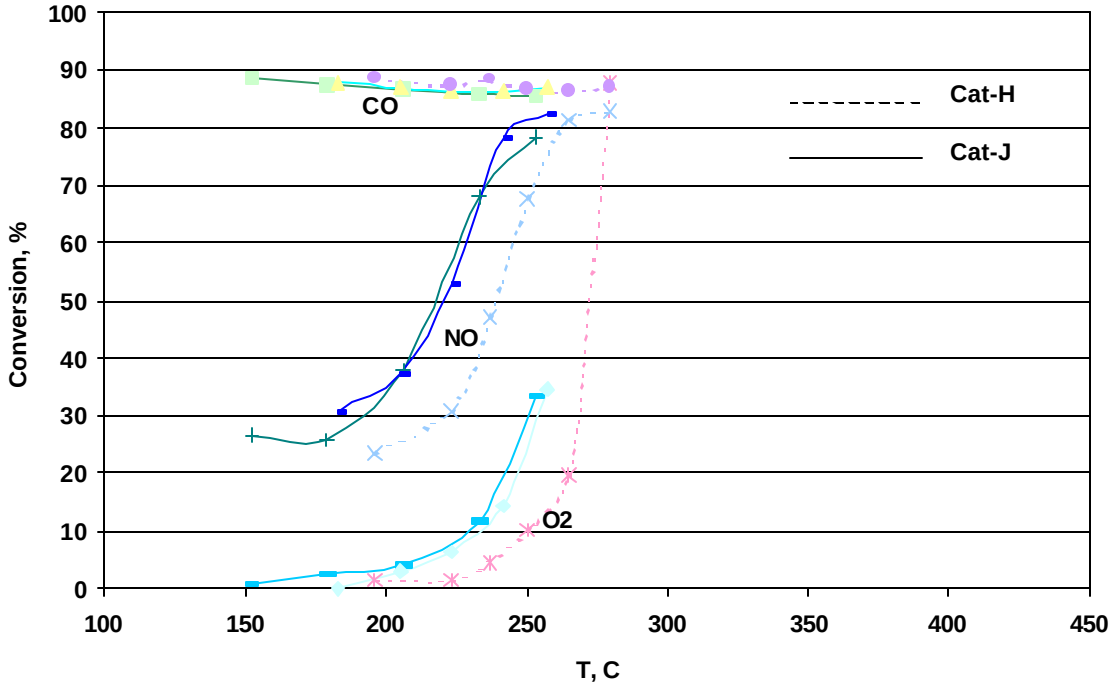

Figure 3-10. Effect of Ce on Catalyst Performance

3.1.6 Loading Effect

As discussed earlier, the catalyst reactivity increased as its total loading of metals increased. A new parameter of total loading, i.e. Fe+Cu+Ce, has been used to analyze its effects on the catalyst reactivity. In general, the test result showed that the catalyst reactivity increased as the total loading increased even as contributions from Cu, Fe and Ce were different (Figure 3-11). In general the maximum NOx conversion increased as total loading increased, except for the case

with Ce addition (J-1). Although J-1 exhibited a lower T_{50} and had an initial reduction of close to 30% at low temperatures, it did not have high maximum NO reduction.

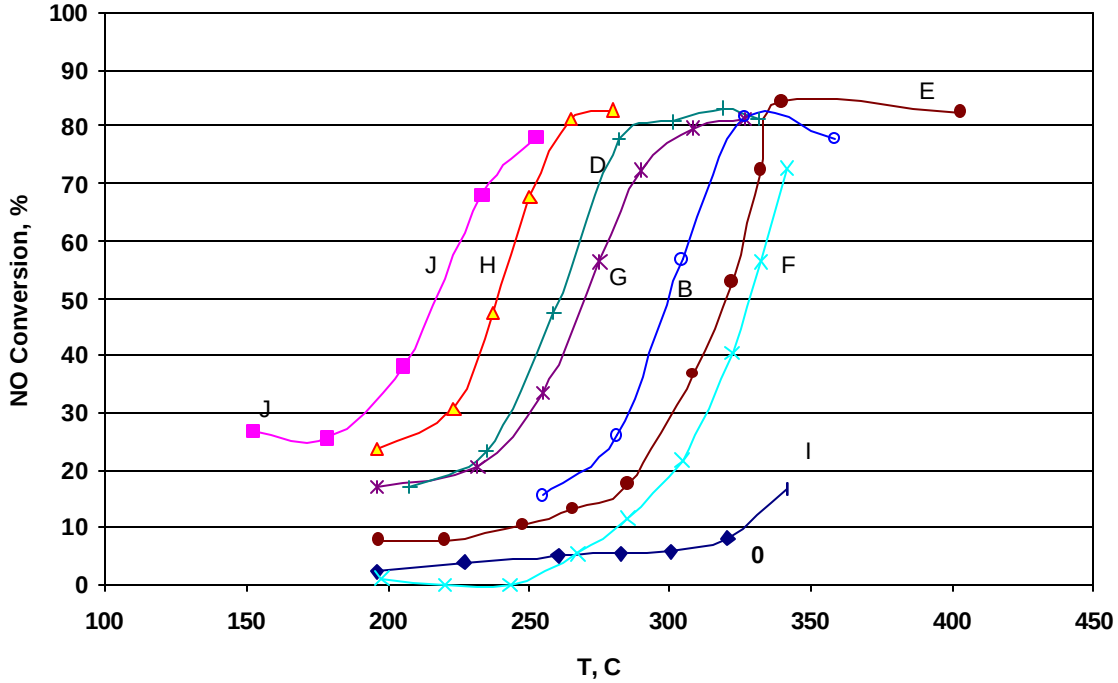

Figure 3-11. NO Conversion Performance for Various Catalysts

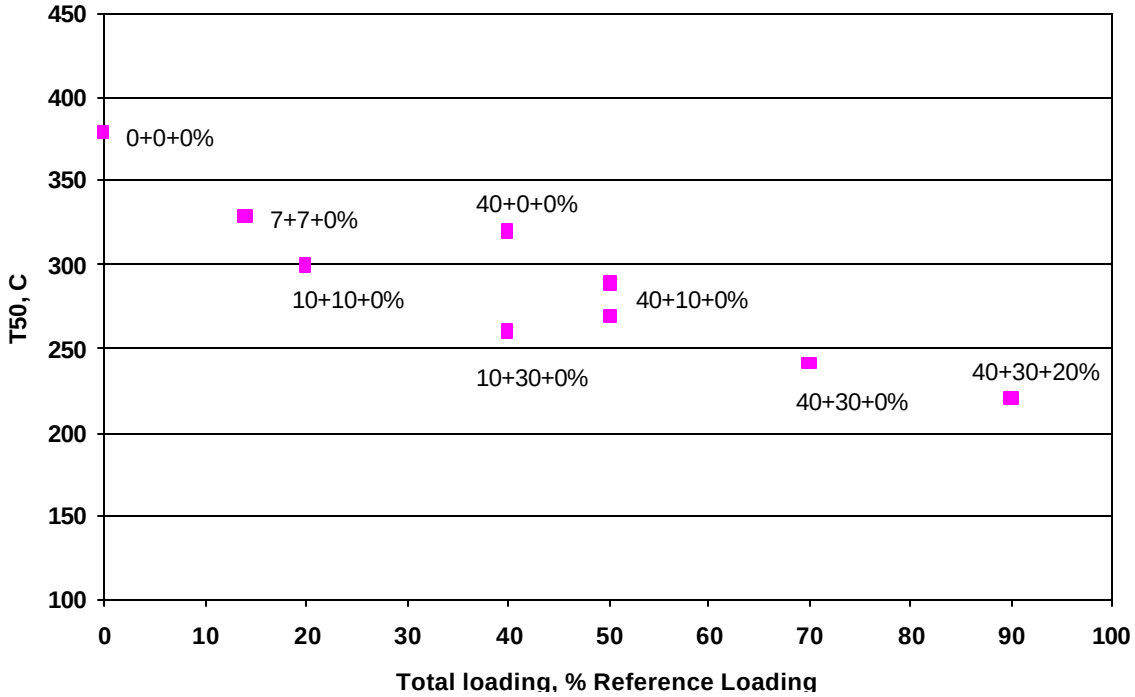

Figure 3-12. Effect of Total Loading on Reactivity Index T50

It should be pointed out that the contribution or effectiveness of different metal component is different. Some catalysts had better performance than others with the same or even higher total loadings. As shown in Figure 3-12, catalyst-B with lower total loading (10% Fe and 10% Cu) was more active than the catalyst-E with higher total loading (Fe+Cu=40%+0%). The same is true for the comparison between catalyst-D (Fe+Cu=10%+30%) and catalyst-G (Fe+Cu=40% +10%). It shows again that Cu plays an important role in NO reduction by CO by altering the reaction pathways as discussed earlier.

3.1.7 N_2O Generation

N_2O emissions were measured for the tests performed in May and June, including catalysts E, F, G, H, I, and J. As plotted in Figure 3-13, overall the NO to N_2O conversion was small, with the highest measured N_2O conversion at only 12 %. The reference AC (I) did not generate any N_2O through the entire temperature range. Other catalysts with metal loading converted some NO to N_2O, and the conversion increased with increasing catalyst bed temperature. Another trend seen from the data in Figure 3-13 is that the catalysts with higher total metal loading tend to generate more N_2O and at lower temperatures.

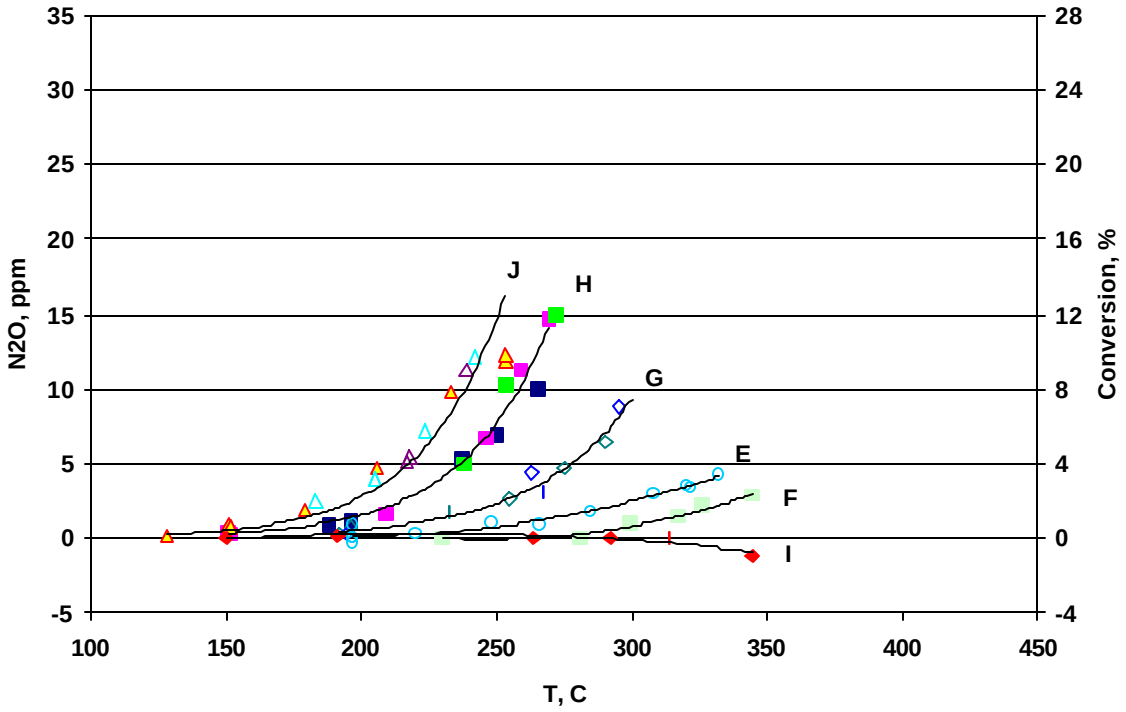

Figure 3-13. NO to N_2O conversion

3.1.8 O_2 Consumption and CO

The catalyst with the lowest metal loading (Type F, 7% Fe / 7% Cu) was selected to investigate the effect of initial small loading on activated carbon. For this low loading catalyst, the

maximum NOx reduction occurred at about 350°C. Similar to the reference AC only tests, as temperature exceeded 270°C, the NOx-carbon reaction started as a result of the support AC burning. The familiar "light off" was seen for this low loading catalyst, as with the reference AC only case (Figure 3-9). Shown in Figure 3-14, O_2 concentration and CO generation were in sync. However, since the initial O_2 concentration and its consumption were orders of magnitude higher than the initial CO concentration in the feed stream, clearly most of O_2 was consumed by combustion of carbon to generate predominantly CO_2, as well as some CO.

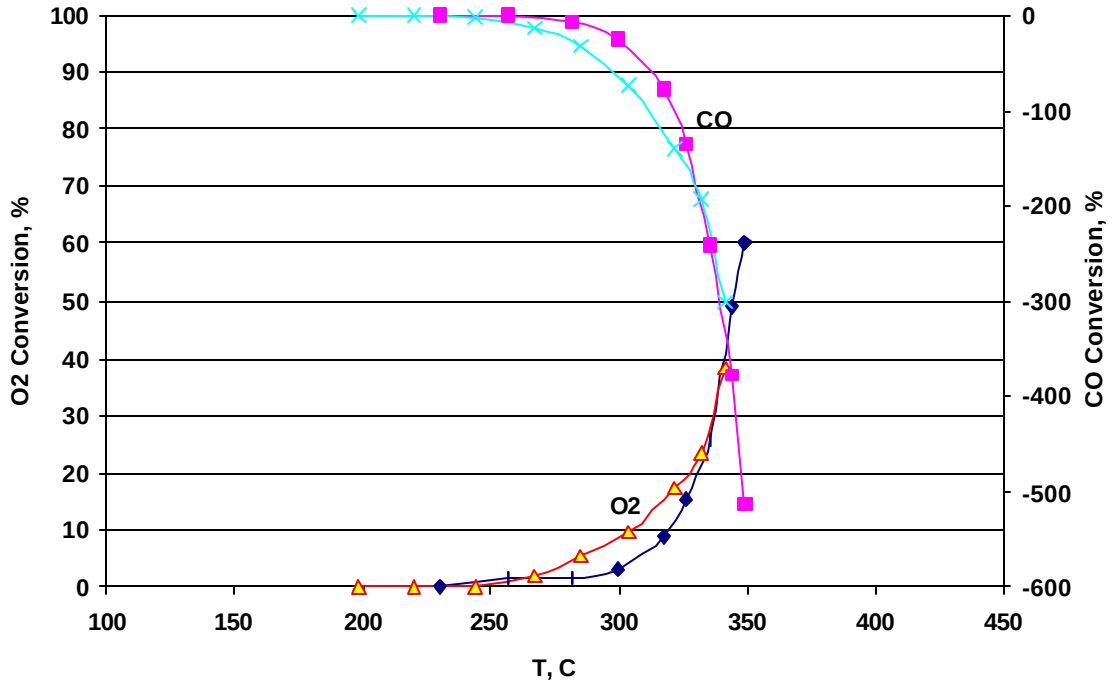

Figure 3-14. CO and O2 Conversions for Catalyst F

There are clearly two categories of the relationships between conversions of CO and O_2. For reference AC only and low Cu catalysts, CO generation was proportional to the amount of the O_2 consumed (Figure 3-15). For the high Cu catalysts (catalysts G, H, and J), the CO conversion stayed at 80-90% of the feed concentration for a wide of operation temperature range from 150 to 380°C, regardless of O_2 consumption by carbon, which means with these catalysts, the carbon reaction was nearly complete to produce predominantly CO_2. In Figure 3-16, one can see that the carbon combustion (as indicated by O_2 consumption) was promoted by the total metal loading. However, for the high loading catalysts with sufficient Cu, even with significant carbon burning, the CO level still remained very low.

In summary, the catalysts with sufficient Cu loading reduced CO efficiently in a very wide temperature range. This is a very important feature since some carbon burning is expected when AC support is used.

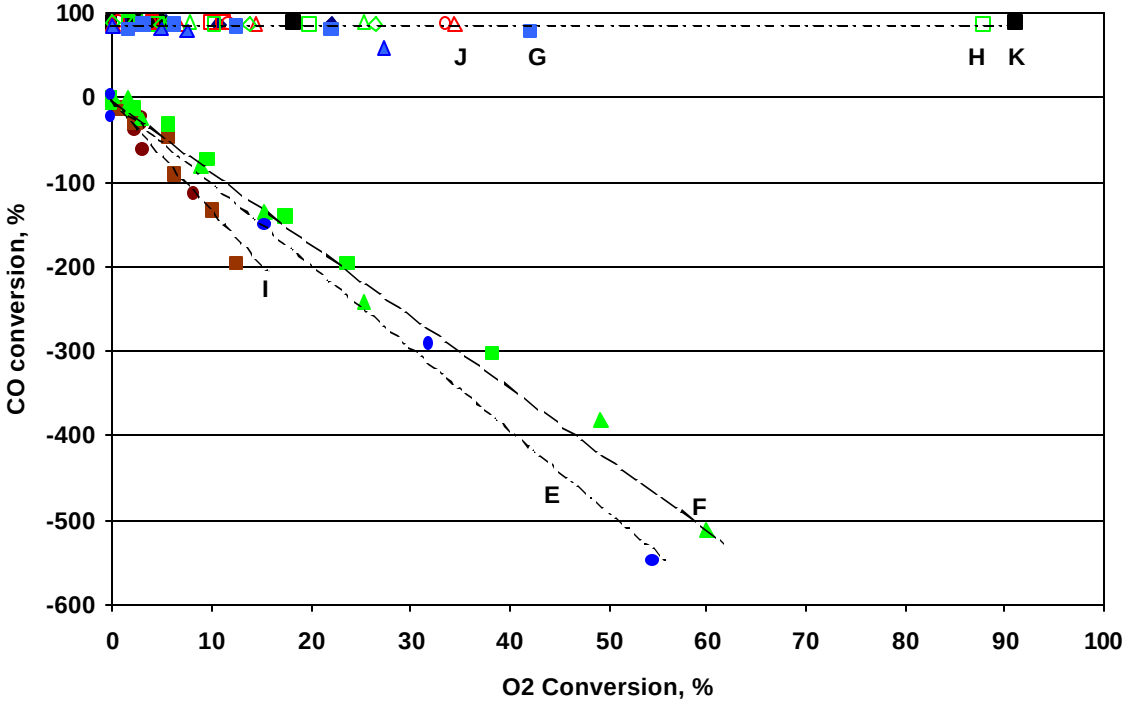

Figure 3-15. Relationship between CO and O_2 Conversions

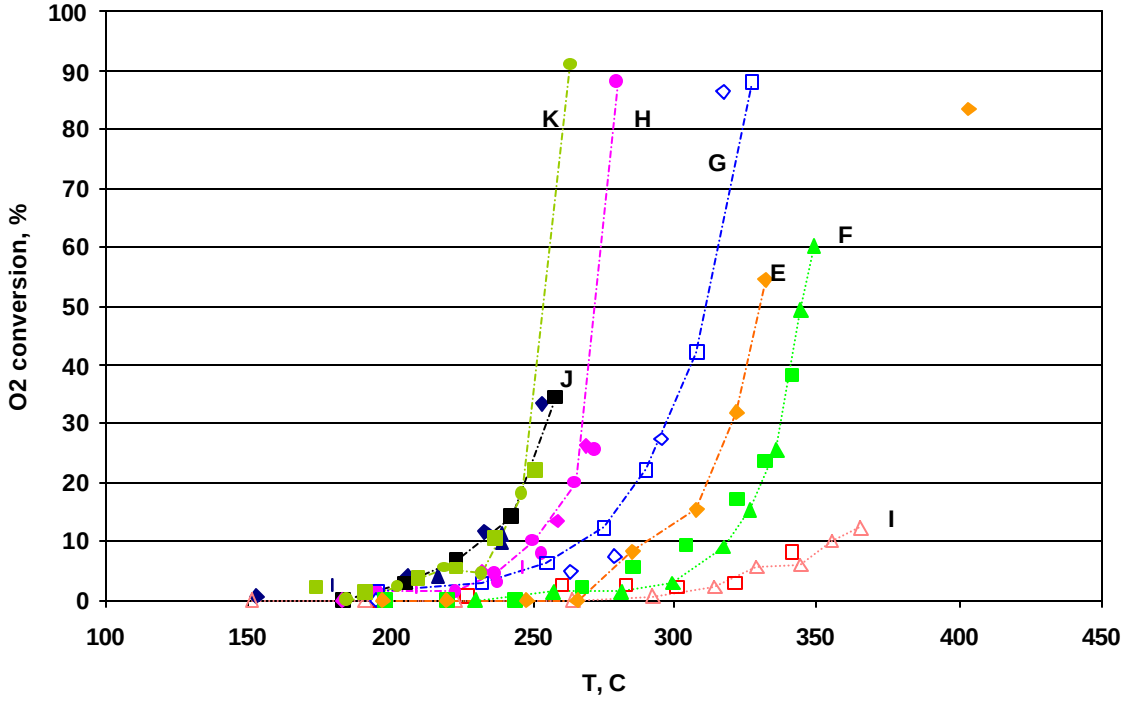

Figure 3-16. Effect of Catalyst Type on O2 Conversion

3.1.9 Catalyst Stability

Some of the catalysts were tested for longer durations under constant conditions to check their stability.

As shown in Figure 3-17, the stability of the catalyst D was demonstrated by operating at 275°C under steady state conditions for nearly 12 hours. The system was well operated and maintained at a steady state condition with approximately 86% NO reduction. No significant reactivity decay was seen during the test.

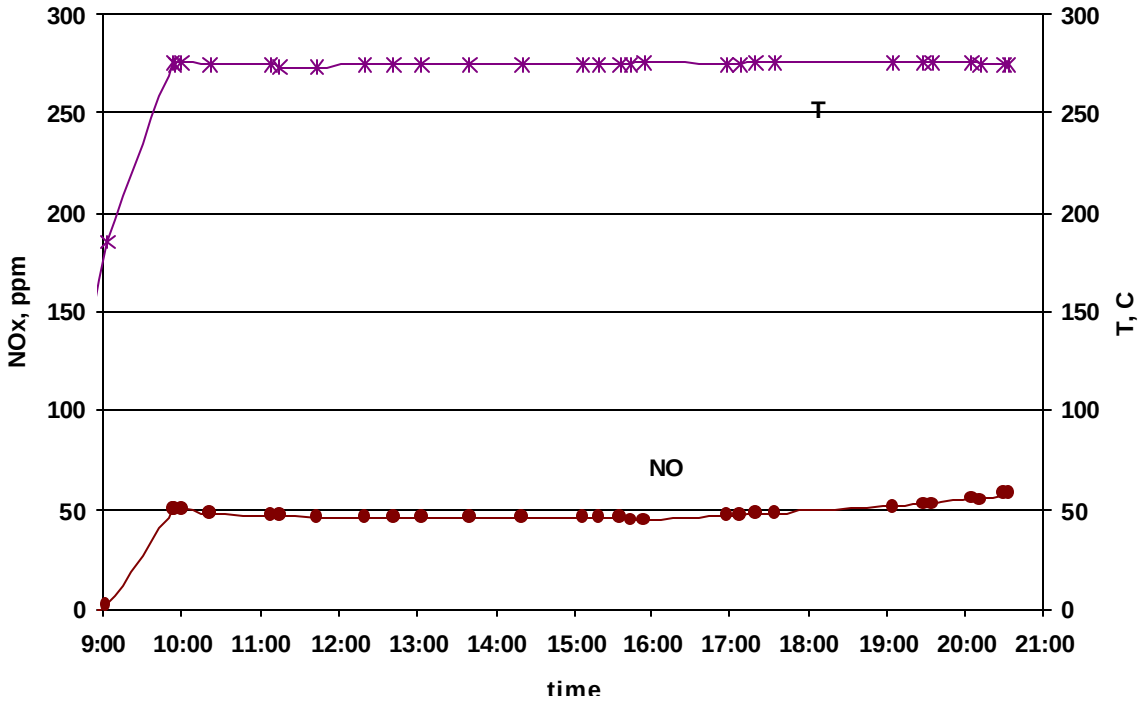

Figure 3-17. Long Duration Test at Constant Conditions

3.1.10 Effects of Moisture and SO_2

Effects of Moisture and SO_2 Over the Fe/Cu/AC and Fe/Cu/Ce/AC Catalysts: Selected catalysts with high reactivity were tested to study the effects of moisture injection and simultaneous addition of moisture and SO_2 on the activity and selectivity. It was shown in the previous discussions that both Catalyst H and Catalyst J (see Table 2-1) were active catalysts for NO reduction in the presence of dry simulated flue gas.

To study possible inhibition/poisoning effects of moisture and SO_2 over these two catalysts, the additives were injected into the reactant gas stream after establishing the steady-state activity in the dry, SO_2-free gas mixture. Upon addition of 8% moisture to the gas stream, the concentrations of the other components decreased accordingly to the following:

NO	CO	O_2	H_2O	CO_2	N_2
240 ppm	480 ppm	2.8 %	8.0%	12.9%	76.3%,

and the overall GHSV was 1140 hr^{-1}. The usual observation upon injection of moisture was initially (1) desorption of a quantity of NO, (2) desorption of a smaller quantity of CO, and (3) enhanced consumption of O_2. This was typically followed by a return to the approximately the same levels as the original NO and CO conversions and a much slower decrease in the O_2 consumption with time on-stream. An example for Catalyst M (duplicate of H) test is shown in Figure 3-18.

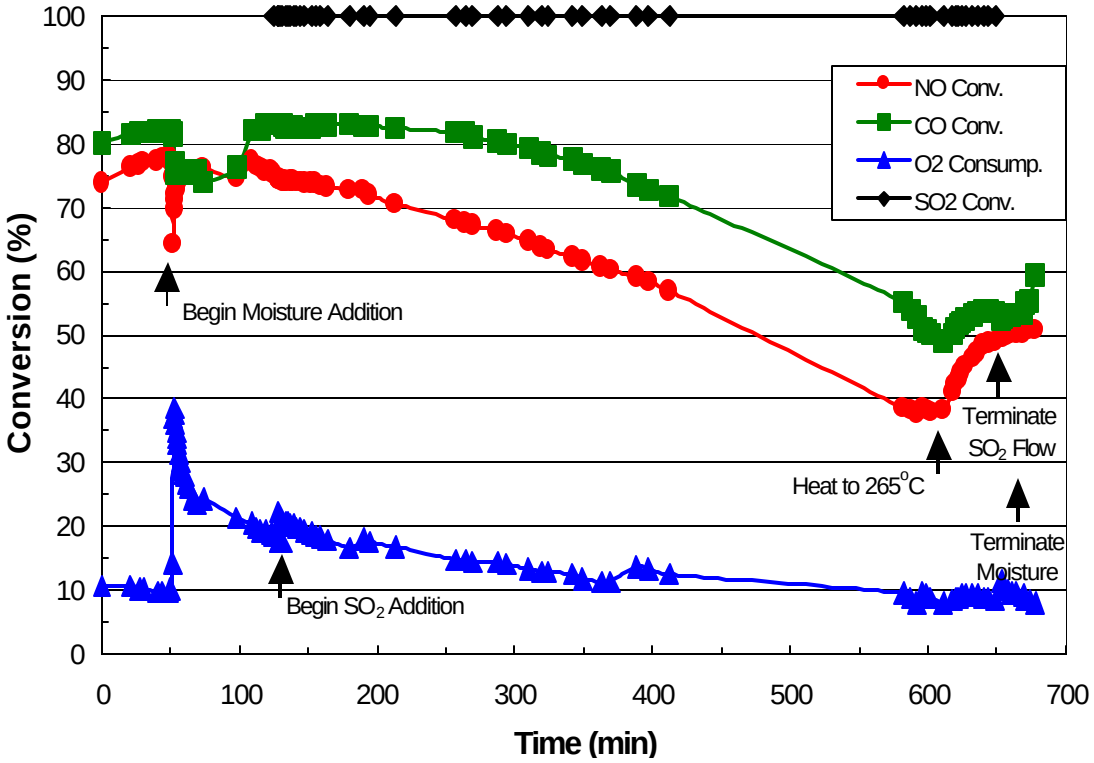

Figure 3-18. NO, CO, O_2, and SO_2 Conversion Over the 40% Fe/30% Cu/AC Catalyst at Approximate 257°C (M-3)

Also shown in Figure 3-18 is the effect upon subsequent addition of 200 ppm SO_2 to the reactant gas stream, where the flow rate of the SO_2/N_2 was compensated by proportionately decreasing the flow rate of the N_2 stream. It is evident from Figure 3-18 that the presence of SO_2 over the catalyst led to a gradual decrease both the NO and CO conversions. At the same time, there was little effect on the O_2 consumption other than an initial discontinuity. About 7.5 hr after addition of the SO_2 to the gas stream, it appeared that the NO and O_2 conversion levels had reached steady-states, while the CO conversion rate was still declining. Increasing the reaction temperature 8°C led to a significant enhancement in the NO reduction level, a smaller improvement in the CO conversion, and no significant effect on the O_2 consumption. During the addition of SO_2 to the gas stream, all of the SO_2 was removed from the reactants.

Similar testing with Catalyst J containing Ce was carried out. After reaching steady-state at 239°C, the injection of moisture was begun. As shown in Figure 3-19, initial exposure of the 40% Fe/30% Cu/20% Ce/AC catalyst to H_2O vapor led to transient desorption of quantities of NO and CO, as well as to enhanced consumption of O_2. Addition of SO_2 to the gas stream led to gradual decline in the observed NO reduction activity, but with this catalyst there was no accompanying decline in the CO removal rate observed with time on-stream. Indeed, the catalyst temperature decreased a few degrees and about 98% CO conversion was maintained. Upon termination of the injection of both moisture and SO_2, the NO removal rate stabilized at about 50%.

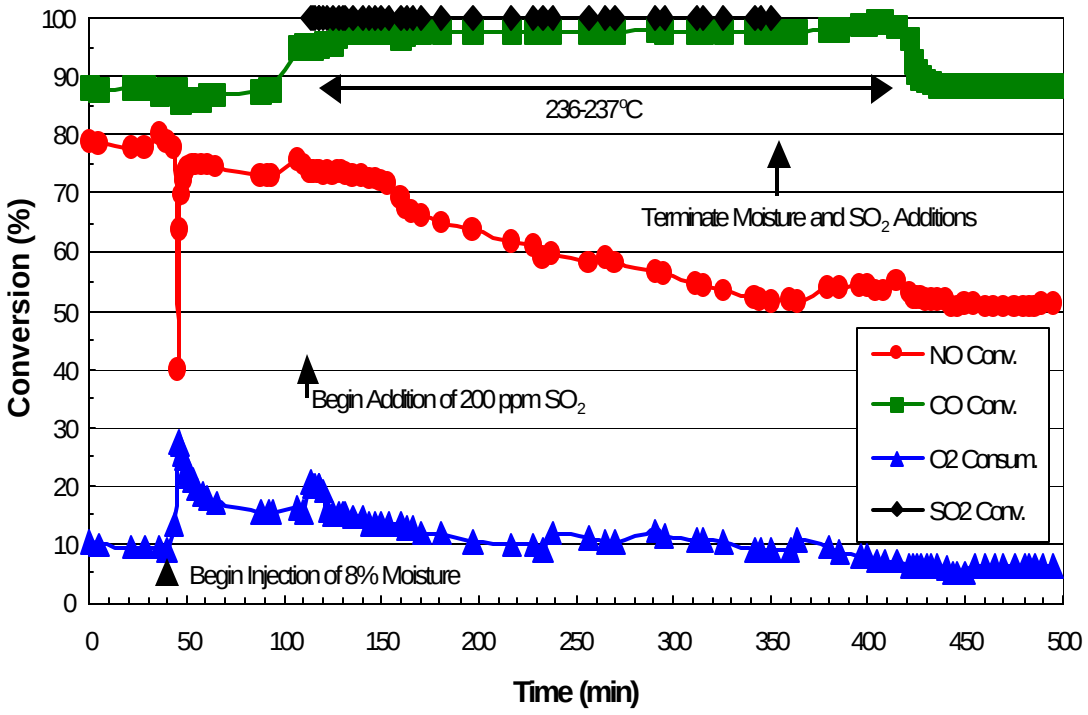

Figure 3-19. Conversions of NO, CO, O_2, and SO_2 Over the 40% Fe/30% Cu/20% Ce/AC Catalyst at 239oC

While moisture and SO_2 were being fed into the gas stream, the consumption of O_2 gradually declined and stabilized at 10% O_2 removal from the reactant gas. Removal of both moisture and SO_2 from the inlet gas resulted in a further lowering of the O_2 consumption to a steady-state level of about 6%. Once again, all of the SO_2 in the inlet gas stream was converted upon passing over the catalyst.

After purging the catalyst with N_2 as it cooled and at ambient temperature overnight, the catalyst was retested under dry conditions. The observed conversions and N_2O selectivity are shown in Table 3-2 as Day 5 Test results. Between the entries for the Day 5 tests, the catalyst had been tested at higher temperatures, including at 254°C where the NO, CO, and O_2 conversions were

83%, 87%, and 13%, respectively. Therefore, high conversions were attained after the Day 4 testing with moisture and SO_2 and after purging with N_2 overnight.

Table 3-2. Conversions and N_2O Selectivity over the 40% Fe/30% Cu/20% Ce/AC Catalyst J at 239 ± 1°C.

Test	%NO Conv.	%N_2O Sel.	%CO Conv.	%O_2 Conv.	%SO_2 Conv.
Day 3 Test - Dry	82	6.2	89	9.8	---
Day 3 Test - with 8% Moisture After 2 hr	74	1.7	89	14.4	---
Day 4 Test - Dry	79	3.9	88	9.7	---
Day 4 Test - with 8% Moisture After 1 hr	71	1.6	88	15.4	---
Day 4 Test - with 8% Moisture + 200 ppm SO_2 After 4 hr*	51	3.7	98	9.2	100
Day 4 Test - 2.25 hr After Terminating Moisture and SO_2	51	1.6	88	6.5	---
Day 5 Test - Dry: After 4 hr	64	5.1	88	2.3	---
Day 5 Test - Dry: After Higher Temp. Treatment and then 2 hr at 240°C	59	5.6	89	1.4	---

*Temperature had decreased to 236°C.

Activity of the Cu-Free 40% Fe/AC Catalyst in the Presence of Moisture and SO_2: As shown in the previous sections, the temperature index T_{50} for NO reduction observed for the Fe/Cu/AC catalysts is strongly dependent on the presence or absence of Cu and its content in the catalysts. For example, for Cu loadings of 0, 10, and 30% in a 40% Fe/AC catalyst, T_{50} declines from 320°C to 270°C to 240°C, respectively. It was shown for the 40% Fe/30% Cu/AC catalyst (Figure 3-18) that injection of moisture into the inlet gas mixture produced only transient decline in NO and CO conversions, while addition of 200 ppm SO_2 to the reactant produced a gradual decline in both conversions.

The catalytic behavior of a fresh portion of the Cu-free 40% Fe/AC catalyst (Catalyst L, duplicate of E) was utilized to probe the effect of moisture and SO_2 on this single component supported catalyst. The activity of this catalyst was first determined in the dry reactant gas mixture, and it was verified that the temperature "light-off" curve was reproducible and that T_{50} was also reproduced. Upon testing for Days 2 and 3, the NO conversion at about 320°C tended to reach higher level relative to that observed for Day 1.

Upon injection of moisture, the NO conversion immediately increased, as shown in Figure 3-20. This contrasts with the behavior of the 40% Fe/30% Cu/AC catalyst (Figure 3-18), where the measured NO conversion decreased, apparently due to transient desorption of NO from the catalyst. At the same time that the NO conversion increased over the Cu-free catalyst, the consumption of O_2 dramatically increased. As shown in Figure 3-20, the conversions were maintained at high levels until the addition of SO_2 was initiated. As the SO_2 began passing over the catalyst, the conversion of O_2 sharply dropped, approaching the consumption level observed with the dry reactant gas mixture. At the same time, the NO conversion level more gradually declined to approximately half of the activity shown in the wet reactant gas mixture.

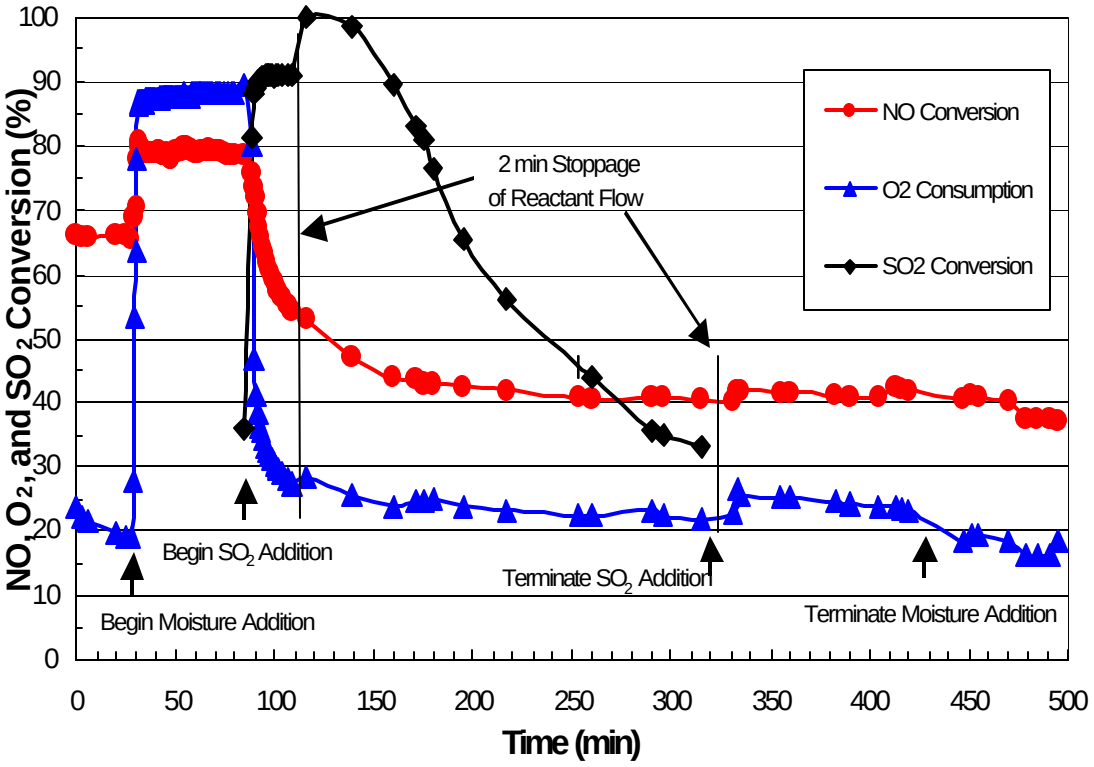

Figure 3-20. NO, O_2, and SO_2 Conversion Over the Cu-free 40% Fe/AC Catalyst in the Presence of Moisture and SO_2 at 321°C

For both NO and O_2, the conversion levels reached steady-state values, with the catalyst not exhibiting further deactivation. Termination of SO_2 injection did little to change the observed removal rates of NO and O_2, but termination of the moisture addition tended to decrease the conversion levels of both of these reactants.

It is interesting that addition of SO_2 to the reactant mixture did not lead to complete conversion of this "poison" until after the gas flow was interrupted for about 2 min to measure and verify the inlet gas composition. This momentary stoppage of the gas flow apparently altered the catalyst in some way so that conversion of the SO_2 was promoted. However, the conversion of SO_2

gradually declined with time. This behavior was not observed with the copper-containing catalysts such as the 40% Fe/30% Cu/AC catalyst.

It is noted that in all of the tests with this Cu-free catalyst, relatively large amounts of CO were generated, corresponding to the significant conversion of O_2. This is apparently due to partial oxidation of the carbon support by the O_2 in the presence of the Fe catalyst component at the high reaction temperatures required by the absence of Cu in the catalyst. The O_2 consumption was much higher than the stoichiometric amount required for CO generation, indicating the dominant combustion product was CO_2. This again verifies that Fe is a good catalyst for carbon gasification and combustion, but it does not have a sufficient catalytic function for the CO oxidation reaction.

3.1.11 Effect of Potassium

Ce and K had been reported to enhance catalytic redox processes. Cerium is widely used in automobile three-way catalysts as an oxygen transferring agent due to its redox behavior. We have shown here (Figure 3-19) that Ce also maintains the CO oxidation reaction to deplete CO in the presence of SO_2. Potassium is a basic component that can function as a combustion catalyst. A 40% Fe/30% Cu/20% K/AC catalyst was prepared using KNO_3 as the impregnation reagent.

This K-doped catalyst (Catalyst K) exhibited a high catalytic activity for NO reduction and CO oxidation at low reaction temperature, similar to the Fe/Cu/Ce/AC catalyst. Steady-state conversions seemed to take longer to achieve, but the initial NO conversion upon start-up in the 170-205°C temperature range was >30%. The index temperature T_{50} observed upon multiple-day testing was in the 205-220°C range. At the same time, the CO and O_2 conversions were 88-91% and 2-5%, respectively. Little N_2O was formed, and the selectivity to N_2 tended to stabilize at about 98% with time-on-stream.

An experiment in which moisture was added to the reactant gas stream at 235°C is shown in Figure 3-21. The behavior of this K-containing catalyst very much resembles that of the K-free 40% Fe/30% Cu/AC catalysts, e.g. see Figure 3-18. As usual, there was a small exotherm as the initial moisture passed over the catalyst. In addition there was a large desorption of NO, a smaller desorption or lower conversion of CO, and a promotion of O_2 consumption. The NO reduction reaction recovered and the NO conversion in the presence of moisture was higher than the initial conversion under dry conditions. Interruption of the gas flow through the reactor for about 2 min led to subsequent improvement of the NO and CO conversion levels but had no effect of the O_2 consumption. Termination of the moisture addition led to slight decreases in the NO and CO removal rates and a somewhat larger decrease in O_2 consumption. However, the NO reduction level remained higher than the initial activity observed upon start-up under dry conditions.

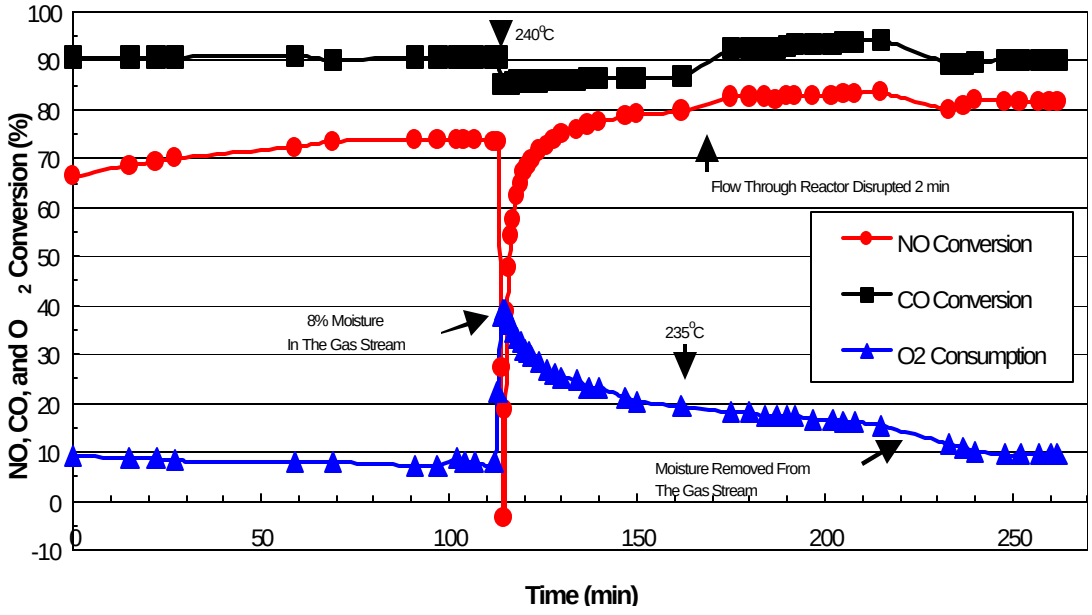

Figure 3-21. NO, CO, and O_2 Conversions Over the 40% Fe/30% Cu/20% K/AC Catalyst Before, During, and After Moisture Injection at 235ºC

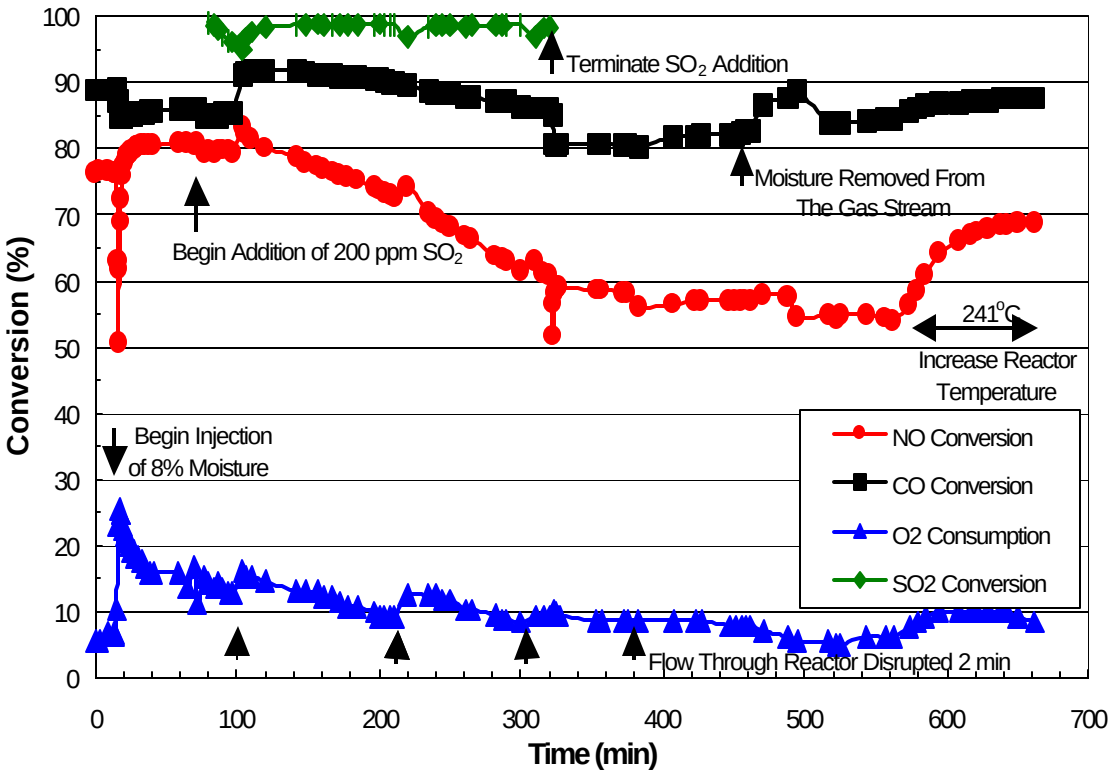

Figure 3-22. Conversions of NO, CO, O_2, and SO_2 Over the 40% Fe/30% Cu/20% K/AC Catalyst at 232ºC

During a subsequent day of testing at about 232°C, moisture was again injected, followed by the addition of SO_2. The observations for this test are shown in Figure 3-22. The effects of moisture in the gas stream were the same as observed in Figure 3-21. Upon addition of SO_2, very little change in the conversions was initially observed. At the same time, most (but not all) of the SO_2 was converted. A discontinuity in the conversion curves was caused by interruption of the gas flow through the reactor, which led to transient higher conversions of all reactants. With continued time-on-stream, the NO conversion gradually declined, while CO conversion and O_2 consumption showed smaller decreases. Upon termination of the SO_2 addition, the conversions of all reactants stabilized, with CO conversion tending to increase slightly. Removal of moisture from the gas stream led to slightly lower conversions of NO and O_2, while the CO conversion continued to increase with time. Increasing the catalyst temperature to 241°C caused a significant increase in the NO conversion from 54% to 69% and smaller increases in the CO and O_2 conversions.

3.1.12 Additional Discussions

The incorporation of Ce (Catalyst J) and K (Catalyst K) into the 40% Fe/30% Cu/AC catalyst (Catalyst H) increased the activity of the catalyst by shifting the NO "light-off" curves to lower temperature (lower T_{50}), as shown in Figure 3-23. At the same time, there was little change in the CO conversion and O_2 consumption under these dry conditions.

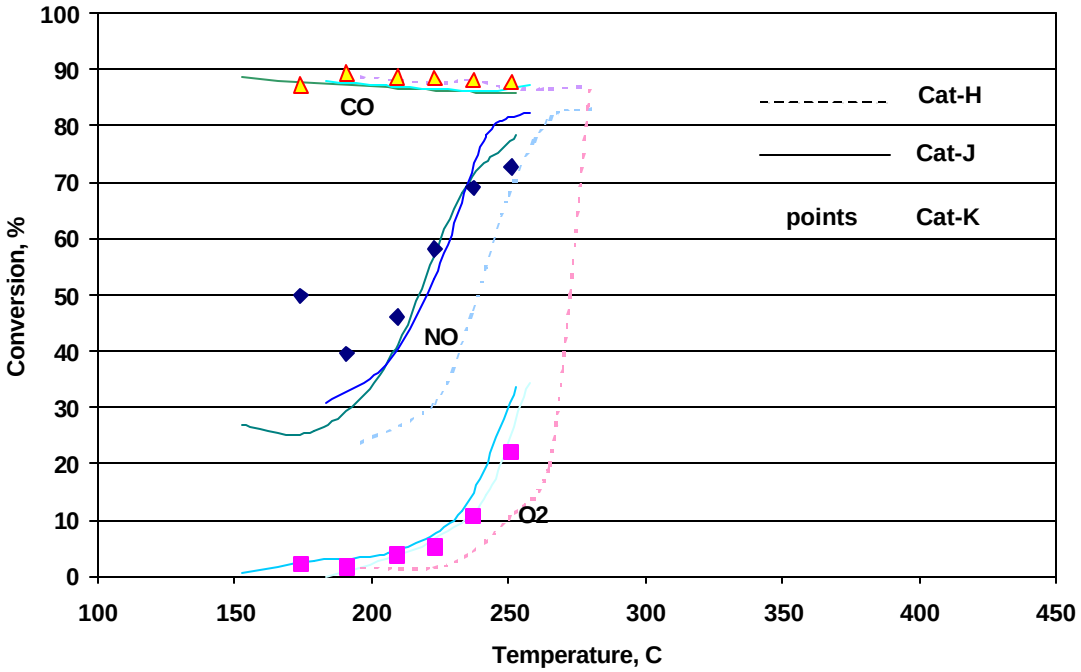

Figure 3-23. Comparisons of K- and Ce-Containing Catalysts

Compared with other catalysts, catalysts H, J, and K (all containing 40%Fe/30%Cu/AC) exhibit high NO reduction activity with only low levels of O_2 consumption, as shown in Figure 3-24. In this figure, Catalyst G contained a reduced level of 10% Cu, while Catalyst I was the unpromoted aqueous-treated AC. Catalyst F contained lower quantities of both Fe and Cu. The data shown for Catalysts E and L (E) are the two tests of the Cu-free 40% Fe/AC, and it is clear that without the presence of Cu in the catalyst, the iron oxide component promotes the consumption of O_2 by greatly enhancing the catalytic combustion of the carbon support.

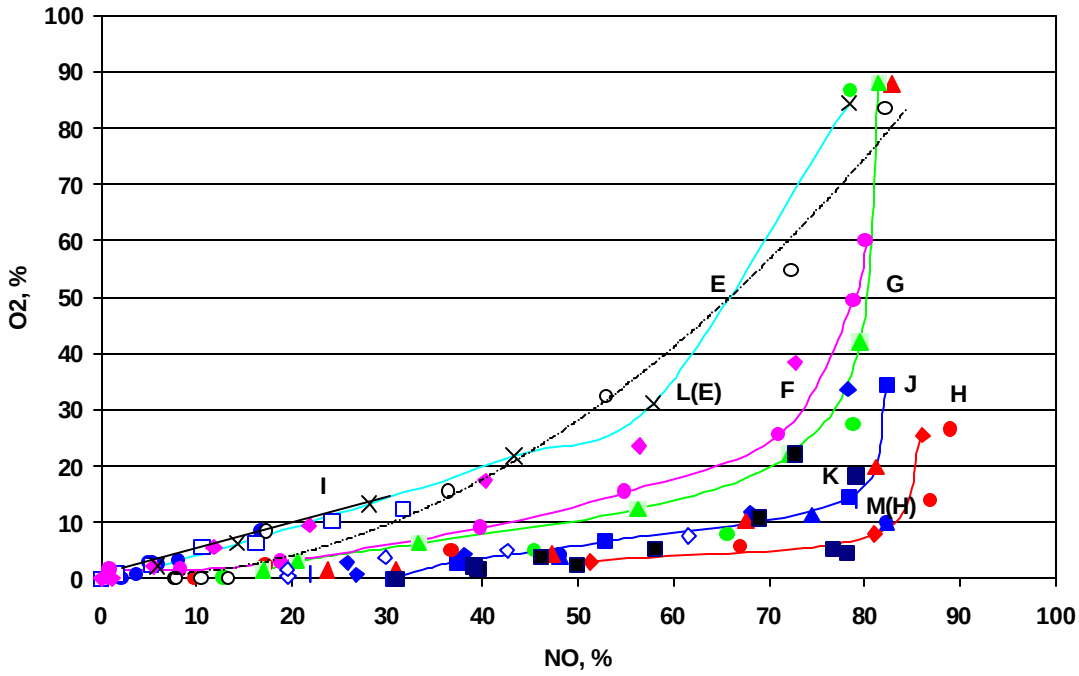

Figure 3-24. Conversion of O_2 vs NO under Dry Conditions

Comparisons of the same catalysts in terms of CO Conversion/Generation *vs* NO Conversion are shown in Figure 3-25. The catalysts that contained high levels of Cu all exhibited high conversions of CO to CO_2. It is noted that Catalysts H, J, and K contained 30% Cu in addition to the 40% Fe, while Catalyst G contained 10% Cu. Catalysts E and L are the Cu-free catalyst tests, where large quantities of CO were generated and the quantity increased as the reaction temperature was increased. This behavior is clearly shown in Figure 3-26.

As noted earlier in the report, the inhibition of the NO reduction reaction over Catalysts J, K and M (all containing 40%Fe and 30% Cu) with SO_2 in the inlet gas stream was more gradual than catalysts without copper (e.g. Catalyst L or E). This is more clearly shown by replotting the NO conversion data in terms of ppm NO remaining in the outlet stream, as in Figure 3-27. This figure also shows that the deactivation rates due to SO_2 for the catalysts J, K and M were similar. In all cases, the NO reduction activity stabilized upon removal of SO_2 from the simulated flue gas stream.

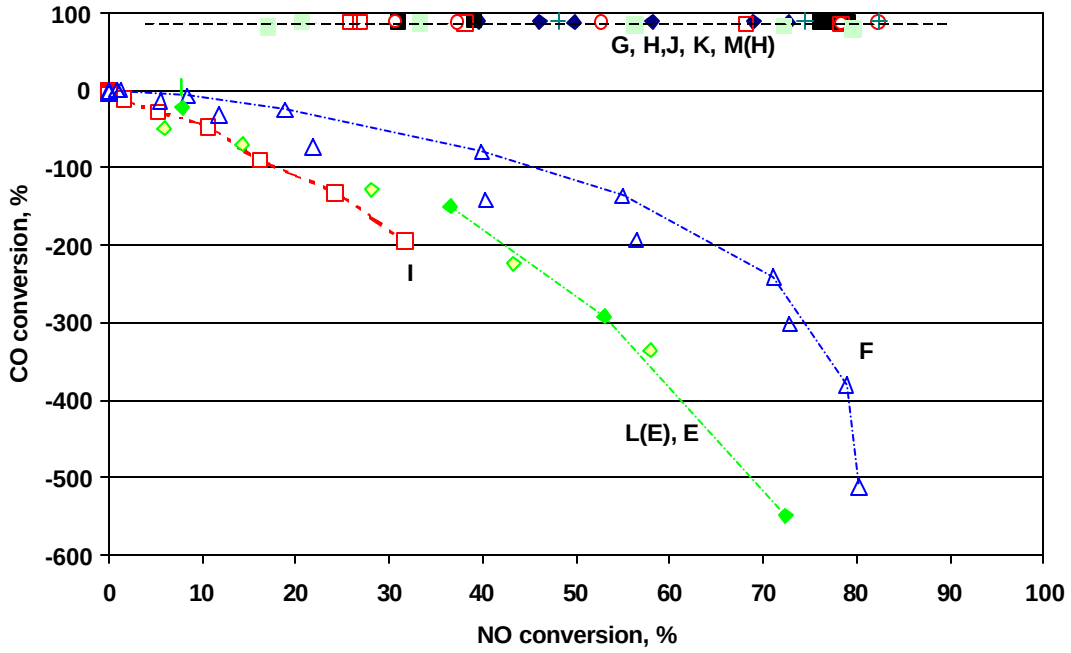

Figure 3-25. Comparisons of CO vs NO Conversions

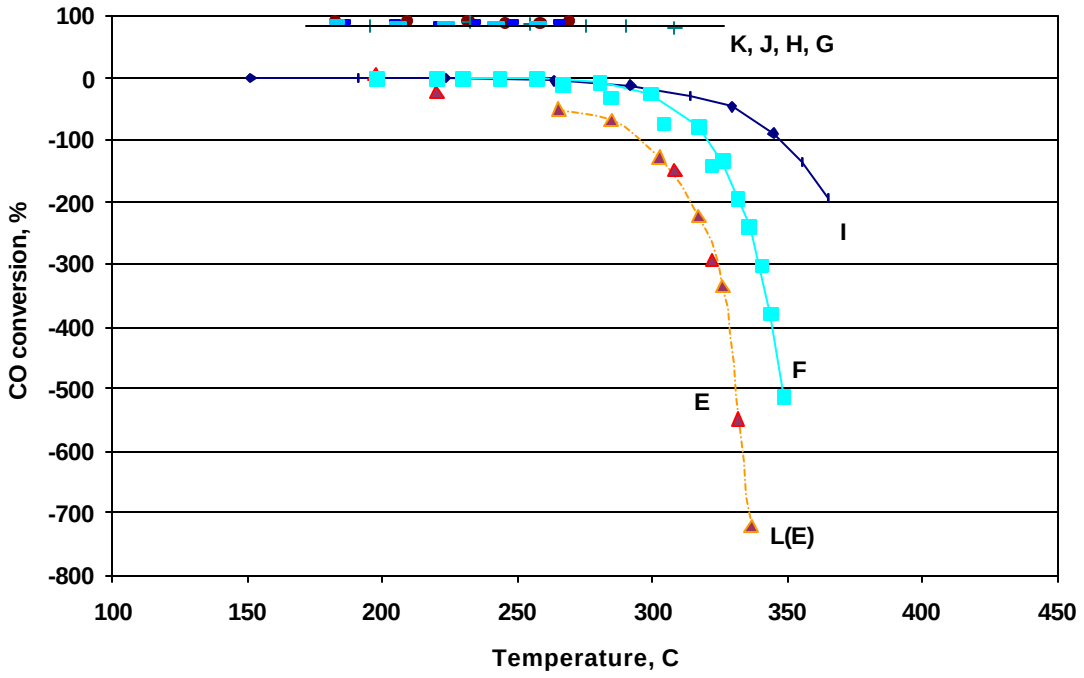

Figure 3-26. Conversion / Generation of CO vs Temperature

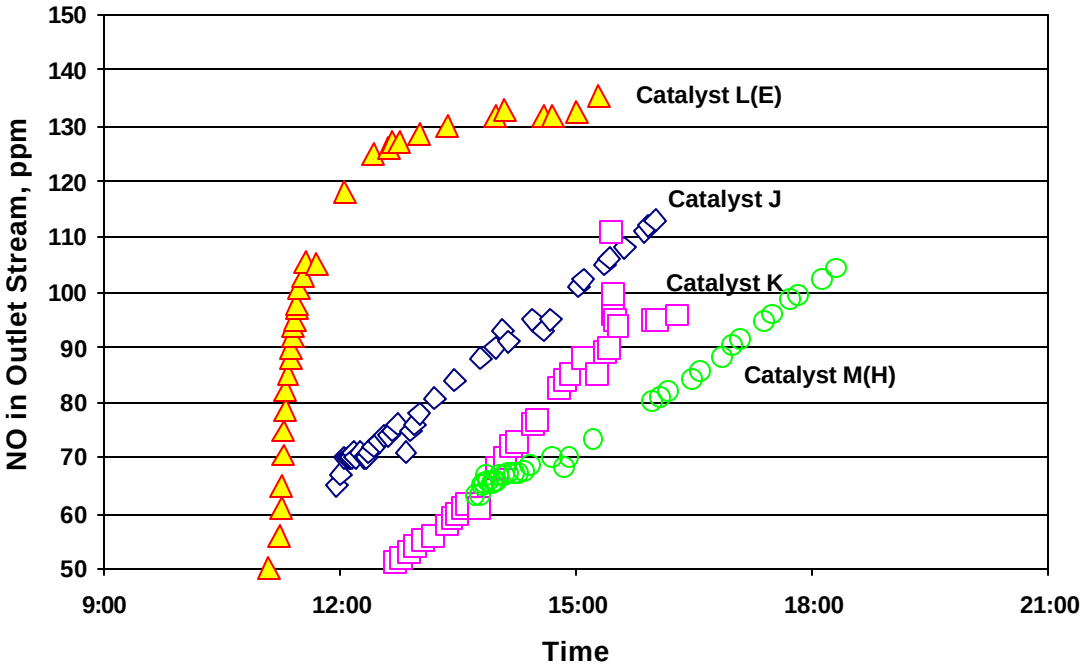

Figure 3-27. Effect of SO_2 Exposure on NO Conversion

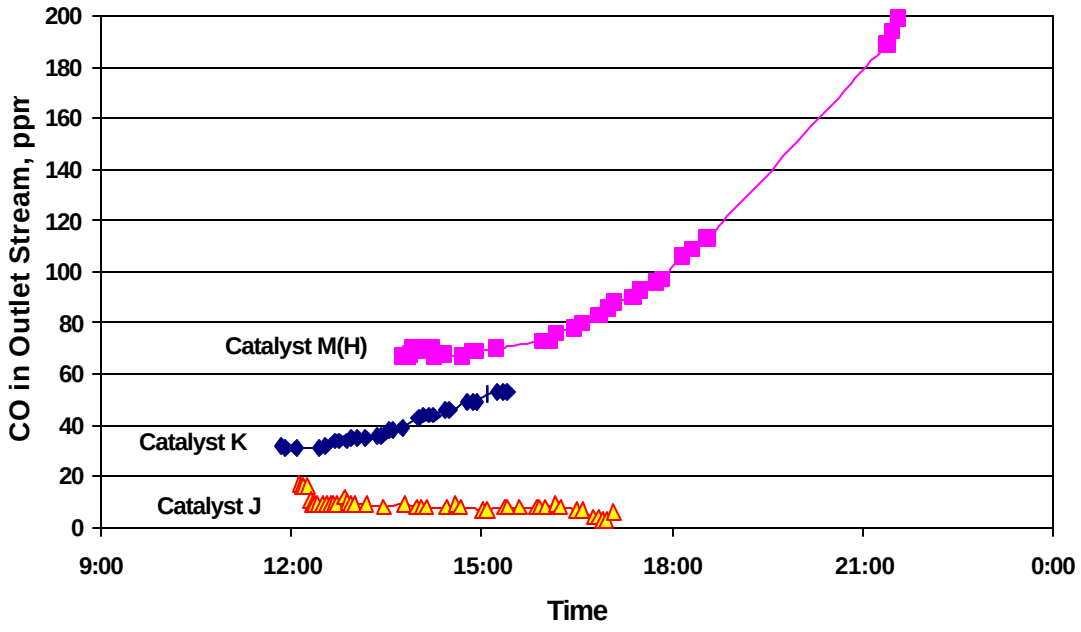

Figure 3-28. Effect of SO_2 Exposure on CO Conversion

Figure 3-28 shows that effect of 200 ppm SO_2 on CO conversion for catalysts J, K and M (all containing 40%Fe and 30% Cu). During the SO_2 exposure, the Ce-containing catalyst J

maintained very high CO conversion, while the CO activity for catalyst M were reduced by the presence of SO_2.

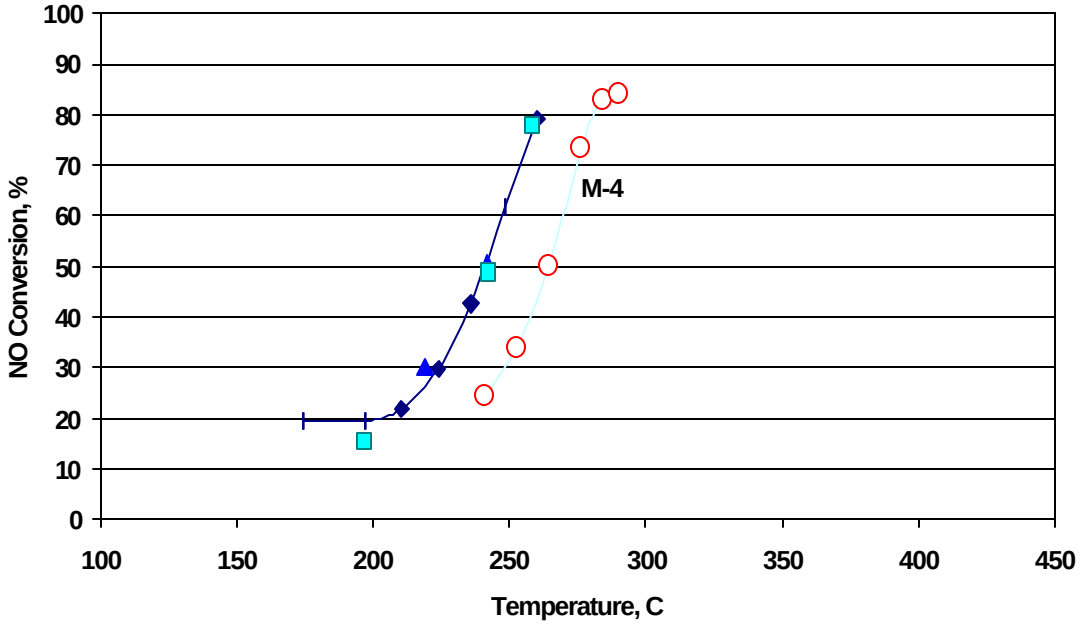

Figure 3-29. Restoration of NO Activity After SO_2 Exposure for Catalyst M (H)

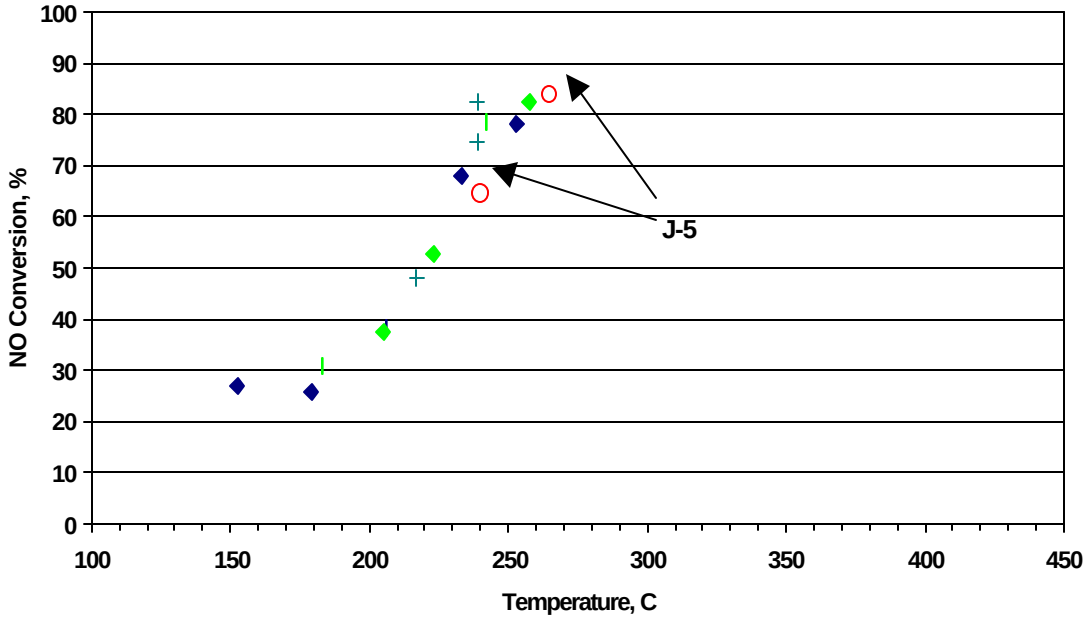

Figure 3-30. Restoration of NO Activity After SO_2 Exposure for Catalyst J

As discussed in section 3.1.10, the catalyst samples, after SO_2 exposure and cooling in nitrogen purge, were re-tested in dry, SO_2-free gas environment. In Figure 3-29, test data for catalyst M (Fe/Cu/AC) after SO_2 exposure (M-4, open circles) are plotted along with those before SO_2 exposure for the same catalyst. Catalyst M achieved over 80% NO conversion even after SO_2 exposure. By increasing the reaction temperature about 25 ºC, the NO conversion profile for M-4 was restored to a similar pattern as the earlier tests.

As shown in Figure 3-30, catalyst J (Fe/Cu/Ce/AC) exhibited complete recovery of NO activity. The after SO_2 exposure test data (J-5, open circles) fell right on the original NO conversion profile before the exposure. High NO conversion (>80%) was achieved at a low reaction temperature. Similarly, test data of catalyst K (Fe/Cu/K/AC) after SO_2 exposure also shown restoration of original NO activity at low temperatures.

3.2 Activated Alumina Based Catalysts

3.2.1 Reaction Pathways

Literature review and test data analysis have revealed that the performance of the NO - catalyst - CO system was influenced mainly by the following four competing reaction pathways:

1. Direct reduction of NO by CO, either added in the test gas mixture or generated *in situ* from the AC support, i.e., $NO + CO \rightarrow N_2 + CO_2$;

2. Destruction/oxidation of excess CO, i.e., $CO + O_2 \rightarrow CO_2$;

3. Partial combustion/gasification of the supporting activated carbon, i.e., $C + O_2 \rightarrow CO + CO_2$; and,

4. Direct reaction of NO with the carbon support, i.e., $NO + C \rightarrow N_2 + CO_2$

Depending on reaction temperature, type of substrate, and type / amount of metals applied, different reaction pathway(s) may dominate the performance under given operating conditions.

The catalysts tested in previous quarters were all activated carbon based. Beyond its function as a catalyst support, activated carbon also directly participate in reactions involving both NO and CO (reaction pathways 3 and 4 above), especially at higher temperatures. These two reactions are absent for activated alumina based catalysts. Therefore the AA based catalysts test data, together with earlier AC based test data, provide an opportunity to understand the interactions and relative importance the reactions in the NO- catalyst-CO system.

3.2.2 NO and CO Conversions

The first AA catalyst tested was Type N, prepared using as-received activated alumina. Figure 3-31 summarizes the test data for Catalyst N on five separate days, in dry, SO_2 free gas mixture as described in Chapter 2. During Day 4 testing the catalyst was exposed to moisture and SO_2, therefore Days 5 and 6 represent the catalyst performance in dry, SO_2-free environment after the exposure.

The Days 1-3 test data for Catalyst N can be compared with the typical performance of AC-based catalysts with same metal loading (40% Fe and 30% Cu, M and H), shown in Figure 3-32. The AA catalyst reached 50% NO removal in the temperature range of about 240-250 ºC, which was similar to the AC based catalysts. The AA catalysts also achieved over 80% NO removal, but at reaction temperatures about 20 ºC higher than those of AC catalysts for the same NO conversion.

Both AA and AC catalysts gave excellent CO conversion over the entire temperature range. The fresh AA catalyst actually did slightly better (at about 90% conversion) than the AC catalyst. These data show that, even in the absence of carbon related reaction pathways 3 and 4, the

Fe/Cu/AA catalyst is capable of NO and CO removal levels similar to that of AC based catalyst, albeit with a somewhat flatter NO - temperature profile.

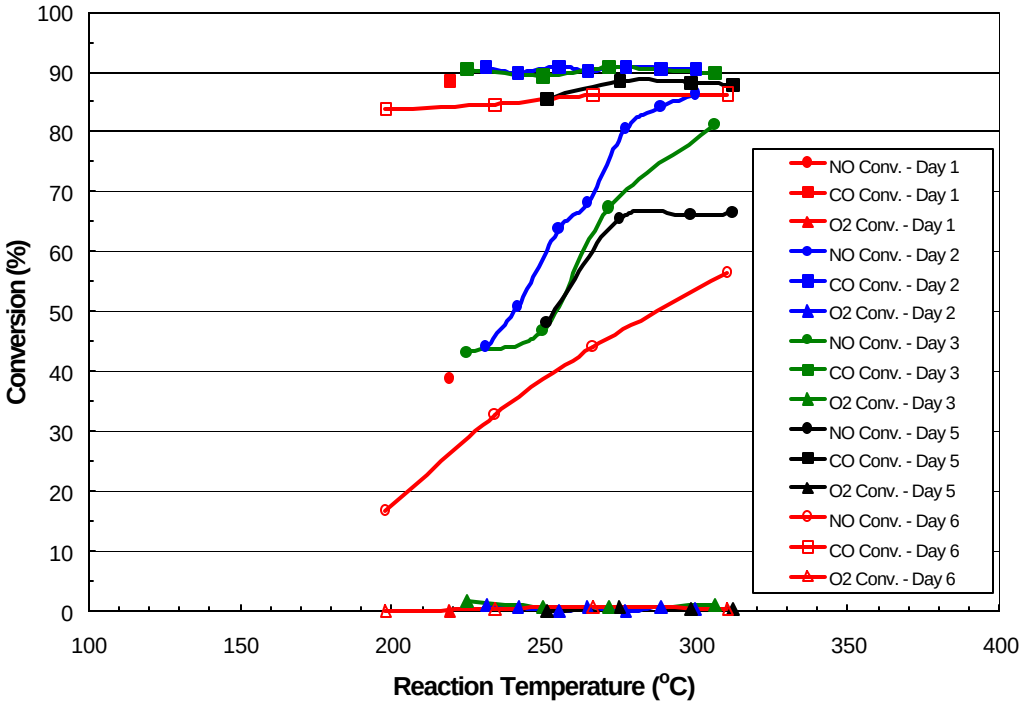

Figure 3-31. NO, CO and O_2 Conversions over 40% Fe/30% Cu / AA Catalyst N

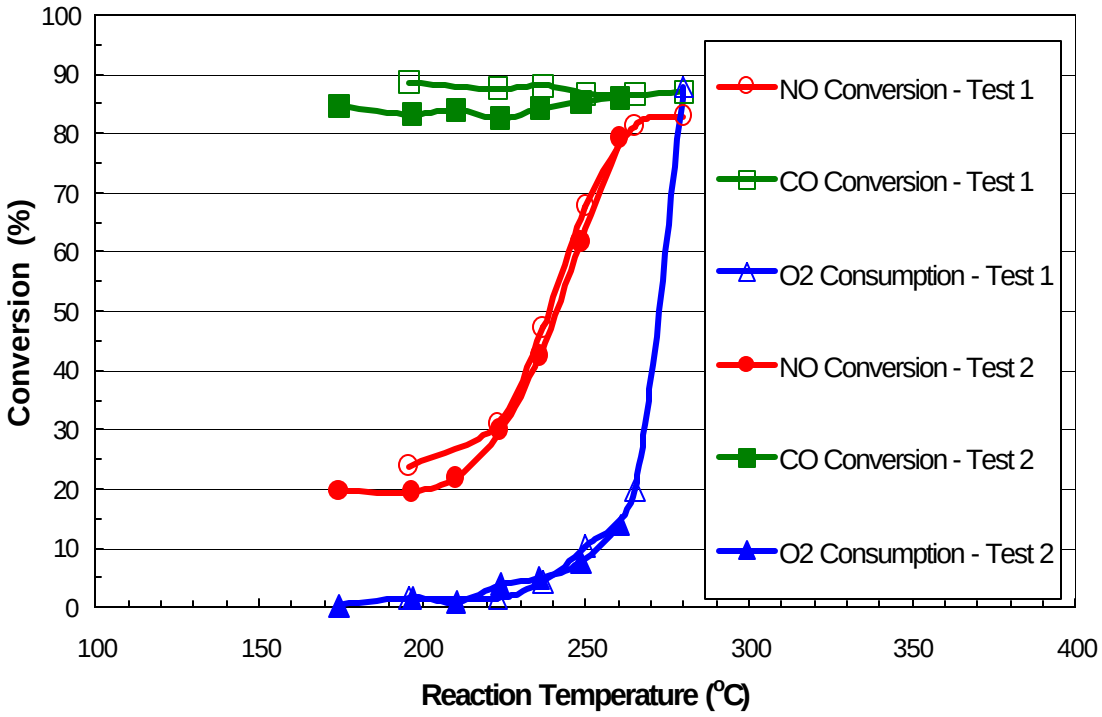

Figure 3-32. Conversion of NO, CO, and O_2 over 40% Fe/30% Cu / AC Catalyst

3.2.3 Oxygen Consumption and CO

At higher temperatures, the AC based catalysts displayed significant depletion of oxygen in the reactant gas mixture, due to the partial combustion of carbon substrate (pathway 3)

As expected, the AA based Type N data in Figure 3-31 showed little O_2 loss over the entire temperature range. Since the dry reactant gas mixture contains 520 ppm CO and 3% O_2, complete oxidation of all the CO (via pathway 2 above) would consume about 0.8% of oxygen in the mixture assuming it being the sole oxidant. Most test data with AA-based catalysts (N, O, P, Q) have oxygen conversion in the range of 0.4 - 0.8%, which suggests that CO oxidation is the only reaction consuming oxygen.

3.2.4 Exposure to H_2O / SO_2

During Day 4, catalyst N was exposed to moisture and SO_2. Figure 3-33 shows the transient data of Day 4 test.

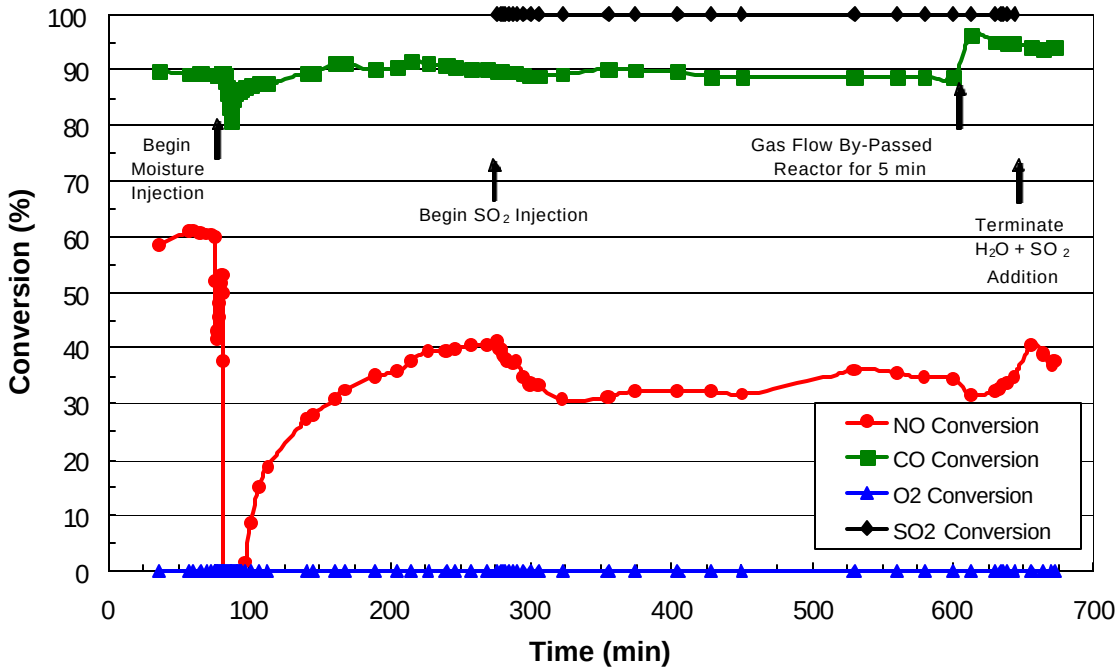

Figure 3-33. Historical Data of Catalyst N upon Exposure to H_2O/SO_2

At the beginning, steady state conditions were reached at 275 ºC reaction temperature and in dry, SO_2 free gas mixture, with a NO conversion of 61%. Upon introduction of water vapor to the gas stream (8% H_2O in the mixture), a large amount of NO was desorbed from the catalyst. NO levels as high as 300% of the inlet concentration were measured briefly from the outlet gas. At the same time a small drop in CO conversion was observed, indicating some desorption of CO from the catalyst. Both CO and NO conversions recovered gradually with CO conversion

restored to the original level of about 90%. NO conversion was slower in recovery and only reached about two-thirds of the original activity after three hours.

Compared to AC based catalysts subjected to similar test conditions, the AA catalyst had a larger amount of NO desorption and a larger loss of NO activity due to water addition. This is clearly shown in Figure 3-34, in which the NO concentrations in reactor outlet gas immediately before and during water vapor addition are plotted for several AC and AL based tests.

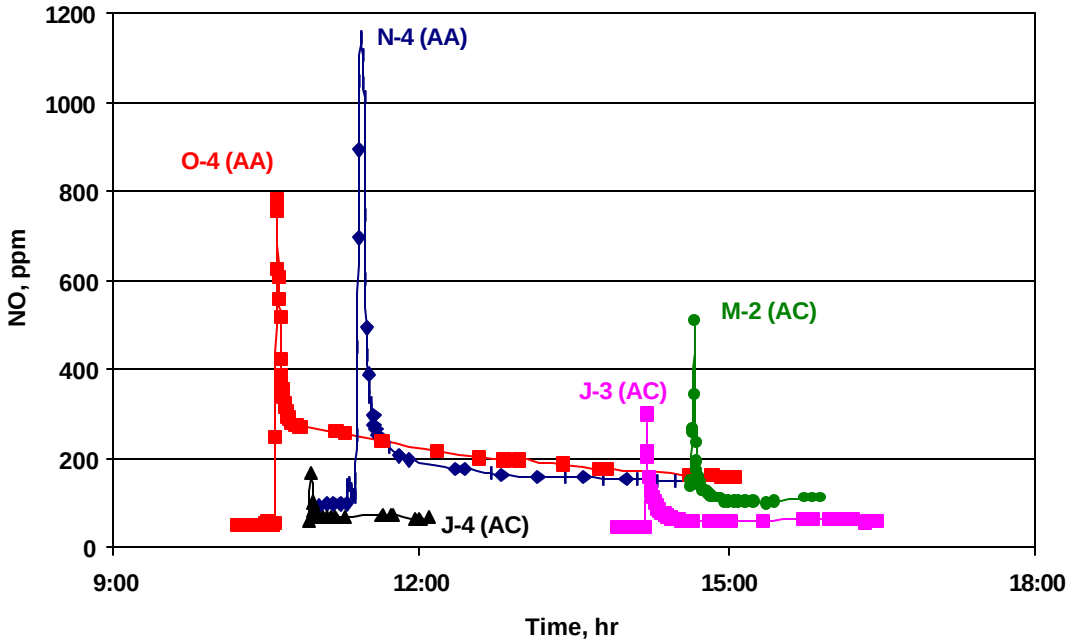

Figure 3-34. Transient NO Concentrations before and after the Start of Water Addition

Addition of 200 ppm SO_2 to the reactant gas stream led to a small reduction in the NO activity. Unlike the AC based catalysts that displayed a continuous decay of NO activity during SO_2 exposure, the activity of AA catalysts did not reduce further after the initial drop. Type N even regained some activity over the next several hours. The CO conversion was only slightly lowered upon introduction of SO_2, and was holding steady thereafter.

Towards the end of the Type N testing, the gas flow to the reactor was bypassed for five minutes to measure inlet gas composition. This caused a jump in CO conversion. Terminating H_2O /SO_2 resulted a small surge in NO activity, but no noticeable effect on CO conversion.

During the entire test, oxygen in the gas mixture remained unchanged. No SO_2 was detected in the outlet gas. The fate of the SO_2 needs to be investigated in the future.

The catalyst using calcined AA support (Type O) was also exposed to H_2O/SO_2 during Day 4. As seen in Figure 3-35, the Type O test data are consist with Type N and support the observations described above.

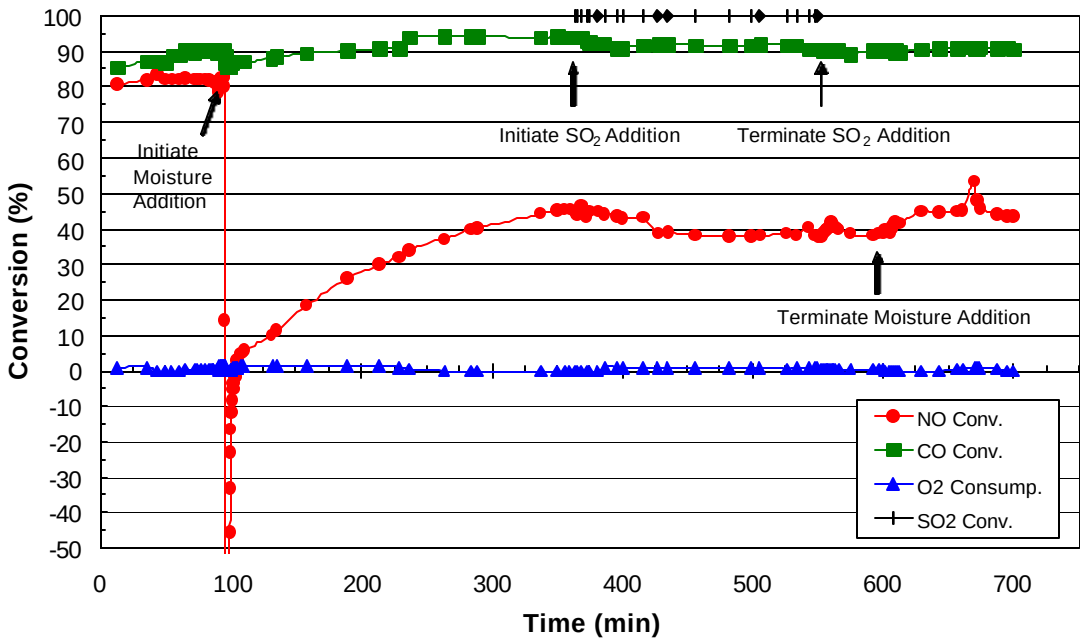

Figure 3-35. Historical Data of Type O Catalyst upon Exposure to H_2O/SO_2

3.2.5 As Received Versus Calcined AA

As described in Chapter 2, a separate catalyst sample was prepared by impregnating metals onto calcined activated alumina. The calcing of as-received AA in a furnace maintained at 500 ºC overnight exhibited a 14.4% weight loss. The BET surface areas of the as-received and calcined AA and their associated catalysts are given in Table 3-3. Catalyst O with calcined AA had higher surface areas before and after the impregnation. For both catalysts, the surface areas after the tests were higher than that before the tests, indicating that the micro pore structure remained intact through testing. Type O had lower surface area after the tests, possibly because O was subjected to more testing time (8 days versus 6 days for N).

Table 3-3. BET Surface Area (m^2/g) of Type N and O Catalysts

	N - As Received AA	O - Calcined AA
Before Impregnation	127	162
Before Cat. Tests	115	134
After Cat. Tests	201	153

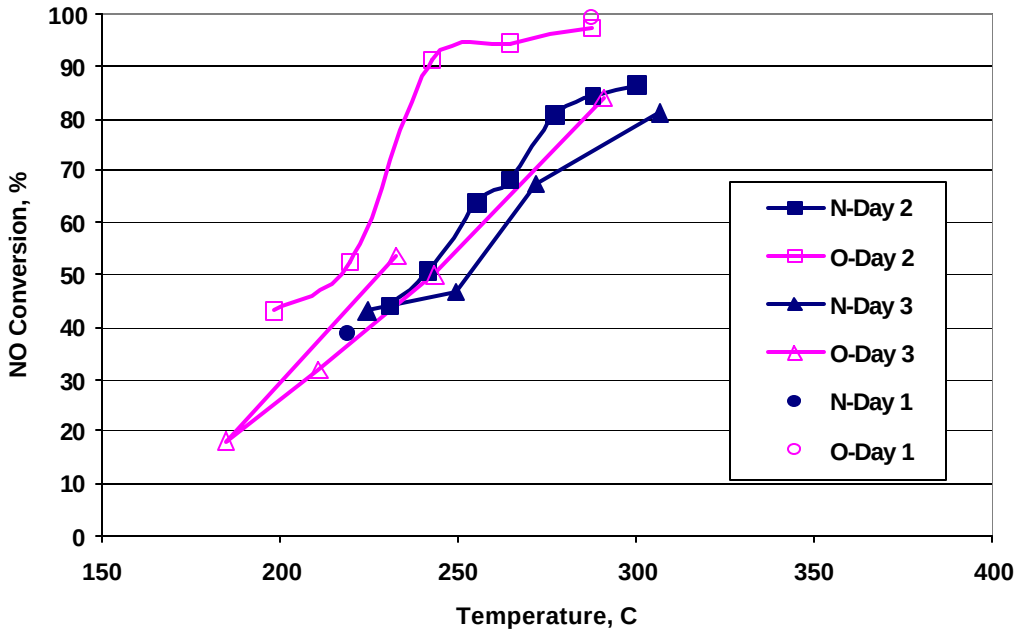

Figure 3-36. NO Conversion for N and O Catalysts

The behavior of Type O catalyst was very similar to Type N, except that O had a higher initial NO activity. Figure 3-36 shows the NO conversion data of the first three days of testing for both O and N, in dry, SO_2 free gas mixture. Type O, based on calcined AA, achieved higher NO conversion at lower temperature when same day test profiles are compared with each other.

3.2.6 Deactivation

It is clear from Figure 3-36 that both N and O catalysts exhibited higher light-off temperatures and lower final NO conversions for later tests. This deactivation trend is more evident in Figure 3-31 where five days of test data are plotted together. Although the Days 5 and 6 tests were conducted after H_2O/SO_2 exposure, their data seem to fit the general deactivation trend. This level of deactivation was not observed during the earlier tests with AC based catalysts.

The fact that Day 5 test after H_2O/SO_2 exposure achieved significantly higher NO conversion than Day 4 (> 65% versus 30-40% for Day 4) suggests that moisture and SO_2 did not cause permanent damage to the catalyst and its NO activity were regenerable after exposure. It is also important to point out that AA based catalysts exhibited excellent and stable activity for CO reduction. The CO conversion of both O and N catalysts did not change significantly over time, even during and after H_2O / SO_2 exposure.

3.2.7 N_2O Formation

As reported during previous quarters, the AC based catalysts had very high NO to N_2 selectivity, with only minor N_2O formation. The amount of N_2O found in the reactor outlet gas depended strongly on the reactor temperature and the type of AC catalysts. In Figure 3-37, NO to N_2O

conversion data of all tests with AA based catalysts are plotted along with that of two tests of AC catalysts with the same metal loadings. No significant N_2O formation was observed for AA based catalysts. This seems to suggest that the N_2O formation in the current tests (either as a final or intermediate product of NO reduction) may be promoted by the activated carbon, rather than by the metal ingredients (Fe and Cu) which are common to both AA and AC catalysts.

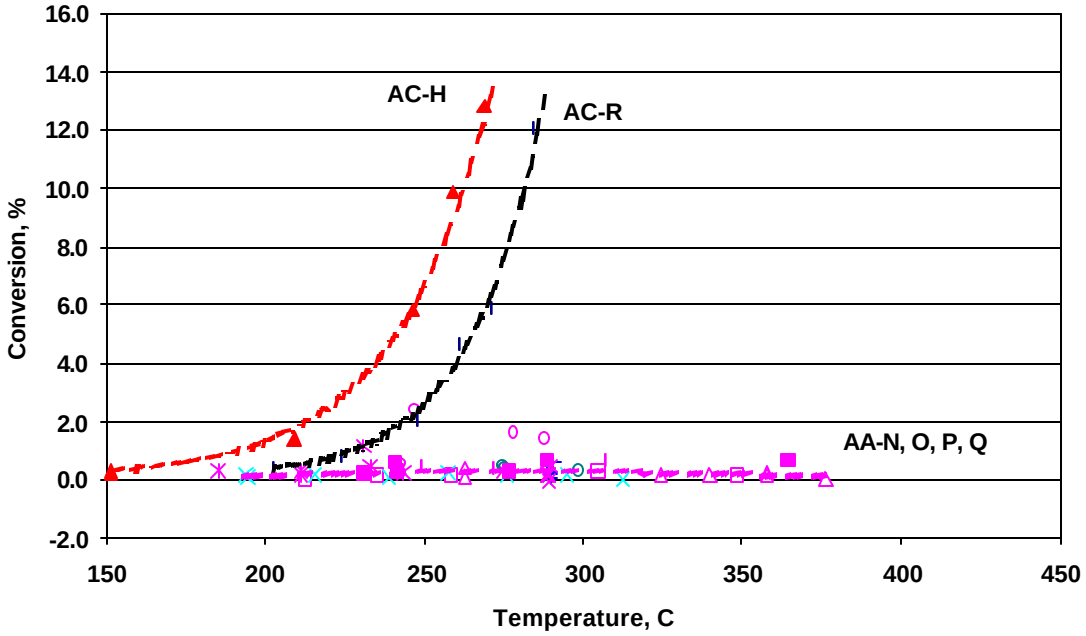

Figure 3-37. NO to N_2O Conversion for AC and AA Catalysts

3.2.8 Testing with High Space Velocity

Tests with high space velocities were carried out with the same flow rate of the same reactant gas mixture, as described in Chapter 2. Instead of the normal 20 ml layer of catalyst, only 4 ml was loaded into the reactor, resulting in a gas hourly space velocity (GHSV) of 5250 hr^{-1} in dry, SO_2 free gas mixture. This space velocity is five times the normal space velocity used in other tests. As shown in Table 1, catalyst type Q and R are duplicate samples of O and H, used for high GHSV tests.

As seen in Figure 3-38, the AA based catalyst Q (a fresh duplicate of O) tested at high space velocity achieved 60% NO conversion, compared to over 90% for the same catalyst tested at low space velocity. Also the NO activity curve became much flatter, and the temperature needed for 50% NO conversion, T_{50}, was about 60 ºC higher at high space velocity. This large difference indicates that the short gas-catalyst contact time was limiting the NO conversion at the high space velocity.

The AC based catalyst, on the other hand, achieved high NO conversion at high space velocity, although higher reaction temperature was needed as indicated by a general shift of the activity

curve toward higher temperatures. Recalling the reaction pathways discussed earlier, at high space velocity, a higher reaction temperature is needed to compensate for a smaller catalyst volume. The fact that AC based catalysts have two NO reduction pathways (1-through reaction with CO, and 4-reaction with carbon), and both reactions speed up with higher temperature, may explain why high NO conversion was achieved by AC based, but not by AA based catalysts at the high space velocity.

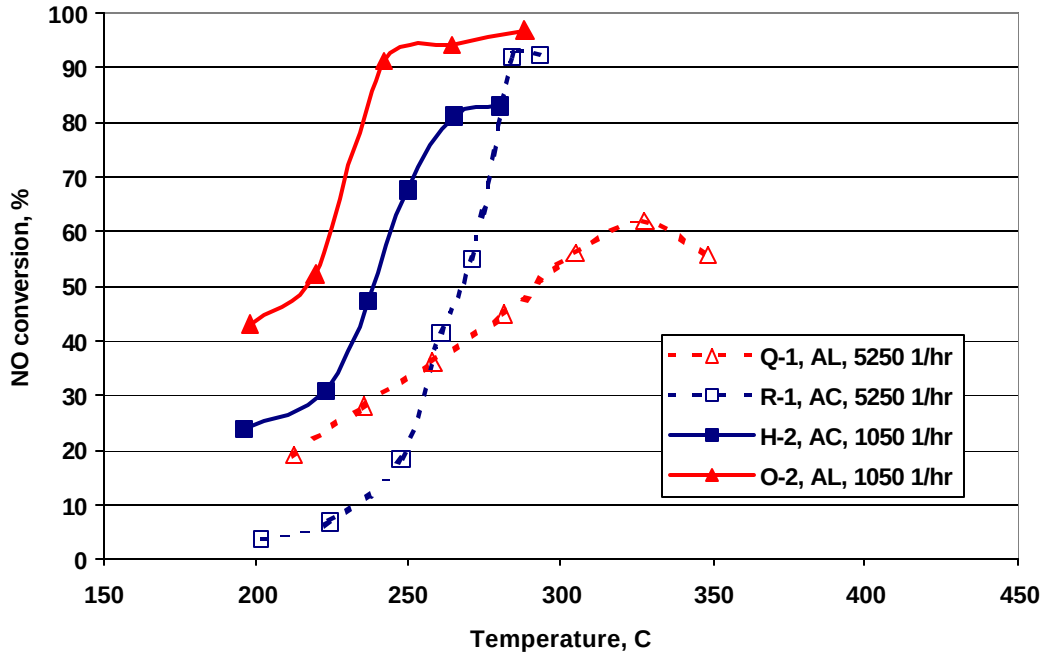

Figure 3-38. Effect of Space Velocity on NO Conversion for AC and AA Catalysts

Another catalyst sample tested at high space velocity is type P, which is the remaining sample of catalysts O after eight days of testing. Figure 3-39 compares the performance of type P with that of type Q (fresh duplicate sample of type O).

As can be expected from earlier discussions of deactivation for AA based catalysts, the previously tested type P had its activity profile shifted about 40 ºC towards higher temperature, and achieved lower final NO conversion. It is also interesting to note that, with increasing reaction temperature, the NO conversion of both P and Q reached a maximum and then decreased with further increase in temperature. A possible explanation for this is that at high temperatures, the rapid oxidation of CO by oxygen (reaction pathway 2) may have depleted the CO needed for NO reduction (pathway 1). This maximum NO conversion was generally not observed for AC based catalysts, because NO is converted by the dual reactions with CO and carbon (pathways 1 and 4), and at high temperatures CO generated through burning of carbon substrate (pathway 3) more than replenishing the depletion due to pathway 2.

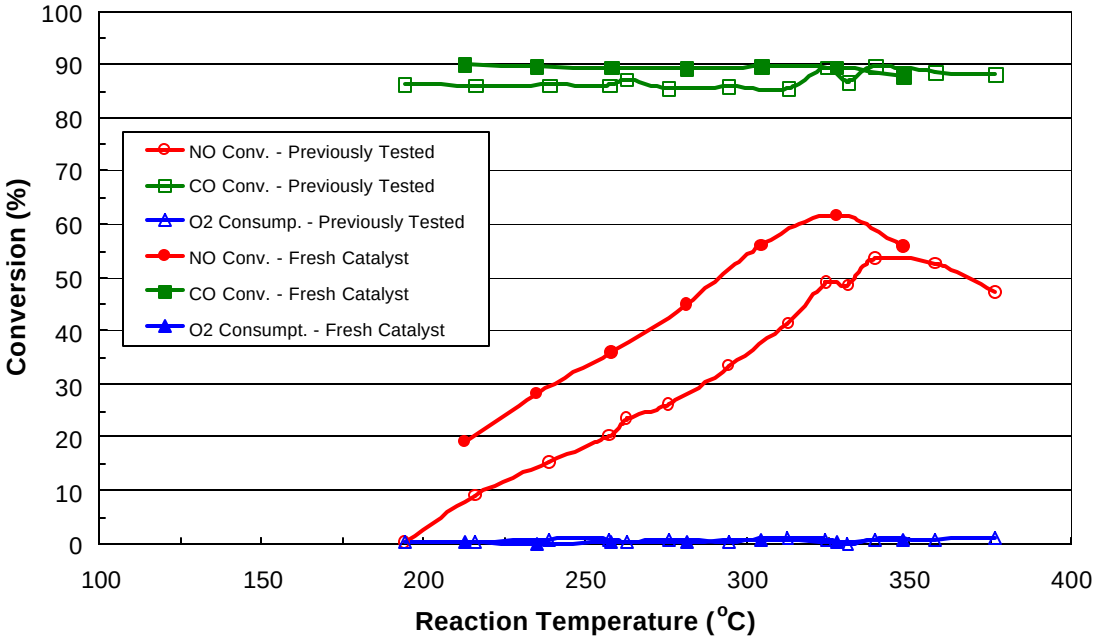

Figure 3-39. NO, CO and O_2 Conversions over Previously Tested (P) and Fresh (Q) 40% Fe / 30% Cu /AA Catalyst with GHSV = 5250 hr^{-1}

Even at the higher space velocity, the CO conversion remained very high during entire reaction temperature range, and the previously tested catalyst showing only slightly lower CO conversion. As with earlier AA-based catalyst testing, no significant oxygen consumption was observed.

4.0 FURNACE OPTIMIZATION

The objective of this task is to investigate a means of producing an adequate ratio of CO/NO upstream of the catalyst reactor. A 3-D CFD simulation of the furnace was performed using the computer program, FW-FIRE. The outlet conditions of the FW-FIRE model were then applied as the inlet conditions to a 2-D Fluent model of the heat recovery area (HRA) to predict CO and NO at the HRA outlet. Since the FW-FIRE model does not include the finishing superheater and finishing reheater (located between the furnace outlet and the HRA inlet), the outlet temperature distribution from these banks was calculated using the Foster Wheeler program, HEATEX.

4.1 Computer Program Description

FW-FIRE (Fossil Fuel, Water-walled Furnace Integrated Reaction and Emission Simulation) simulates furnace combustion, heat transfer and pollutant formation based on fundamental principles of mass, momentum, and energy conservation. The FW-FIRE computer program incorporates the latest state-of-art coal combustion/gasification, pollutant formation, and physical analysis techniques based on extensive empirical research. The FW-FIRE code performs general three dimensional multiphase gas combustion steady state analysis of reactive fluid flows. The program is fully capable of analyzing gas-fired, oil-fired, and coal-fired boilers although FW-FIRE was initially tailored for pulverized coal combustion and gasification.

HEATEX is a Foster Wheeler general-purpose program for thermal/hydraulic analysis of tube banks. The program performs heat transfer calculations on a local basis by dividing the tube bundle into a number of small heat transfer elements.

Fluent is a general purpose commercial CFD software, which can be used for simulation, visualization, and analysis of fluid flow, heat and mass transfer, and chemical reactions.

4.2 Furnace Model

4.2.1 Model Geometry

An FW-FIRE model was made of a current 400 MWe pulverized coal furnace. The model simulates the furnace, in height from the bottom of the hopper to the roof, in depth from the front wall to the rear wall, and in width from the left sidewall to the right side wall. The furnace has a total of 24 opposed wall-fired burners (3 vertical x 4 horizontal x 2 walls) and 10 over fire air ports. The radiant heat transfer surface consists of 2.75” OD waterwalls and five 2.0” OD partial divisional wall panels. Water is circulated in the furnace by natural circulation. Fine meshes are used to model the burners and over-fire air (OFA) ports. The model contains 528,840 (117x113x40) nodes and is shown in Figure 4-1.

4.2.2 Boundary Conditions

The input data required by FW-FIRE include fuel analysis, coal particle size distribution (mass percentage for each size bin), waterwall fluid temperatures, and the velocities, flow rates and

temperatures of primary and secondary gas streams. The waterwalls of the furnace are assumed to be gray and diffusive. The wall temperature at each location is calculated based on the fluid temperature and the heat flux at the wall cell. Coal kinetic parameters were applied for Illinois #6 coal.

Parametric runs were conducted to determine the effects of outlet oxygen concentration and over-fire air (OFA) flow rate on outlet NO and CO.

4.2.3 Baseline Case

The baseline (design) case for this unit is 3% O_2 at boiler outlet and 30% OFA. The corresponding boundary conditions were applied to the computational model and FW-FIRE was run until steady state conditions were achieved.

The modeling results for the baseline case are summarized in Table 4-1. The coal burnout shown in the table is the percentage of dry ash-free based coal burned. The loss on ignition (LOI) represents the percentage of unburned carbon in the ash. The furnace exit gas temperature (FEGT) shown in the table is the average temperature of flue gas before the finishing superheater (vertical plane above the nose. Figure 4-2 presents a plot of gas temperature in a vertical plane through the second burner column and at the furnace outlet (before the finishing superheater). The mole fraction of O_2 through the second burner column, at the OFA elevation, and at the furnace outlet is presented in Figure 4-3. CO mole fraction and Flue gas velocity at the second burner column and at the furnace outlet is presented in Figures 4-4 and 4-5. Figure 4-6 is a plot of the NO concentration in a vertical plane through the second burner column and at the furnace outlet.

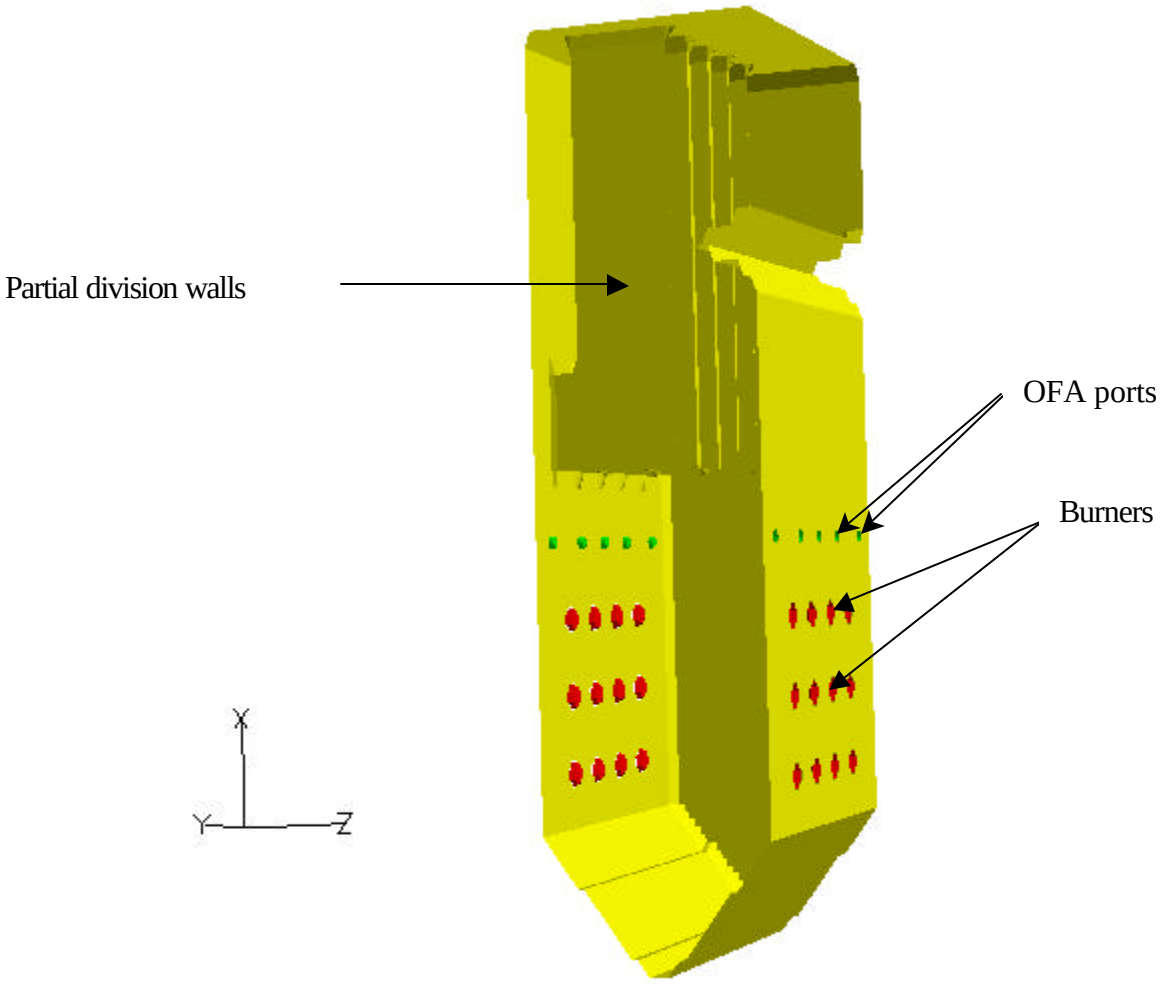

Figure 4-1. Computational Model of Furnace (with right side wall removed)

Table 4-1. Summary of Furnace Baseline Case Simulation

Burnout	%	99.66
LOI	%	2.61
CO furnace	ppmvw	1537
NOx	ppmvw	227
FEGT	F	2100

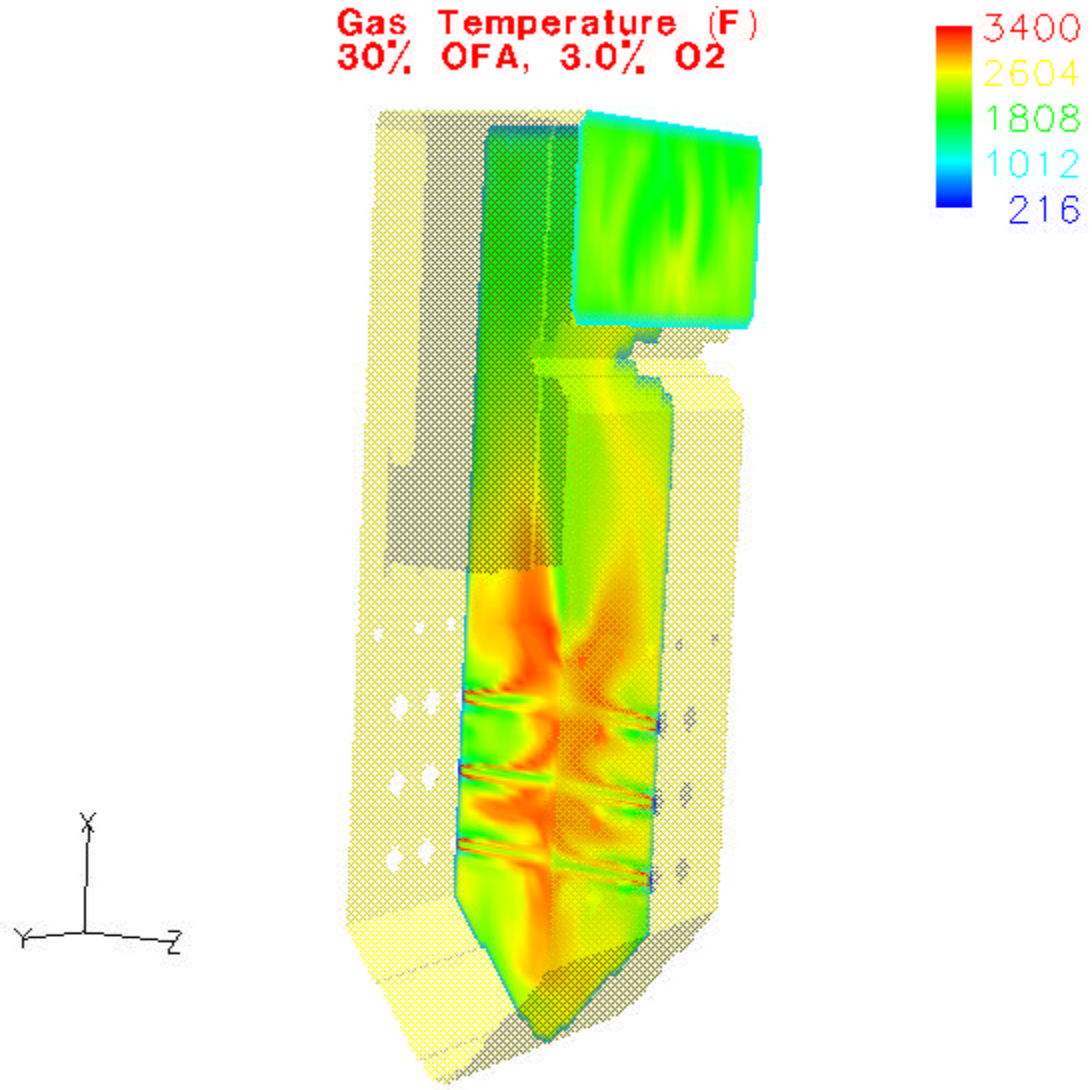

Figure 4-2. Furnace Gas Temperature

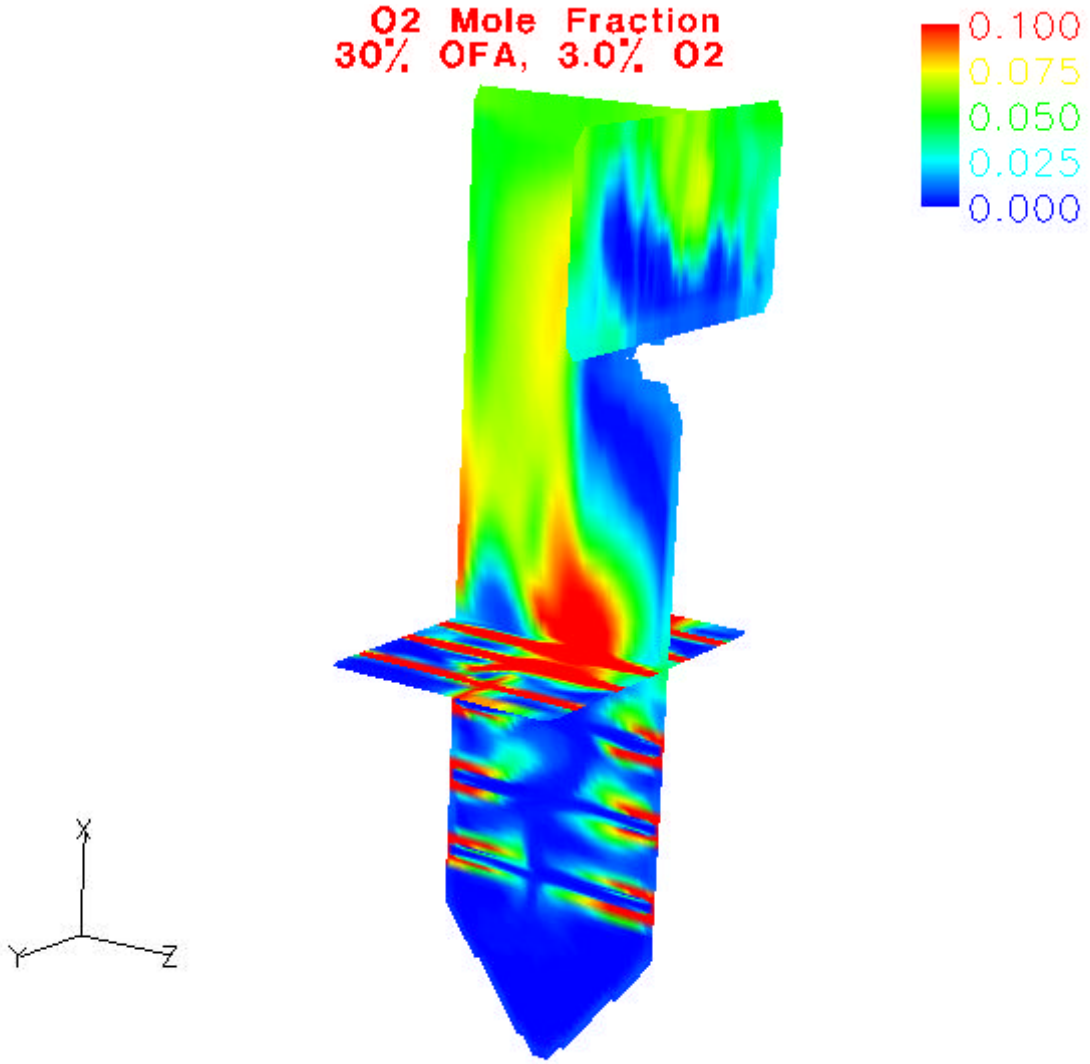

Figure 4-3. Furnace O_2 Mole Fraction

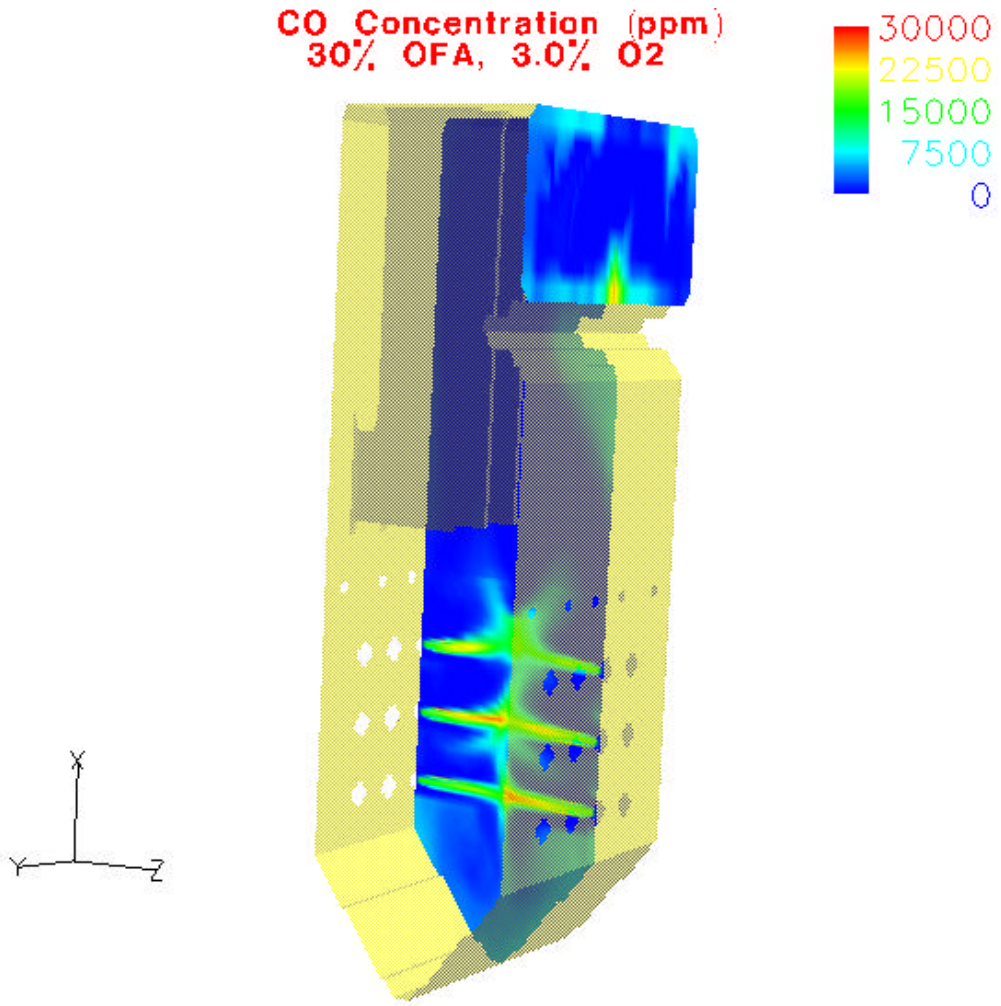

Figure 4-4. Furnace CO Concentration

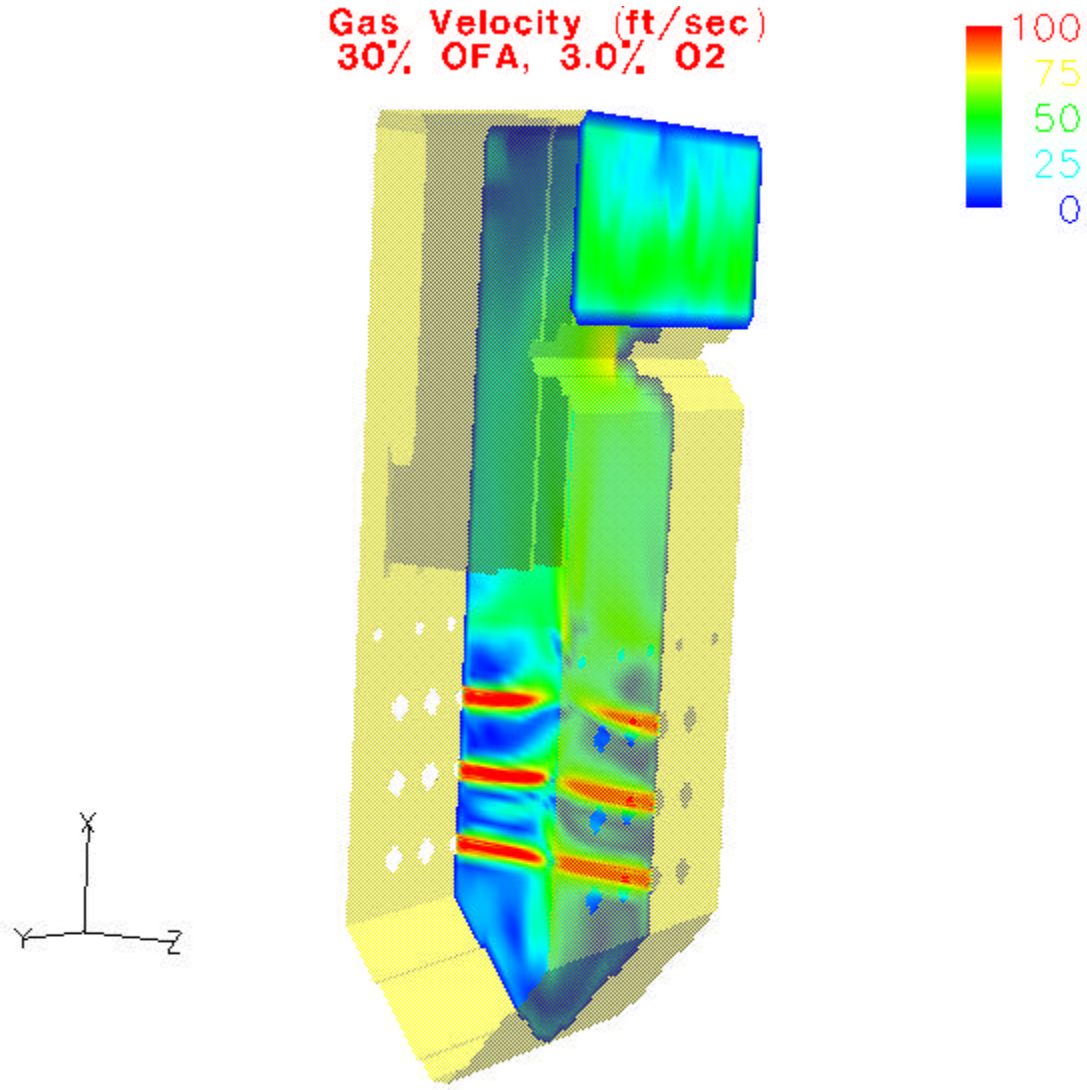

Figure 4-5. Furnace Gas Velocity

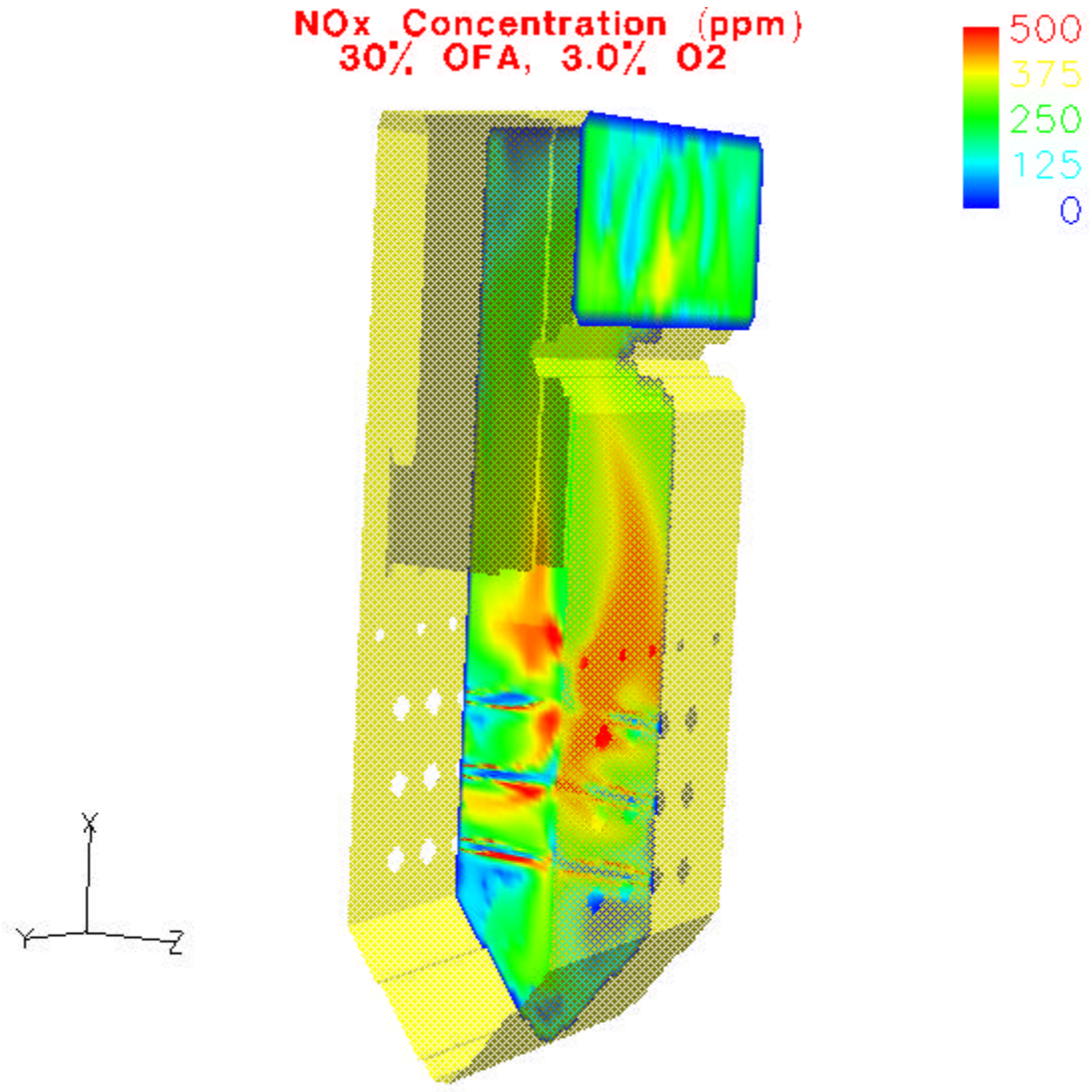

Figure 4-6. Furnace NOx Concentration

4.3 HRA Model

Since the conditions at the furnace outlet tend to be uniform in the width direction, to simplify the analysis a two-dimensional (height versus depth) model of the HRA and finishing superheaters were utilized.

4.3.1 Finishing Superheater and Reheater

An HEATEX model was made of the finishing superheater and finishing reheater tube bundles. Inlet temperature and flow distribution were obtained from the FW-FIRE furnace model outlet conditions. Figure 4-7 presents the corresponding furnace outlet (finishing superheater inlet) and HRA inlet (finishing reheater outlet) flue gas temperature profiles.

4.3.2 Fluent Model

A two dimensional fluent model was made of the HRA. Figure 4-8 shows the geometry of the HRA. The HRA model simulates the heat transfer, hydraulic resistance, and turbulence of the primary reheater, primary superheater, upper economizer, and lower economizer. The model includes approximately 21,000 cells.

Heat transfer to the tube banks is simulated by distributed heat sinks. Tube bank hydraulic resistance is simulated by a combination of individual tube modeling and distributed resistance. The magnitude of the heat sinks and distributed resistances are calculated to match the predictions of the Foster Wheeler Boiler Performance Computer Program.

Species transport was modeled using the finite rate/eddy dissipation model. CO reaction rate kinetics were obtained from Adams et al 2000 as follows:

$CO + ½\ O_2 \rightarrow CO_2$

$$\frac{d[CO]}{dt} = A[CO]^{1.0}[H_2O]^{0.5}[O_2]^{0.25} e^{-(\frac{E}{RT})}$$

A = 2.61 E+12 kg-mol/m^3
E = 45,566 Kcal/kg-mol

Reaction of NO with O_2 was neglected (due to low gas temperature). The reaction of CO with O_2 is very sensitive to temperature as shown in Figure 4-9, which depicts the fraction of the CO remaining for given residence time at a constant gas temperature for fully mixed gas flow. Note that in the HRA the residence time is approximately 4 seconds with a gas inlet temperature of 1550ºF and a gas outlet temperature of 725ºF. In the Fluent model the eddy dissipation model is applied to simulate the turbulence-chemistry interaction, which limits the reaction rate and reduces the maximum CO reductions shown in Figure 4-9.

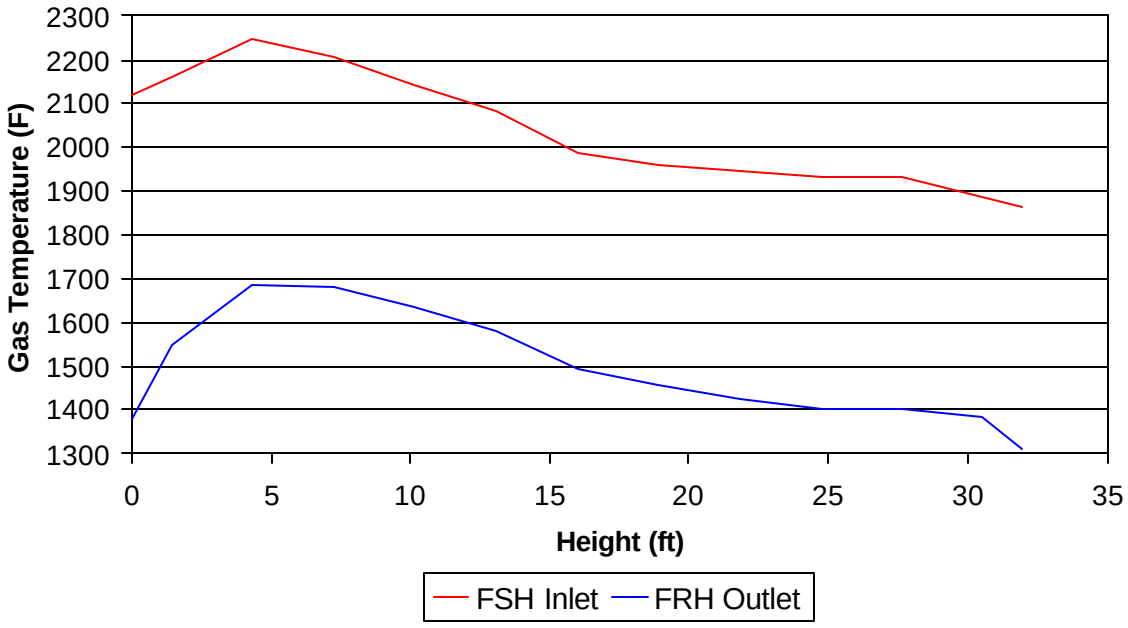

Figure 4-7. Flue Gas Temperature Vs. Height at Furnace Outlet and HRA Inlet, Baseline Case

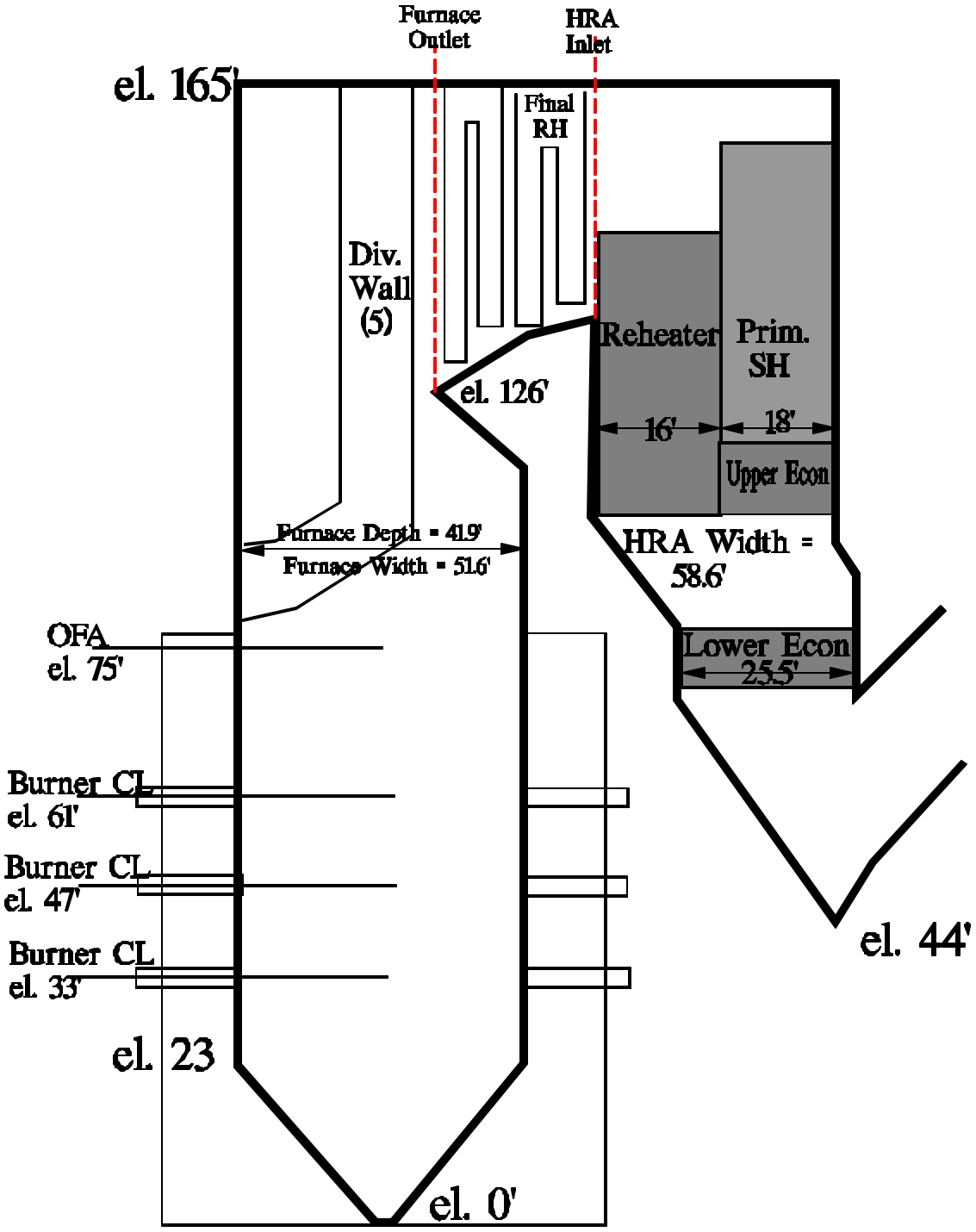

Figure 4-8. 400 MWe Boiler Design

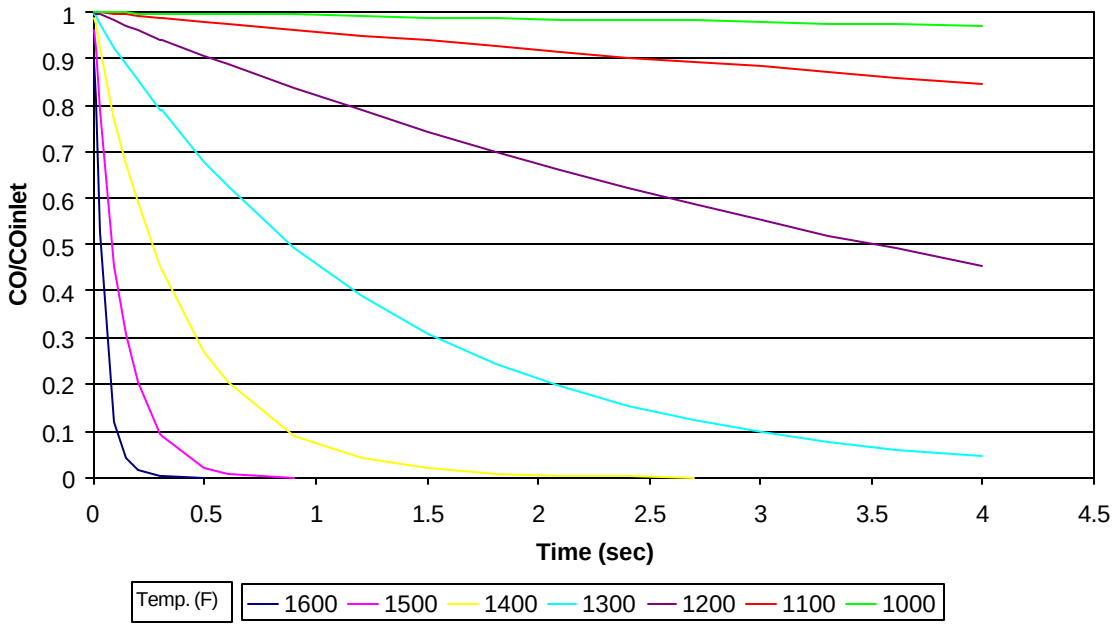

Figure 4-9. Ratio of CO/CO_{inlet} Vs. Residence Time and Temperature

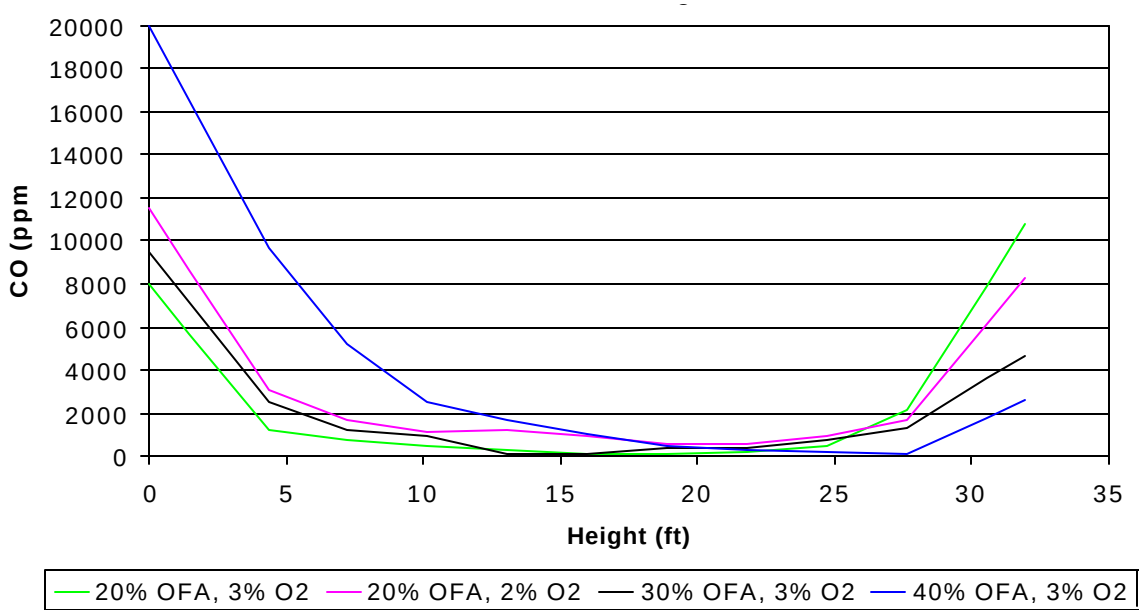

Figure 4-10. CO Concentration at HRA Inlet Vs. Height

4.3.3 Boundary Conditions

Properties (velocity, CO, NO, and O_2) at the furnace outlet plane of the FW-FIRE furnace model were averaged in the width direction to produce a profile versus height at the HRA inlet. Gas temperature versus height was obtained from the HEATEX temperature distribution at the finishing reheater outlet. Figure 4-10 presents the HRA inlet CO concentration for several cases.

4.4 Baseline Simulation Results

The boiler analyzed is designed for an outlet O_2 of 3% and an OFA flow rate of 30% (OFA/Total combustion air). Figure 4-12 presents the temperature distribution in the HRA. As shown in Figure 4-9 most of the CO reduction takes place above 1100ºF. Consequently significant CO reduction takes place only upstream of the primary reheater and primary superheater and in the upper section of the primary reheater. This is shown Figure 4-13, which depicts the CO concentration. Average CO concentration at the HRA inlet is 1600 ppm and at the HRA outlet is 150 ppm. Figure 4-14 presents the NO distribution in the HRA. Average NO concentration in the HRA is 225 (average NO concentration is constant through the model since no NO reduction mechanism is included). The ratio of CO/NO is presented in Figure 4-15, which shows the CO/NO ratio at the HRA outlet ranges from approximately 0.4 to 0.85 with an average value of 0.66. When the outlet OFA is raised to 40%, Figure 4-16 presents the ratio of CO/NO, which at the HRA outlet ranges from approximately 0.4 to 2.7 with an average value of 1.46. Since these ranges of CO/NO may not be acceptable to catalyst performance, a mixing device such as a static mixer may be required between the economizer outlet and the catalyst inlet. Static mixers are routinely used currently for mixing upstream of SCR reactors.

4.5 Parametric Cases Simulation Results

A series of runs were made to determine the HRA outlet CO and NO as a function of outlet O_2 and over-fire air flow. Figure 4-17 presents the concentration CO and NO concentrations and CO/NO ratio at the HRA outlet as a function of boiler outlet O_2 for an OFA flow of 20%. The CO/NO ratio ranges from 0.45 at 3% O_2 to 1.55 at 1% O_2. Figure 4-18 presents the CO and NO concentrations and CO/NO ratio at the HRA outlet as a function of OFA flow for an outlet O_2 of 3%. The CO/NO ratio ranges from 0.21 at 0% OFA to 1.46 at 40% OFA. Increasing OFA flow and/or decreasing boiler outlet O_2 can have a negative effect on fuel burnout. Figures 4-19 and 4-20 present the fuel burnout versus outlet O_2 and OFA flow. Fuel burnout is reduced from 99.74% to 99.45% by reducing outlet O_2 from 3% to 1% and reduced from 99.90% to 99.65% by increasing OFA from 0% to 40%. It is judged that this magnitude in fuel burnout reduction is relatively small. Changes in O_2 and OFA can also influence furnace exit gas temperature, which is important for performance, fouling, and metal temperatures. For the ranges of outlet O_2 and OFA flow studied, the maximum change in FEGT is less than 50ºF, which is judged to be a relatively small effect.

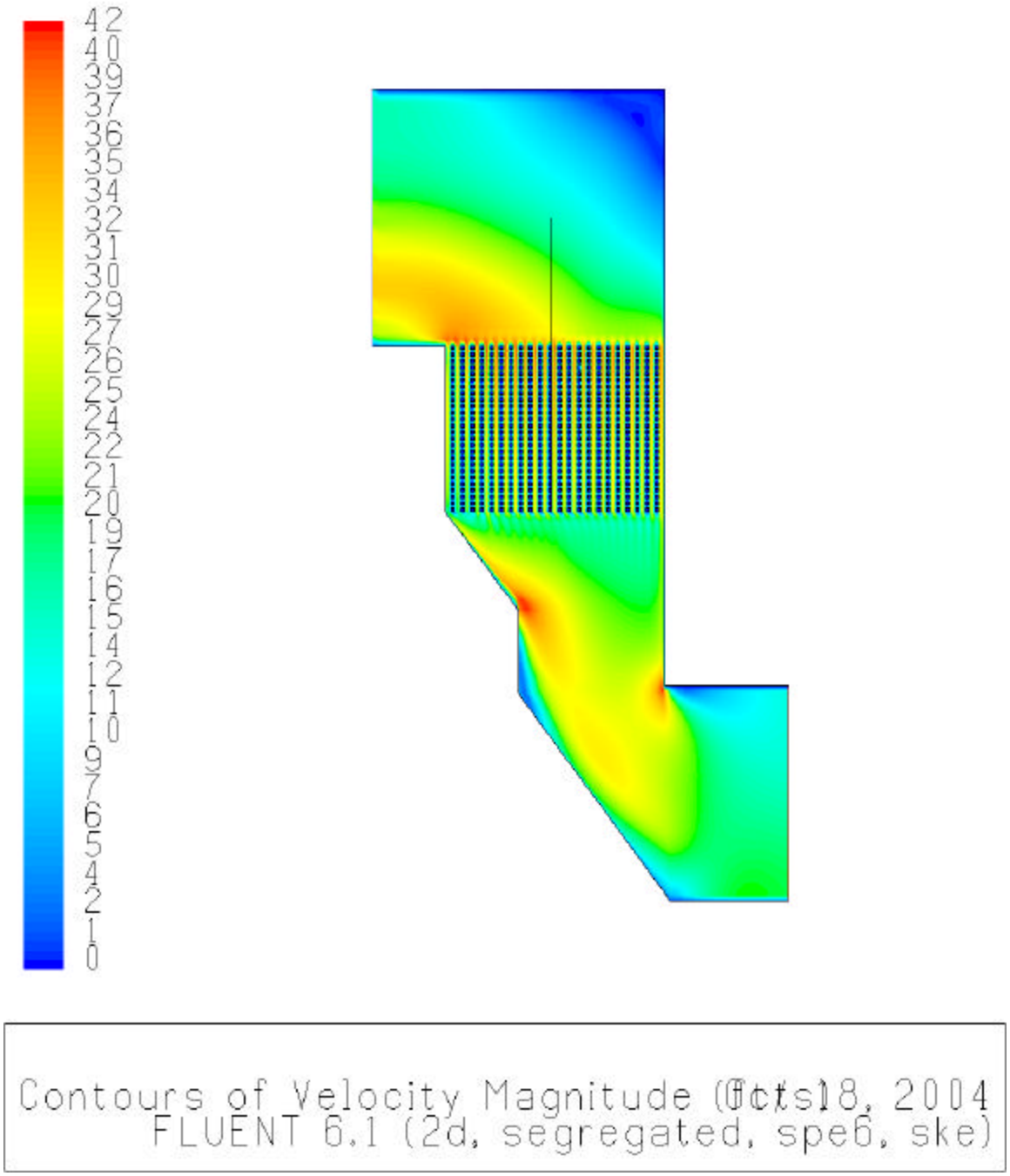

Figure 4-11. Flue Gas Velocity Distribution in HRA, Baseline Case

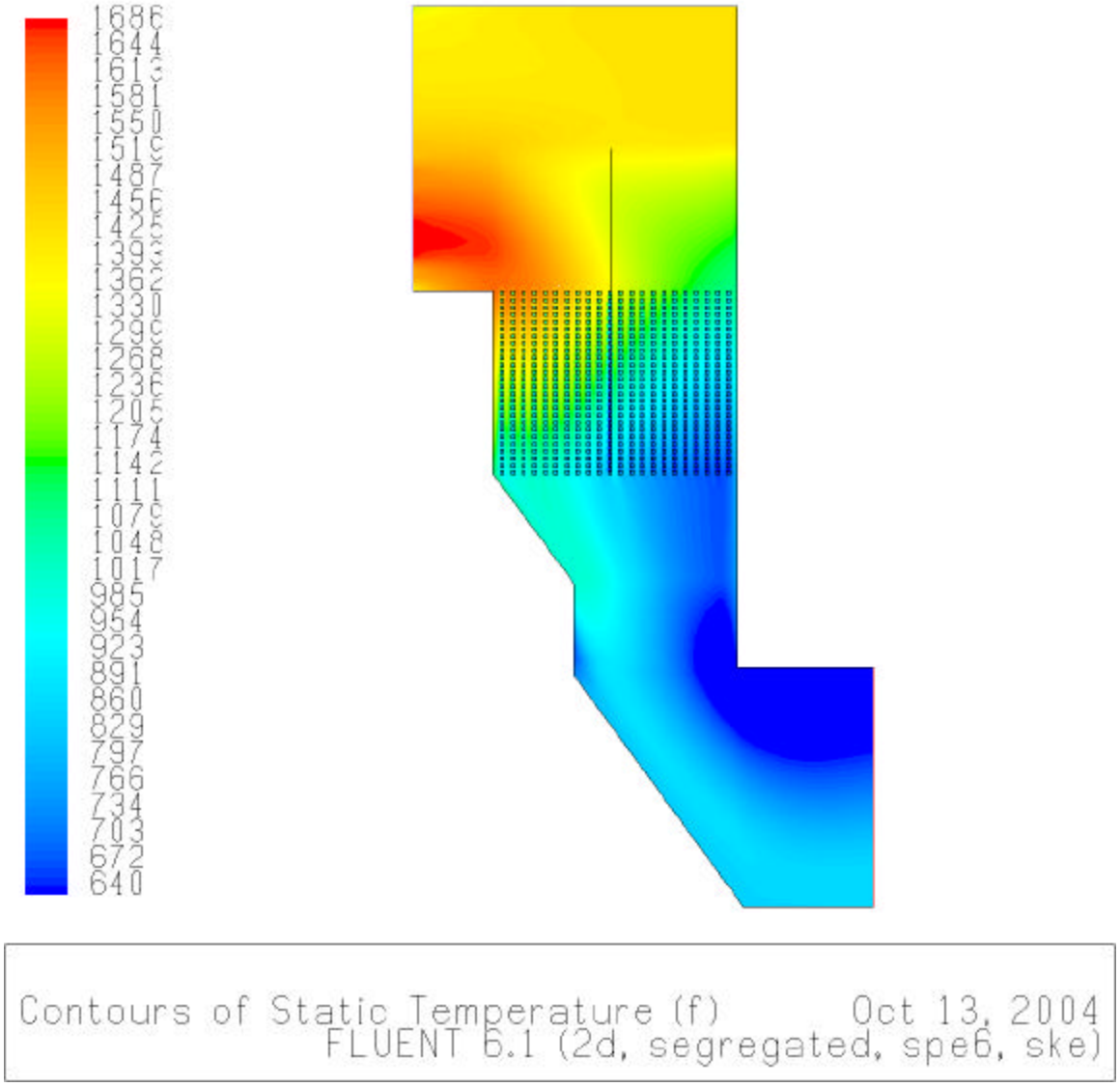

Figure 4-12. Flue Gas Temperature Distribution in HRA, Baseline Case

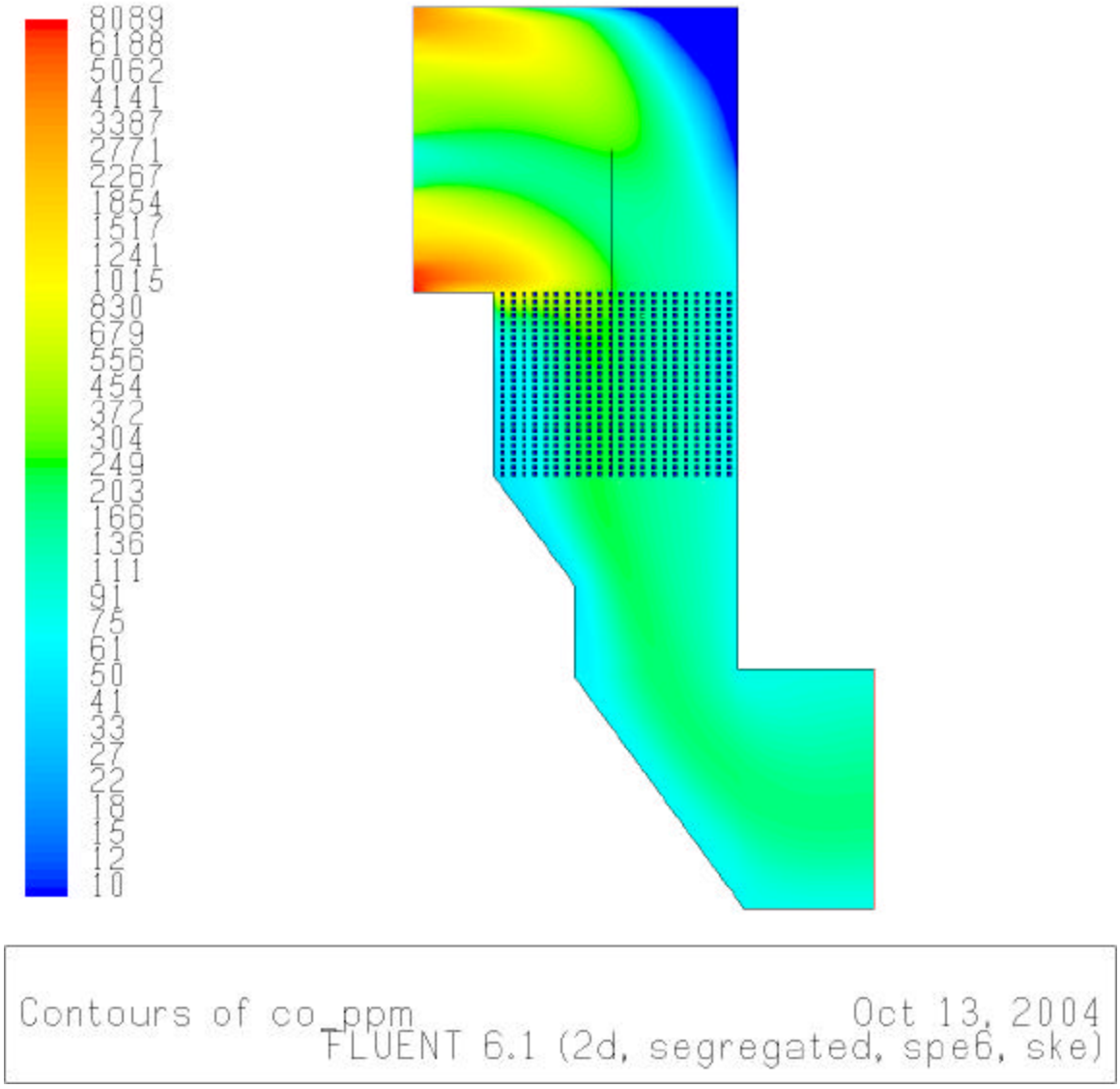

Figure 4-13. CO Distribution in HRA, Baseline Case

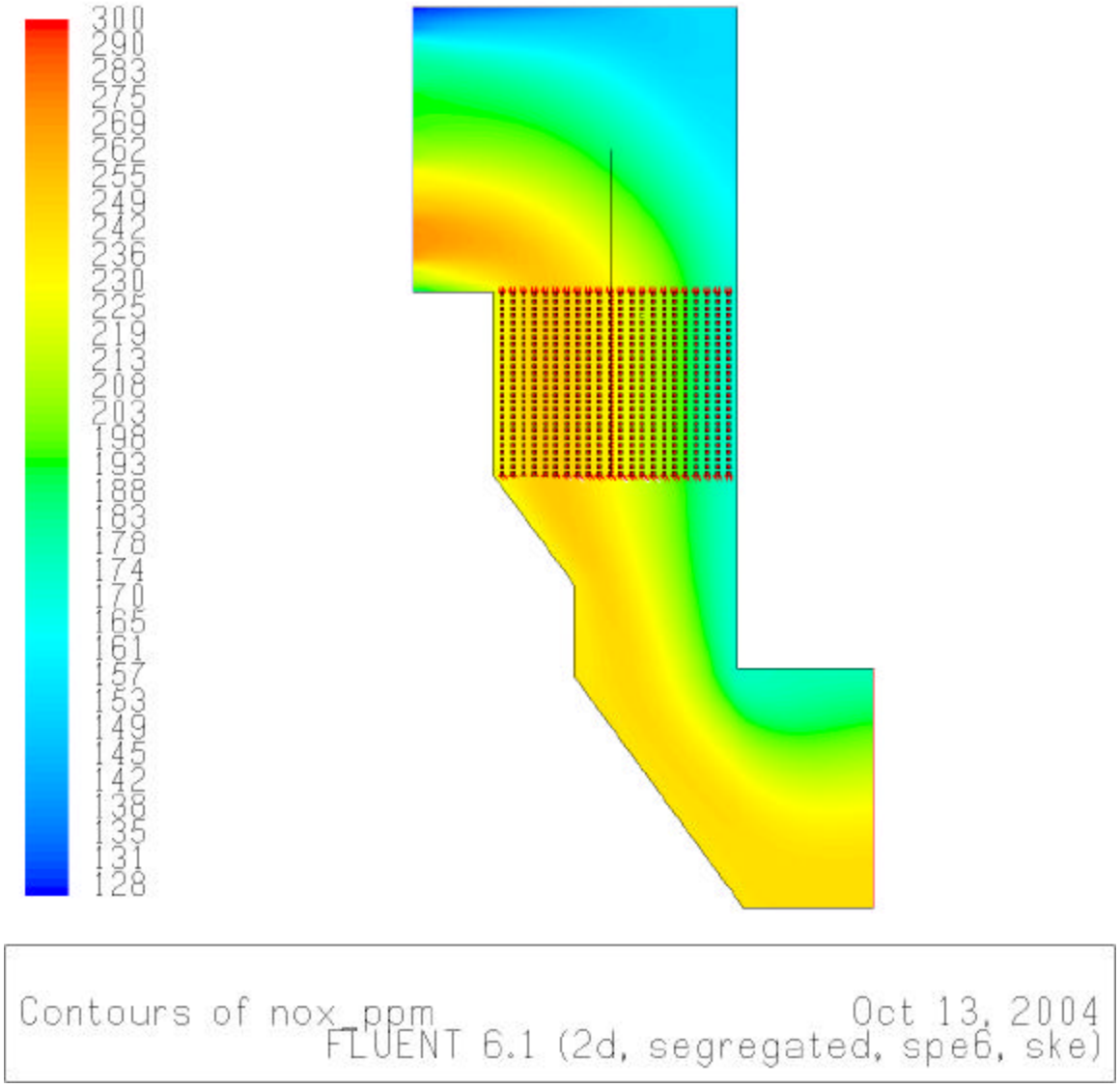

Figure 4-14. NO Distribution in HRA, Baseline Case

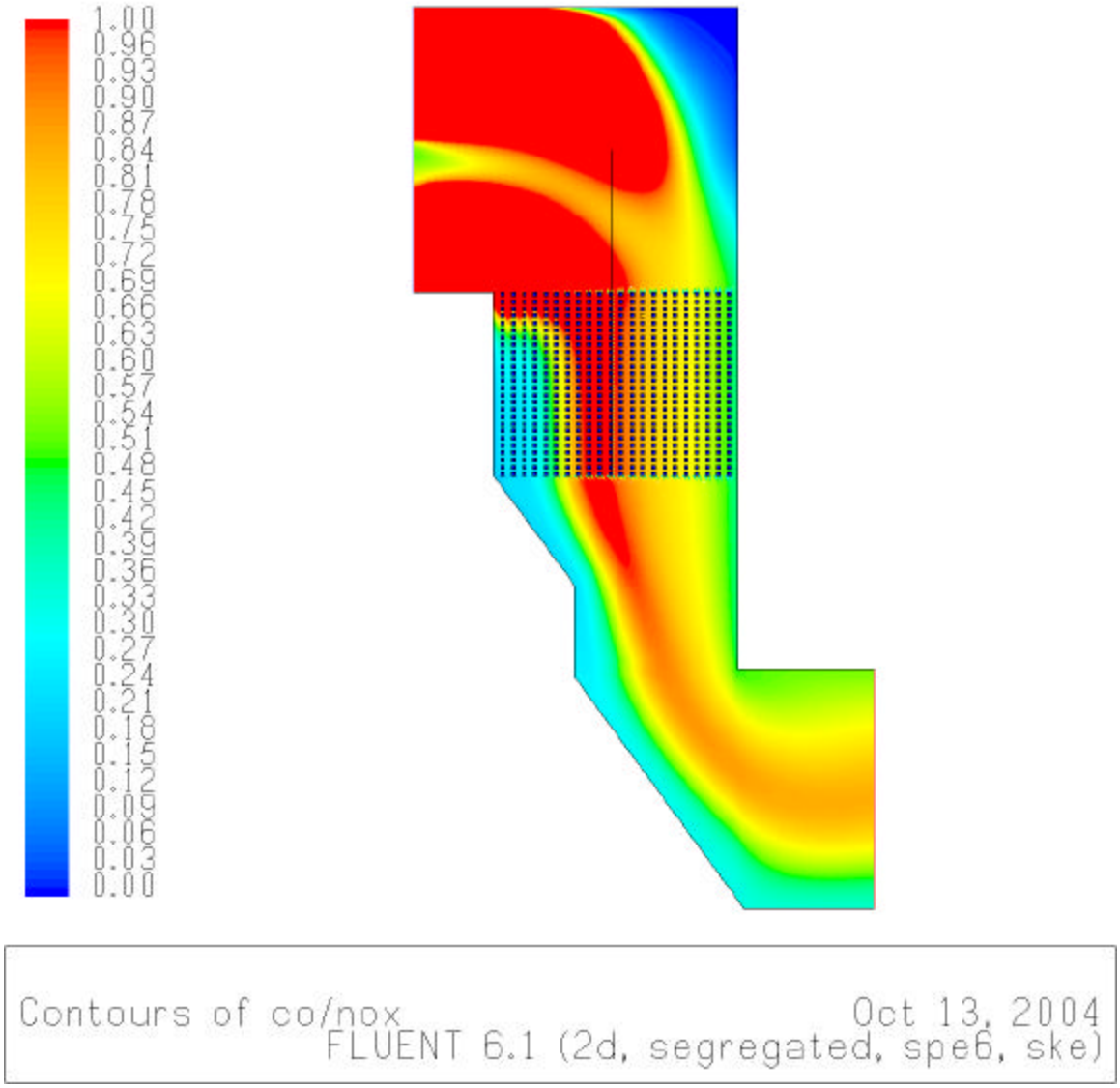

Figure 4-15. CO/NO Distribution in HRA, Baseline Case

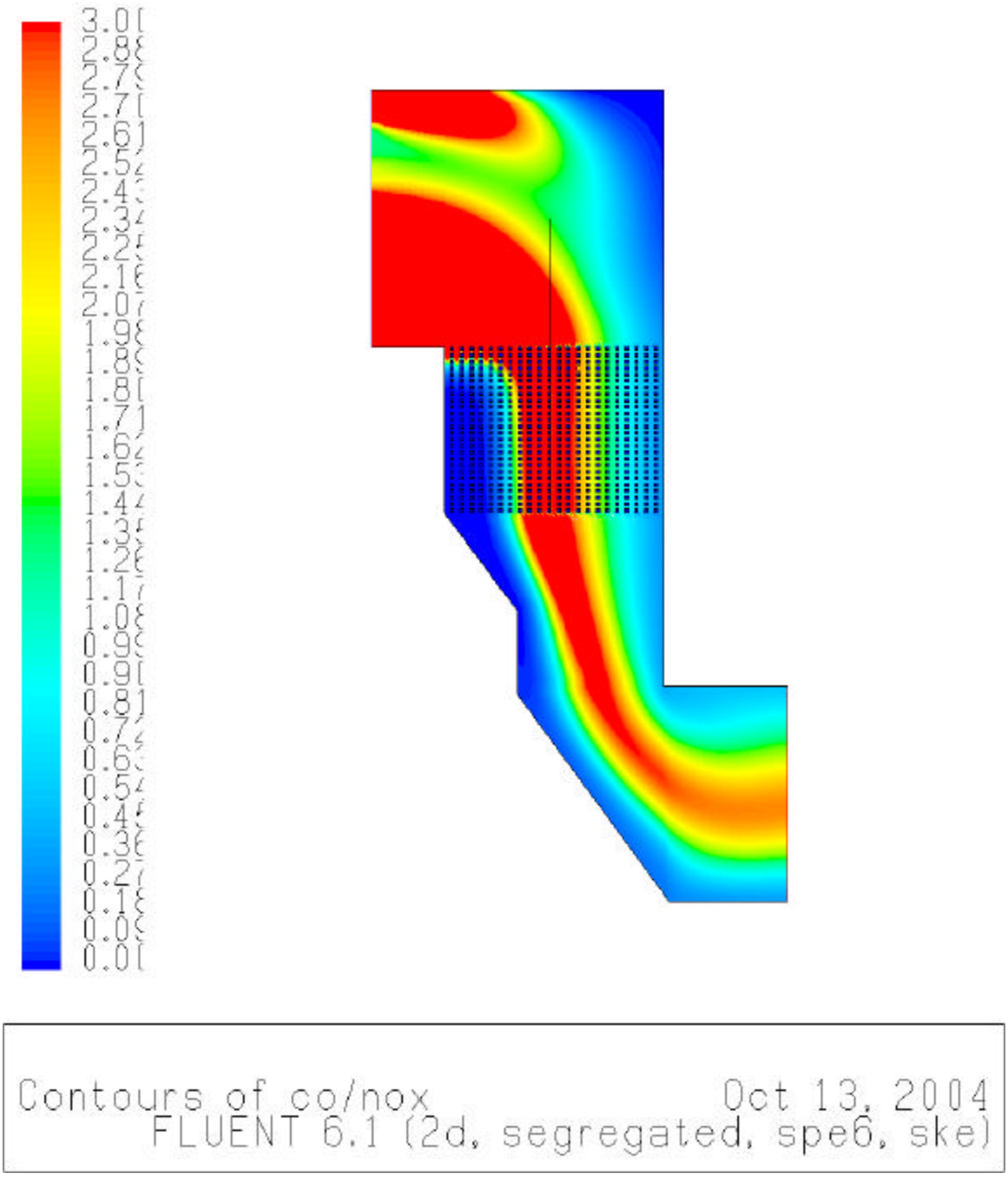

Figure 4-16. CO/NO Distribution in HRA, 40% OFA, 3% O2

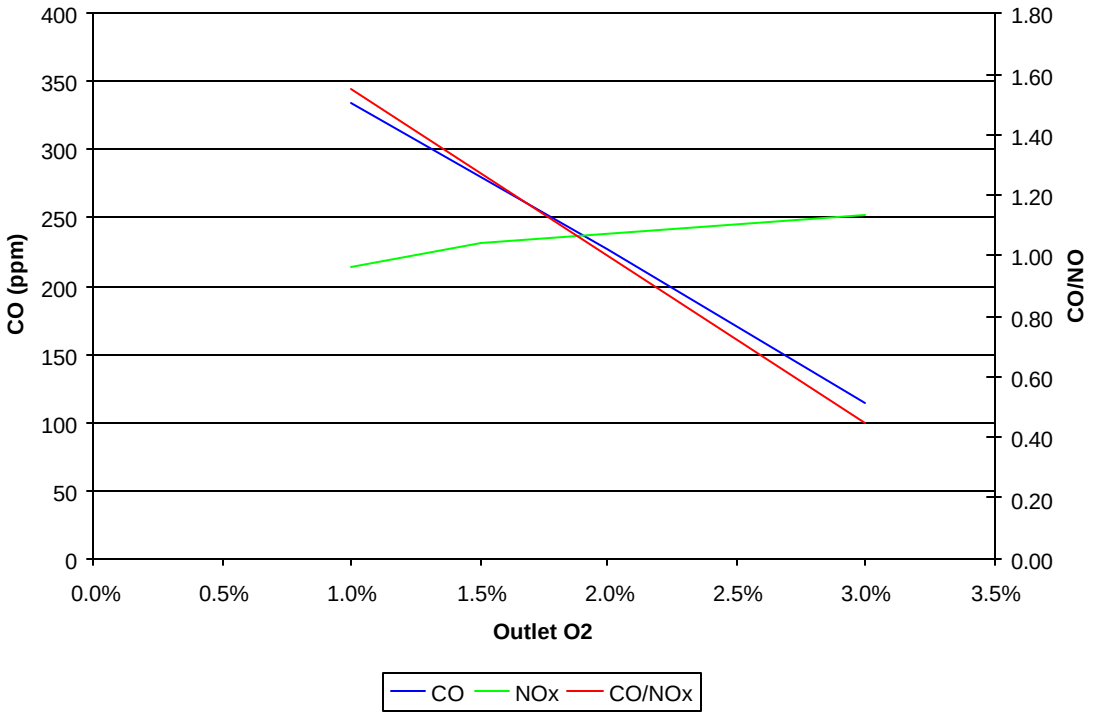

Figure 4-17. HRA Outlet CO and NOx Concentration Versus Outlet O_2

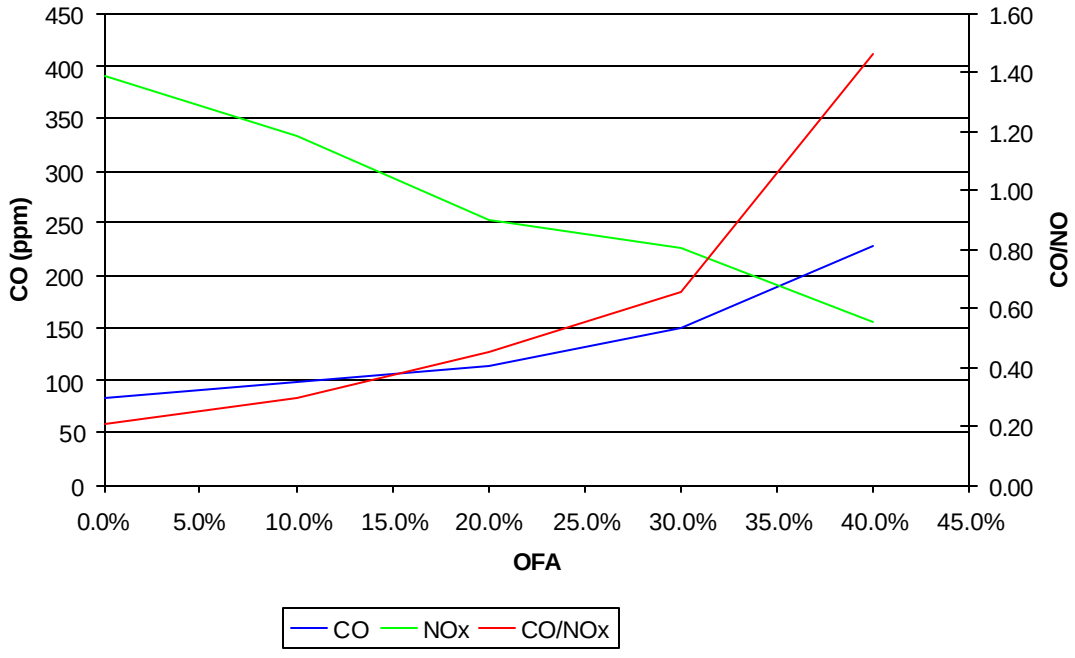

Figure 4-18. HRA Outlet CO and NO Concentration Versus OFA Flow

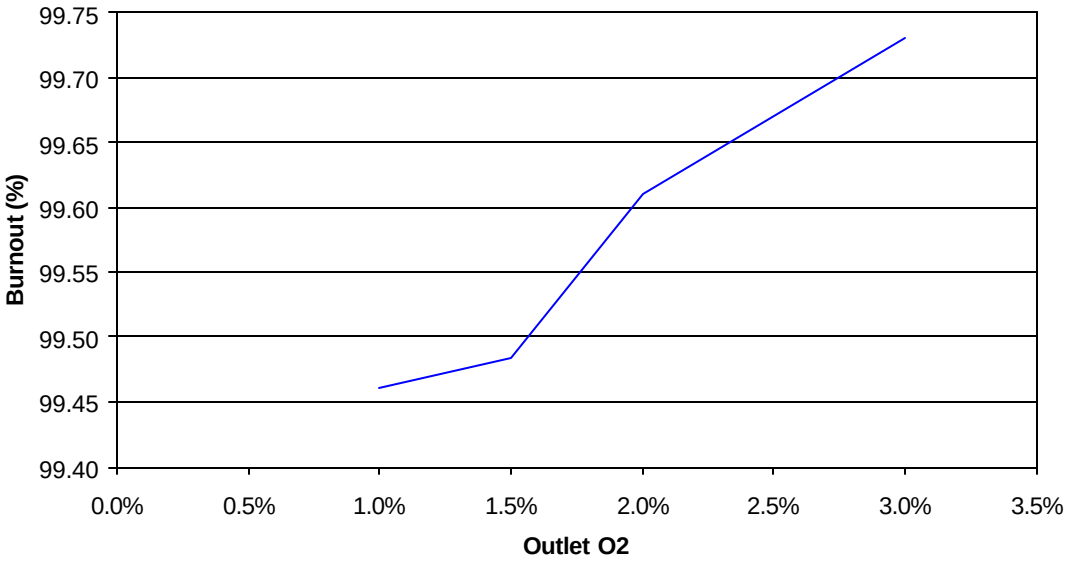

Figure 4-19. Fuel Burnout Versus Outlet O_2

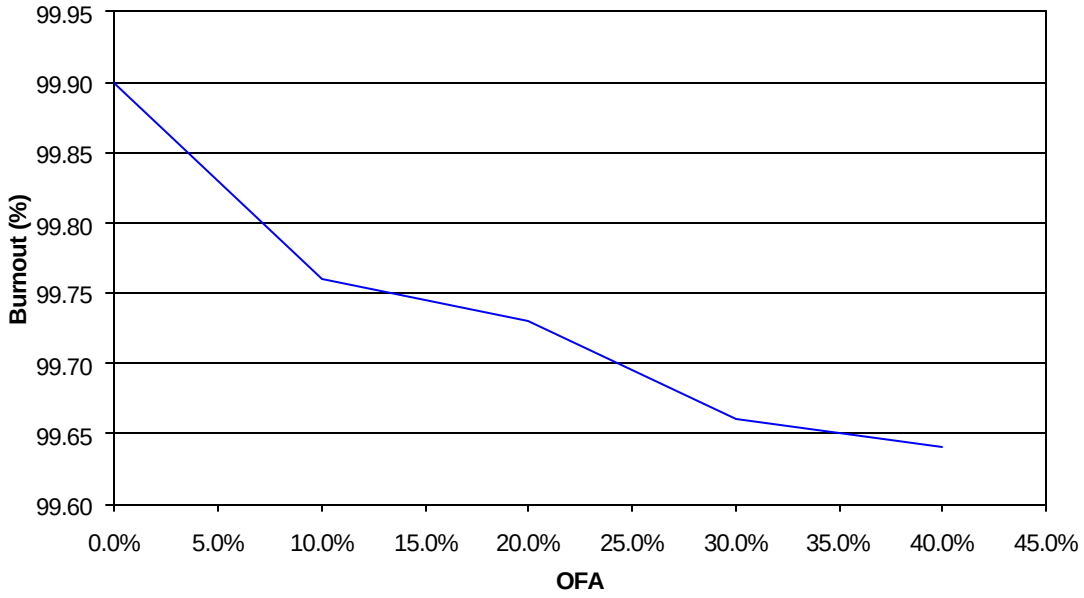

Figure 4-20. Fuel Burnout Versus OFA Flow

4.6 Further Optimization

To achieve even higher CO/NO ratios, additional cases may be investigated including combining lower boiler O_2 with higher OFA flow and taking some burner(s) out of service.

5.0 CATALYTIC REACTOR SCALE-UP AND DESIGN

The basic configuration of the catalytic reactor will be an activated alumina (AA) based, honeycomb type fixed bed reactor. This configuration is selected because of its good structural strength and thermal stability. In addition, it can utilize most of the manufacturing and construction methods currently employed for conventional SCR applications, and will likely be readily accepted by the utility industry. Other configurations, such as entrained flow (injection – capture), granular fixed bed, fluidized bed or moving bed reactors, may be developed to deliver adequate performance and cost-effectiveness, particularly when utilizing low cost carbon-based catalysts. However, these alternative configurations represent a large departure from the current SCR process and therefore may have additional hurdles to gain commercial acceptance.

5.1 Honeycomb Reactor versus Packed Bed of Granular Catalysts

The honeycomb configuration is one that is typical for SCR catalysts, with 7.1 mm pitch, 0.7 mm wall thickness, and 1 m monolith length. The honeycomb is prepared by mixing powders of substrate material, active species and binder material into a homogeneous paste and extruding the paste into monolith form.

As described in Chapters 2 and 3, the catalysts tested in the packed bed rig are activated alumina granules impregnated with active species. The granular material has irregular shape and a median particle size of 1.88 mm. Since the active species are loaded with aqueous impregnation method, a non-uniform distribution of the impregnated species can be expected.

5.2 Transport Phenomena and Limiting Factors of Catalyst Performance

The following transport steps help to determine the catalytic reactor system performance:

- Mass transfer from bulk flow to the outer surface of catalyst.
- Distribution / penetration of active components into the substrate structure. This is particularly important in the case of granular catalysts where active species (e.g. CuO and Fe_2O_3) are impregnated into the substrate.
- Diffusion of reactants (NO and CO) through the catalyst structure to reach inner active sites. The prepared catalysts must have not only sufficient pore volume, but also pores with adequate diameter and free path length to facilitate this diffusion.
- Adsorption of reactants on active sites on the pore surface.
- After reaction, diffusion of the products back to the bulk flow.
- For bi-function, redox catalysts, such as those studied here, the transfer of oxygen between the reducing sites and the oxidizing sites can be an additional limiting factor. The effectiveness of this transfer step is affected by the distance between the two types of sites, which is in turn determined by the relative distribution and density of active species in the substrate structure.

The external mass transfer can be calculated using empirical correlations for various catalyst configurations. The other transport steps described above can be considered using an effectiveness factor, which is defined as (Dogu 1986),

ç = (observed reaction rate / reaction rate if all sites were at external surface conditions)

5.3 External Mass Transfer

To determine the relative importance of external mass transfer, calculations were made for both the packed bed test of granular catalysts and honeycomb reactor. Mass transfer in the fixed bed reactor was calculated from the following equation (Kunii and Levenspiel 1991),

$$Sh = 2 + 1.8\, Re^{1/2}\, Sc^{1/3} \qquad (5\text{-}1)$$

Intra-channel mass transfer of honeycomb monolith was estimated by Equation 5-2 (Gilliland 1934), and Equation 5-3 (Holmgren and Andersson, 1998), separately,

$$Sh = 0.023\, Re^{0.83}\, Sc^{0.44} \qquad (5\text{-}2)$$

$$Sh = 3.53 \exp[0.0298 Re(d_h/L) Sc] \qquad (5\text{-}3)$$

where, d_h and L are hydraulic diameter and length of the monolith channels respectively.

Assuming an inlet concentration of 250 ppm and 80% catalytic reduction of NO, the mass transfer data is summarized in Table 5-1, for both the test rig and a 400 MWe size honeycomb reactor.

Table 5-1. External Mass Transfer Data

	Packed Bed Test Rig	Honeycomb by Eq. 5-2	Honeycomb by Eq. 5-3
Sherwood Number, -	6.5	8.3	4.5
Mass Transfer Co., m/s	1.3E-01	4.9E-02	2.6E-02
Mass Transfer Limit, L_m, kg/s	8.0E-07	1.59	0.86
Total NO Reduced, F_{no}, kg/s	1.6E-09	0.10	0.10
L_m / F_{no}, -	515.7	15.3	8.3

Clearly, the external mass transfer resistance for the packed bed case is negligible. Even for the honeycomb reactor the external mass transfer limit is an order of magnitude larger than the NO reduction rate. Therefore external mass transfer is not a significant rate-limiting factor for the overall reaction.

5.4 Distribution of Active Species in Granular Catalysts

When the catalyst is prepared by the impregnation method, dissolved salts in the solution diffuse through the outer surface into inner pores, and in the mean time they are adsorbed or deposit on

the pore walls physically and/or chemically. This diffusion-adsorption process generates a density distribution for active components, which is high near the particle surface and reduces with depth into the particle. Figure 5-1 is a photo of the cross section of a fresh catalyst particle taken with an optical microscope. Figure 5-2 is a SEM EDX image of the cross section of a similar particle. Both figures clearly show that only a thin outer layer of the substrate is fully penetrated by active components. SEM EDX spectrum analysis of various spots on the cross section also revealed different penetration patterns for CuO and Fe_2O_3 into the alumina substrate: Fe_2O_3 tends to concentrate in a thin shell while CuO tends to diffuse deeper into the particle.

These image analyses also indicate that the granular catalysts used for our laboratory testing can be greatly improved by homogeneously distributing both metal oxides, so that the optimum ratio of the active species can be achieved for the entire volume of the substrate material, thus maximizing the catalyst utilization, reducing required catalyst volume and reactor pressure drop.

Using the aqueous impregnation method, deeper and more uniform distribution can be obtained by using a longer impregnation time, and by using vacuum to withdraw air from the bare support material before impregnation. Since honeycomb elements will be made from uniformly blended fine powders of support material, binder and active components, they will have inherently homogeneous distribution. Therefore the commercial scale reactor with honeycomb catalysts will have higher activity on volume basis than the granular catalysts tested in laboratory.

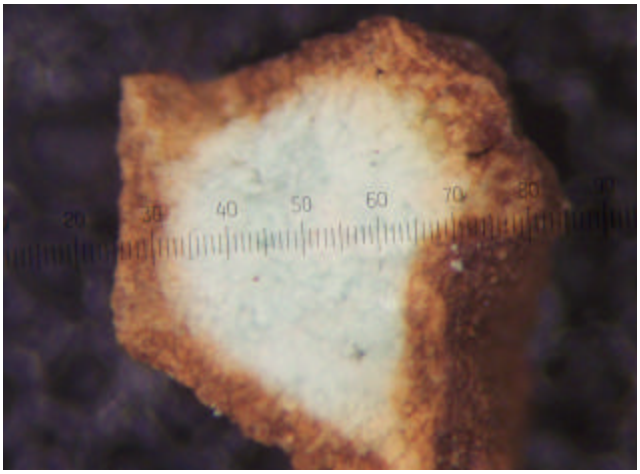

Figure 5-1. Cross Section of a Fresh Catalyst Particle

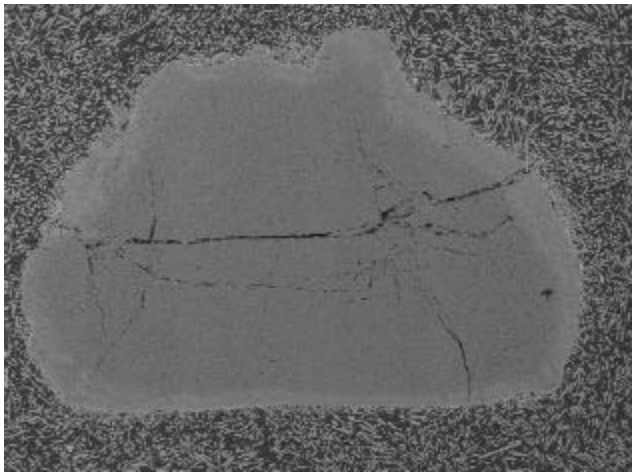

Figure 5-2. SEM EDX Image of Fresh Catalyst Cross Section

5.5 Catalysts Reaction and Scale-Up Model

By introducing the effectiveness factor ç, a general differential catalytic reaction model can be written as,

$$-F\ dC_A = ç\ r_w\ dw = ç\ k_w\ f(C_A)\ dw = ç\ k_w\ f(C_A)\ ñ\ dV \qquad (5\text{-}4)$$

Here F represents the gas volume flow; C_A is the reactant concentration; $r_w = k_w\ f(C_A)$ is the reaction rate per unit mass loading of active component; $f(C_A)$ is a function of C_A depending on reaction order and stoichiometry; ç is catalytic effectiveness factor defined in section 5.2; $dw = ñ\ dV$ is the total mass loading of active components; and ñ is the loading density of active component(s). Solving this differential equation, one will get,

$$-g(x) = - \int (dC_A)/f(C_A) = \int ç\ k_w/F\ ñ\ dV = ç\ k_w\ ñ\ V/F \qquad (5\text{-}5)$$

where x is the fractional conversion of the reactant; g(x) is a function of x, which becomes ln(1-x) for first order reactions.

To get the same g(x), the value of the right hand side of equation (5-5) has to be kept the same. This means that, for a given type of catalyst, same performance (conversion) can be obtained as long as the parameter group $ç\ k_w\ ñ\ V/F$ is kept constant. Therefore, this parameter group represents the scale-up rule for catalytic reactor. For homogeneous catalysts with given ç, k_w, and ñ, the scale-up rule is simplified as V/F, which is catalyst volume based space time (the reciprocal of space velocity). For catalysts with a coating layer of active components, $V = S\ ä$, where S is the external surface area of the coating layer and ä is the coating thickness. With given ç, k_w, ñ, and ä, the scale-up rule becomes F/S, which is the catalyst external surface based area velocity U_s.

Catalyst activity is affected by active component concentrations, their ratios and distributions. The effectiveness factor ç is in fact a measure of the rate of intra-catalyst transport (represented by an effective diffusion coefficient D_{eff}) against the true reaction rate occurring at active sites (k_v), which is a function of temperature for a given catalyst. Solution of the steady state differential equation for the mass conservation of reactant diffusing through the catalyst structure leads to the expression of ç as a function of ö, where ö is the Thiele modulus. For first order reactions, $ö = (k_v/D_{eff})^{1/2}\ ä$, where ä is the equivalent penetration depth. ç can be expressed as,

$$ç = \tanh ö / ö \qquad (5\text{-}6)$$

As shown in Figure 5-3, ç approaches one for very small ö values, and 1/ö for large ö values.

In a complex system, such as those with redox catalysts, the density distributions of active components affect the reaction rate or activity. Let,

$$ç\ k_w \quad A_ç\ e^{-E/RT} \qquad (5\text{-}7)$$

The observed reaction activation energy from equation (5-7) will be a good index to study the parameter group $ç\ k_w$, which can be calculated from equation (5-5) with given $ñ\ V/F$ and g(x) from test data.

If the catalytic reaction is under the pore diffusion limitation (with very large ö), the observed activation energy E will be only half of the true reaction activation energy E_t ($E = E_t/2$). Any change in ö (or ç) will cause E to change between $E_t/2$ to E_t. Only when ç 1.0, E will remain nearly constant ($E \quad E_t$) as ö changes.

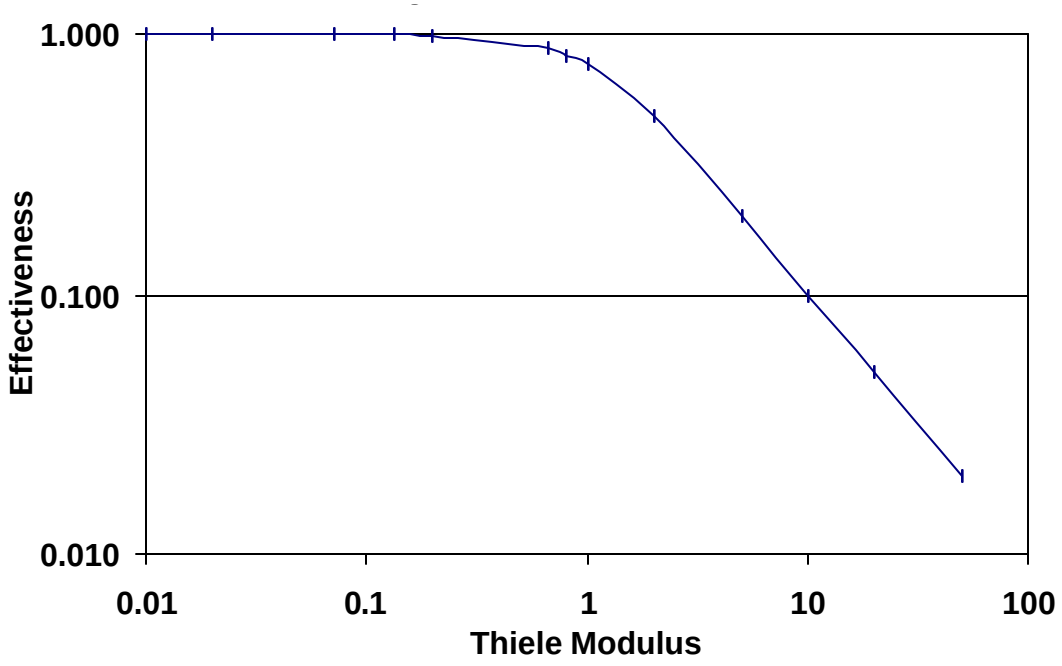

Figure 5-3. Effectiveness Factor as a Function of Thiele Modulus

5.6 Reaction Order and Activation Energy

Different reaction orders can be applied to Equation 5-5. For example, for the first order chemical reaction, $f(C_A) = C_A$ and $g(x) = \ln(1-x)$. The test data have been plotted in the form of conversion versus reaction temperature, as shown in Figure 5-4. Included in the same chart are curves of predicted x for various test conditions by the catalyst reaction model. After trying different reaction orders, it was determined the model with first order assumption gives the best fit for the data, as shown in Figure 5-4.

The observed activation energy for each test can be obtained by plotting ç k_w vs. the reciprocal of reaction temperature, as shown in Figure 5-5, in which the line slopes represent E/R with the unit K. All data series in Figure 5-5, with the exception of J and K, demonstrate an activation energy E/R of approximately $13x10^3$ K. This activation energy means that the reaction rates for these catalysts double every time the reaction temperature is increased for about 15 K, in the temperature range tested. This is comparable with the rate of the typical, kinetically controlled reactions, which as a rule of thumb doubles for every 10 K temperature rise.

Type J and Type K catalysts contains cerium and potassium respectively. As shown in Figure 5-5, the additional promoters Ce ad K lower the observed E/R, to about 30-40% of that of other catalysts.

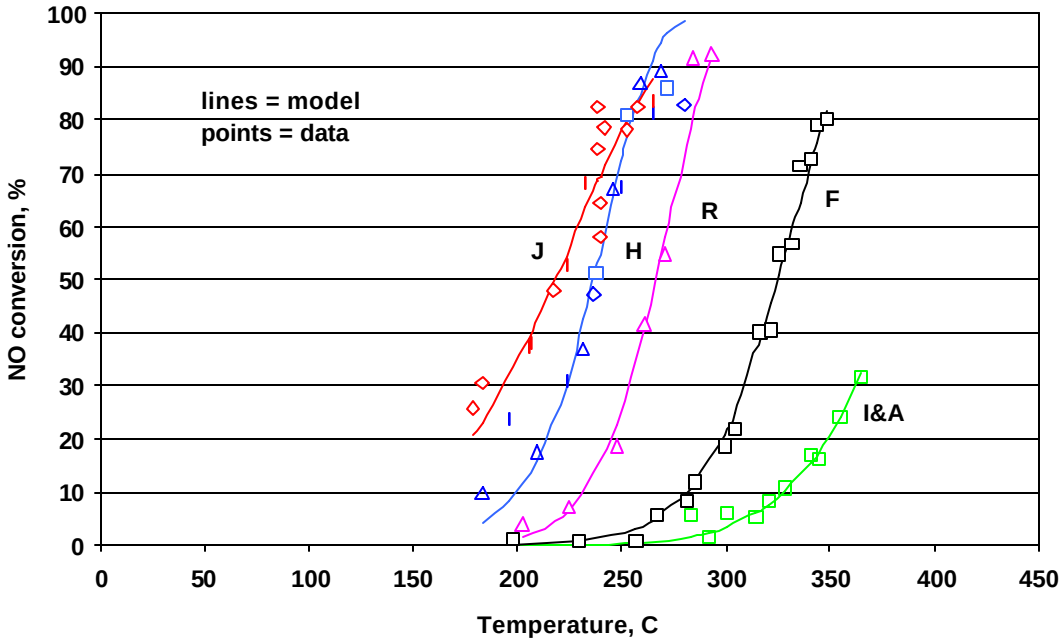

Figure 5-4. Test Data and Model Prediction with First Order Assumption

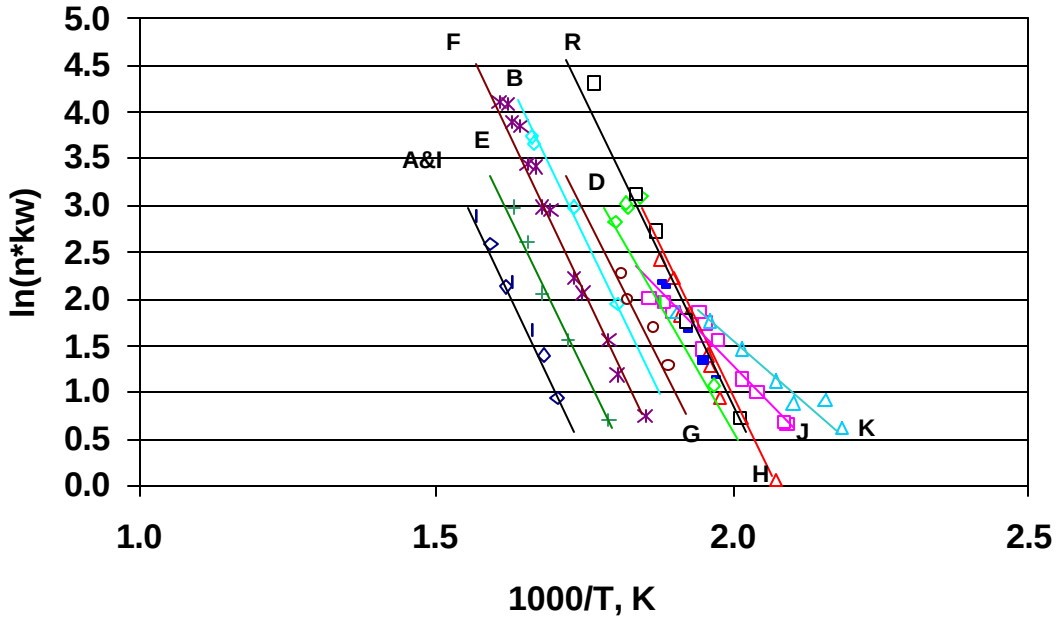

Figure 5-5. Observed Activation Energy of Test Data

5.7 Catalyst Effectiveness Factor

From the discussions in section 5.5, one can see that direct determination of the effectiveness factor involves iteration of Equations 5-5, 5-6 and a given effective diffusion coefficient (D_{eff}) value. Because D_{eff} is unknown for the tested catalysts, indirect methods based on in-depth test data analysis were used to infer the approximate range of the effectiveness factors.

Data series H and R were obtained under different space velocities (5250 1/hr for R and 1050 1/hr for H) with the exact same catalyst (see Table 2-1). Because of the 5:1 ratio in space velocity (F/V), it is expected that higher reaction temperature (and therefore higher k_w) will be needed for series R to achieve the same NO conversion than series H. Based on Equation 5-5, series R must have five times higher ç k_w to get the same conversion level as series H.

On the other hand, the test data show that T_{50} (reaction temperature for 50% conversion) for series R is 27 ºC higher than H. Using observed activation energy, the temperature increase is related to a 4.5 time increase in k_w, indicating ç is about the same for both H and R, and in both cases very close to one.

Using ç k_w of 4.5 to 5, one can also estimate the change of ö from H to R is about 2.1 – 2.2 times, since ö = $(k_v/D_{eff})^{1/2}$ ä , and D_{eff} is relatively insensitive to the small temperature change. This magnitude of change in ö without causing large change in ç is only possible when ö is very small (predominantly reaction rate limitation) and ç is very close to 1.

Now, in order to estimate how close ç is to1, one can make reasonable approximations of D_{eff}. One way is to use the Knudson diffusion coefficient, which can be calculated based on pore size and temperature (Dogu 1986). Knudson coefficient describes the diffusion through capillary (with pore-radius-to-mean-free-path-ratio typically less than 0.1), and represents the lower limit of effective diffusion coefficient, D_{eff}, which includes the effect of both Knudson diffusion and ordinary molecular diffusion.

Table 5-2 summarizes the calculated D_k and $ç_k$. The pore surface area and volume data are from Perry and Chilton (1973). With the diffusion coefficient, ç can be calculated from test data by iterating Equations 5-5 and 5-6. The effectiveness factors given below are for series H and O data at 50% NO conversion.

Table 5-2. Pore Diffusion and Effectiveness Factor Calculation

Type of Substrate	Pore Surface Area, m^2/g	Pore Volume ml/g	Pore Radius, Å	Knudson Diff. Co. D_K, cm^2/s	Effectiveness Factor $ç_k$, -
AC	525	0.59	22	0.0093	0.96
AA	175	0.39	45	0.0185	0.98

Since D_k represents the lower limit of D_{eff}, the true effectiveness factors will be even higher than the values in Table 5.2. By comparative analysis of the data series for the same catalyst tested under different space velocities, for example H and R, or O and P, D_{eff} was estimated to be about 0.04 for catalysts with AC support and 0.07 for those with AA support, in the tested temperature

range. With these D_{eff} values, the effectiveness factors can be determined as over 99% for all tests at low space velocity and over 96% for the tests at the high space velocity.

With the estimated diffusion coefficient, the reactant concentration distribution from the bulk flow to the center of the catalyst element can be determined. Figure 5-6 depicts the relative NO concentration profile for the granular AA catalyst in lab testing as well as the honeycomb configuration to be used for commercial scale design, assuming a D_{eff} of 0.07 cm^2/s.

It is clear that both external mass transfer and pore diffusion are not significant limiting factors for the reaction in both laboratory and honeycomb reactor cases. The above analysis indicates very high catalyst effectiveness was achieved during laboratory tests and the granular catalysts displayed a volume-dependant activity behavior. Because the catalysts had only limited penetration by active components, catalytic performance can be further improved by uniformly distributing active components in the substrate structure. Also because of the high catalyst effectiveness observed from the test data, increasing the active component loading will be an effective way to raise activity of the catalyst. The commercial application will use a honeycomb configuration with homogenous chemical composition and with the flexibility to load various levels of active components. Therefore, the commercial honeycomb catalysts can be designed with high reactivity and effectiveness.

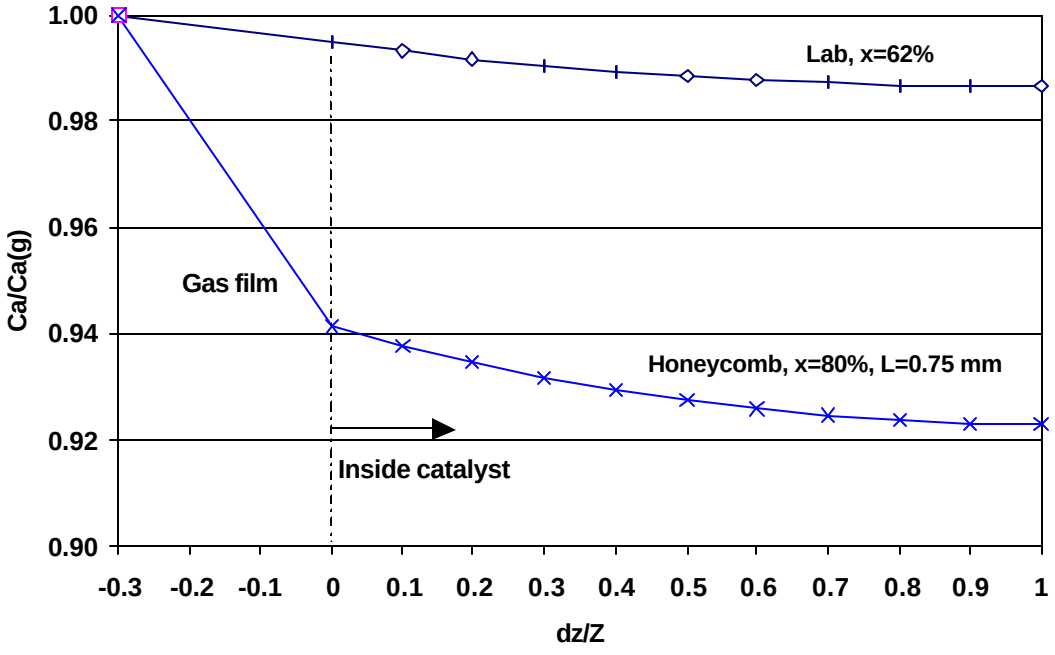

Figure 5-6. Reactant Distribution Profile for Lab and Honeycomb Catalysts

5.8 Reactor Conceptual Design

As the previously reported work in Chapter 4 indicates, adequate CO/NO ratios, as required by the downstream reactor (the AF-SCR), can be obtained by modifying furnace operating conditions, without significant physical changes to the burner and boiler equipment. Therefore, the design and cost impact on the furnace / boiler proper due to the new NOx control system will be minimal, and the system design effort is mainly devoted to the conceptual design of the catalytic reactor.

5.8.1 Selection of Reactor Type

The selected honeycomb configuration is one that is typical for conventional SCR catalysts, with 7.1 mm pitch, 0.7 mm wall thickness, and 1 m monolith length. The honeycomb will be prepared by mixing powders of substrate material, active species and binder material into a homogeneous paste and extruding the paste into monolith form.

5.8.2 Reactor Design and Performance

The basis for the commercial-scale design of the ammonia-free selective catalytic reactor (AF-SCR) is an existing 400 MWe bituminous coal-fired power plant. The plant is assumed to have existing low NOx burners and to add the AF-SCR system to further reduce NOx. The assumed site conditions are an elevation of 425 feet above sea level; a design ambient temperature of 60ºF; and a relative humidity of 60%. The reactor is designed to produce an 80% NOx reduction (outlet NOx = 0.08 lb/MMBtu).

Similar to the conventional SCR catalyst, the AF-SCR reactor will be located in the boiler heat recovery area, between the economizer and the air preheater. The flue gas temperature at the inlet to the AF-SCR is 600 ºF. Table 5-3 presents the performance and geometry of the catalyst. The detailed catalyst test data analyses and modeling revealed that the AA catalysts had very high catalyst effectiveness and catalyst activity can be increased by increasing the amount of active components in the catalyst. Based on this, active components loadings higher than those used in the laboratory testing have been selected for the honeycomb catalysts to reduce the volume of catalyst. Since the active metals were distributed in only a thin layer of the experimentally tested substrate granules as described previously, increasing the metal loadings should be feasible. The catalyst inlet molar CO/NO ratio is 2.0. The CO is reduced by 85% by the catalyst producing an outlet CO concentration of 86 ppmv.

The catalyst volume and monolith geometry detailed in Table 5-3 is similar to current ammonia-based SCR catalysts. Catalyst opening size and gas velocity are selected to maximize catalyst life in a high dust coal-fired power plant. Pressure loss through the reactor is limited to 2.0" H_2O.

Figure 5-7 presents the arrangement of the AF-SCR, which is very similar to the ammonia-based SCR system, but without the ammonia storage, handling and injection system. The dimensions of the reactor are 35'-9" X 53' X 41'-9" (height). Turning vanes (not shown) are provided in the reactor entrance hood to create even downward flow distribution to the catalyst. Upstream of the

catalyst is a rectifier, which straightens the flow to reduce catalyst erosion. The reactor contains three layers with acoustic horns or soot blowers upstream of each layer for ash removal.

Table 5-3. 400 MWe AF-SCR Performance and Catalyst Geometry

Gas Flow Rate	lb/hr	3,500,000
Gas Temperature	F	600
Inlet NOx	ppmv	285
	lb/MM Btu	0.40
Outlet NOx	ppmv	57
	lb/MM Btu	0.08
NOx Removal Efficiency	%	80%
Inlet CO	ppmv	570
Outlet CO	ppmv	86
CO Removal Efficiency	%	85%
Pressure Drop	in H2O	1.9
Catalyst		
Flow Area	ft2	1247
Open Area	%	81.3%
Opening	mm	6.4
Length	m	2.60
Layers		3
Pitch	mm	7.1
Wall Thickness	mm	0.7
Surface Area	ft2	2,026,982
Volume	ft3	13,095
Space Velocity	1/hr	3582
Internal Linear Velocity	ft/sec	21.3
Approach Linear Velocity	ft/sec	17.3

Figure 5-7. 400 MWe AF-SCR System General Arrangement

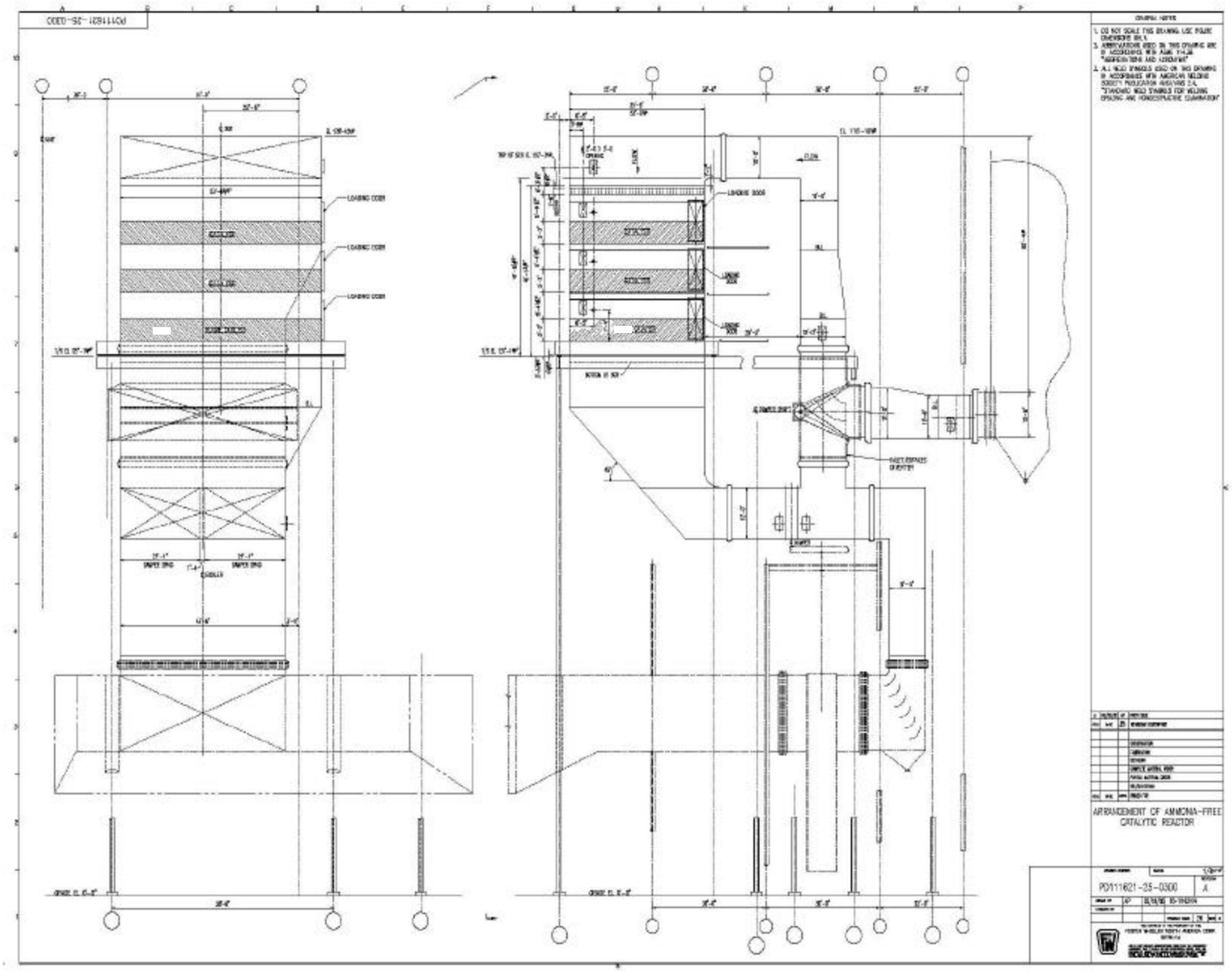

6.0 COST ANALYSIS

As the previous chapters indicate, adequate CO/NO ratios required by the downstream AF-SCR reactor can be obtained by modifying furnace operating conditions, without significant physical changes to the burner and boiler equipment. Therefore, the design and cost impact on the furnace / boiler proper due to the new NOx control system will be minimal, and the cost evaluation effort is focused on the post combustion control by AF-SCR.

6.1 Basis for Cost Analysis

The basis for cost evaluation is the commercial-scale design of an ammonia-free selective catalytic reactor (AF-SCR) retrofitted to an existing 400 MWe bituminous coal-fired power plant, as described in Chapter 5. The plant is assumed to have existing low NOx burners and to add the AF-SCR system to further reduce NOx. The catalyst used is activated alumina (AA) based, honeycomb type, with iron oxide and copper oxide as active components.

6.2 Cost of Catalyst

Cost of catalyst contains the cost of raw materials (including substrate and active components) and cost of manufacturing. It is assumed that the same manufacturing process used today for honeycomb type SCR catalysts will be used for the AF-SCR catalyst. Therefore the cost of the AF-SCR catalyst may be estimated based on the typical cost of conventional SCR catalysts and costs of raw materials. As shown in Table 6.1, the bulk costs for AF-SCR raw materials (activated Al_2O_3, CuO and Fe_2O_3) are significantly lower than those for SCR raw materials. Therefore, the AF-SCR catalyst cost is estimated to be about $90 per cubic foot, which is 29% less than that of conventional SCR catalyst.

Table 6-1. Estimation of AF-SCR Catalyst Cost

SCR Catalyst Cost Calculation		
SCR Catalyst Delivered Cost	$/m3	4500
	$/ft3	127
	$/lb	6.57
Catalyst Real Density	lb/ft3	19.4
SCR Bulk Raw Material Cost		
V2O5 Bulk Cost	$/lb	3.90
WO3 Bulk Cost	$/lb	4.12
TiO2 Bulk Cost	$/lb	2.50
Catalyst Raw Material Cost	$/lb	2.64
Balance of Catalyst Cost	$/lb	3.92
New Catalyst Cost Estimate		
Bulk Raw Material Cost		
CuO	$/lb	2.98
Fe2O3	$/lb	0.39
Activated Alumina	$/lb	0.50
Catalyst Raw Material Cost	$/lb	0.74
New Catalyst Cost	$/lb	4.66
	$/m3	3194
	$/ft3	90.4

6.3 Cost of Ammonia

Conventional SCR systems use anhydrous or aqueous ammonia, or urea as reagent. Of the three, anhydrous ammonia is the most concentrated and least expensive reagent, and requires least on-site processing. Anhydrous ammonia is selected as the reagent for this cost evaluation.

Natural gas is used in the manufacturing of ammonia and accounts for as much as 90% of the product cost of anhydrous ammonia. Since 2002, the natural gas price has risen sharply from under $3/MMBtu to over $10/MMBtu. Figure 6.1 shows the trend of anhydrous ammonia price (CFR at Tampa, Florida, and FOB at Yuzhnyy, Ukraine) over the same period (http://www.fertilizerworks.com/fertreport/pdf/2005/TheMarket-051013.pdf). A price of $350/ton for anhydrous ammonia delivered to the plant is used in this study.

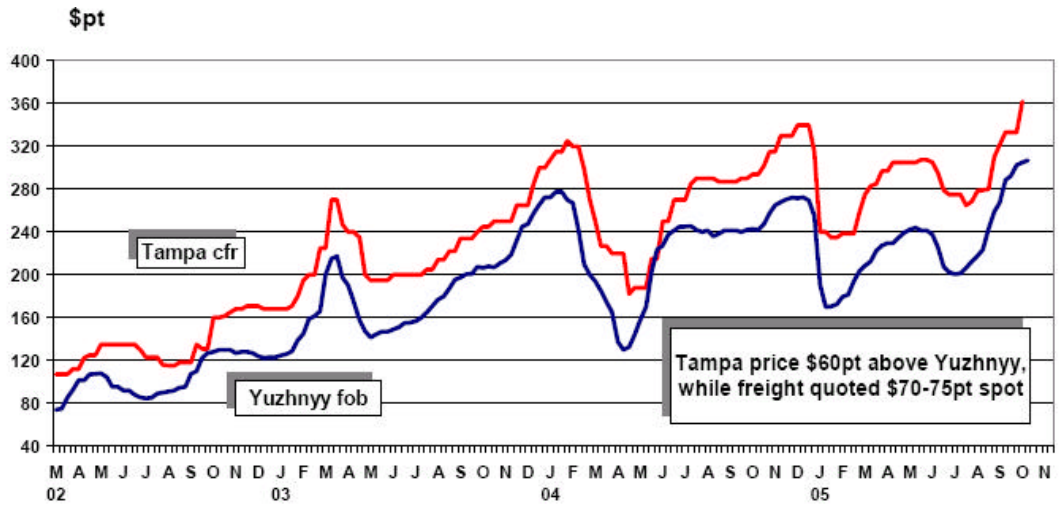

Figure 6-1. Price Trend of Anhydrous Ammonia

6.4 Cost Evaluation of Ammonia-Free NOx Reduction System

Table 6.2 summarizes the overall performance data and cost summary of the AF-SCR and A conventional SCR system for the 400 MWe pulverized coal fired plant described in section 5.8. The AF-SCR has lower capital cost than SCR due to the elimination of the ammonia storage and handling system, and also the low cost catalyst used for AF-SCR. The estimated capital cost for the AF-SCR system is $81/kw, 17% lower than a SCR system which is estimated at $98/kw. For the 400 MWe plant, the savings in capital investment due to AF-SCR is approximately 6.8 million dollars.

The largest O&M cost saving is the avoided cost of ammonia reagent. Smaller savings are projected in catalyst replacement cost, fixed O&M cost and system energy cost. For the 400 MWe plant, the total O&M cost of the AF-SCR system is about 0.89 million dollars per year.

Table 6.3 gives the levelized cost analysis of NOx removal, in both constant 2004 dollars and current dollars. In constant 2004 dollars, the cost of NOx removal by AF-SCR system is estimated as $776/ ton, or 29.5% lower than the removal cost with current SCR technology. For the 400MWe unit, the present value of total cost savings for NOx control due to the AF-SCR system is approximately 19 million dollars.

It should be noted that the cost analysis described here is based on anhydrous ammonia, which is the least expensive ammonia reagent. Anhydrous ammonia is a controlled hazardous substance and is generally not acceptable for plants located in or near cities. Additionally, the analysis includes only direct costs, without considering the costs associated with the special siting, permitting, and safety training requirements for an anhydrous ammonia system. Therefore the cost savings projected above are conservative.

Table 6-2. NOx Control Performance and Cost Summary

Item	Unit	SCR	AF SCR
A. Plant Overall Data			
Plant Net Electrical Output	MWe	400	400
Total Plant Heat Input	MMBtu/hr	3567	3567
SCR Inlet NOx	lb/MMBtu	0.40	0.40
SCR NOx Reduction	%	80.0%	80.0%
Plant NOx Emissions	lb/MMBtu	0.08	0.08
Total Flue Gas Flow	lb/hr	3,500,500	3,500,500
NH3 Consumption (anhydrous)	lb/hr	466	0
Atomizing Air Consumption	lb/hr	9320	0
Total Catalyst Volume	M^3	371	371
Catalyst Life	hours	24,000	24,000
SCR Pressure Drop	"H2O	4.0	4.0
Fan Efficiency	%	70%	70%
Anhydrous Ammonia Cost	$/ton	350	-
Electricity Cost for Plant Use	$/kWhr	0.04	0.04
Plant Annual Capacity Factor	%	85%	85%
Total NOx Removed	ton/yr	4,250	4,250
B. Capital Cost			
Ammonia System Design & Supply	$	2,900,000	-
Initial Catalyst Charge	$	1,669,500	1,184,902
Reactor and BOP Modification D. & S.	$	14,950,217	14,950,217
Total System Erection & Commissioning	$	19,519,717	16,135,120
Total DeNOx Retrofit Capital Cost	$/kW	98	81
	$	39,039,434	32,270,239
Savings in Capital Cost	$		6,769,195
	%		17.3%
C. Operating and Maintenance Cost			
Fixed O&M Cost	$/yr	257,660	212,984
	$/kW-yr	0.644	0.532
Anhydrous Ammonia Cost	$/yr	607,221	-
	mills/kWhr	0.204	-
Catalyst Replacement Cost	$/yr	710,227	504,073
	mills/kWhr	0.238	0.169
Energy Requirement			
Ammonia Heating	$/yr	23,965	-
Atomizing Air	$/yr	3,294	-
Reactor Pressure Loss	$/yr	234,741	234,741
Total Energy Cost	$/yr	261,999	234,741
	mills/kWhr	0.088	0.079
Total Variable O&M Cost	$/yr	1,579,447	738,814
	mills/kWhr	0.530	0.248

Table 6-3. Financial Analysis for NOx Control

Item	Unit	SCR	AF SCR
D. Financial Parameters			
Term	year	30	30
Inflation Rate	%	3.0%	3.0%
Real Escalation	%	0.0%	0.0%
Constant Dollar Cost of Capital	%	6.0%	6.0%
Apparent Escalation	%	3.0%	3.0%
Discount Rate	%	9.2%	9.2%
E. Levelized Cost, Current $			
Levelization Factor for Capital Cost		0.099	0.099
Levelization Factor for O&M Cost		1.361	1.361
Capital Cost	$/yr	3,860,756	3,191,325
	mills/kWhr	1.296	1.071
Fixed O&M Cost	$/yr	350,742	289,925
	mills/kWhr	0.118	0.097
Variable O&M Cost	$/yr	2,150,032	1,005,714
	mills/kWhr	0.722	0.338
Total Levelized NOx Control Cost	$/yr	6,361,530	4,486,965
	mills/kWhr	2.136	1.507
	$/ton NOx	1,497	1,056
Cost Saving	%		29.5%
	$/yr		1,874,565
PV of Total Savings	$		18,955,343
F. Levelized Cost in 2004 $			
Levelization Factor for Capital Cost		0.073	0.073
Levelization Factor for O&M Cost		1.000	1.000
Capital Cost	$/yr	2,836,172	2,344,398
	mills/kWhr	0.952	0.787
Fixed O&M Cost	$/yr	257,660	212,984
	mills/kWhr	0.087	0.072
Variable O&M Cost	$/yr	1,579,447	738,814
	mills/kWhr	0.530	0.248
Total Levelized NOx Control Cost	$/yr	4,673,280	3,296,195
	mills/kWhr	1.569	1.107
	$/ton NOx	1,100	776
Cost Saving	%	-	29.5%
	$/yr	-	1,377,085
PV of Total Savings	$	-	**$ 18,955,343**

7.0 CONCLUSIONS and FUTURE RESEARCH WORKS

Furnace Optimization: Furnace optimization study indicates that adequate CO/NO ratios can be obtained by modifying furnace operating conditions, without any physical changes to the burner and boiler equipment. By reducing the overall excess air level or by increasing the over fire air portion of total combustion air, CO concentration in the flue gas can be increased, and NO reduced. CFD simulation suggests that CO/NO ratio of about 1.5 is achievable by either excess air or over fire air adjustments. The effects by these adjustments on boiler efficiency, unburned carbon in flyash, and furnace exit gas temperature are relatively small and within the range seen in normal power plant operations. Higher CO/NOx ratios may be achieved by combining lower boiler excess air with higher OFA flow, and / or by taking some burner(s) out of service.

Catalyst Development: Although precious metal catalysts have been successfully applied in the automobile industry to convert NO with CO and hydrocarbons as reductants, they require a reducing environment as typically found in the gasoline engine exhaust, and therefore are not suitable for power plant flue gas applications, where oxidizing conditions must be maintained for safety and efficiency considerations. The base metal catalysts, prepared and tested in this study, exhibited very promising NO conversion under simulated power plant flue gas conditions, including 3% oxygen. This is a crucial step towards a practical, ammonia-free, catalytic NOx reduction system for combustion power plants.

The experimental work with multi-component catalysts made from depositing Fe, Cu, Ce and K oxides on activated carbon (AC) and activated alumina (AA) supports has led to the following major observations:

- NO reduction in the range of 80-90% (outlet NO only 25-50 ppmv) was achieved in multiple repeat test runs with operating temperature ranging from 230-350^{o}C for various AC or AA based catalysts.
- All tested catalysts showed excellent N_2 selectivity upon NO reduction. For AC based catalysts, only 0-12% of NO was converted to N_2O, depending on the combination of active components. No significant N_2O formation was observed during the tests with AA based catalysts.
- The AC-based, Fe-only catalyst requires higher reaction temperatures to achieve NO reduction, and at these temperatures it generates large quantities of CO by partial combustion of the carbon support.
- Addition of Cu to the catalysts promotes the NO reduction reaction at significantly lower temperatures and also promotes the oxidation and removal of CO. Similar effects are seen by the addition of Ce or K. High CO conversions (over 80 – 90%) were observed for both AC and AA catalysts with high Cu loadings. The CO conversion level was not significantly affected by temperature, gas composition or test duration in the ranges tested.
- Introduction of SO_2 to the test gas mixture reduces NO activity to various degrees depending on catalysts formulations. After the SO_2 exposure, NO activity can be generally restored to original levels with or without using higher operating temperatures. The impact of SO_2 on catalyst performance and its mechanism need to be studied further.
- Both Fe/Cu/AC and Fe/Cu/AA catalysts were tested with a high space velocity of 5250 hr^{-1}. The AC based catalysts achieved over 90% NO conversion at a higher reaction

temperature than that of low space velocity tests. The AA based catalyst reached a maximum NO conversion of about 60% at high space volocity. CO conversions of 80-90% were achieved for both AC and AA catalysts despite the high space velocity.

In summary, the AC and AA supported base metal catalysts have shown very promising NO conversion and selectivity in oxidizing environment with CO as reductant, as well as excellent CO reduction. It is recommended that both groups of catalysts be further developed and tested at pilot scale, for long duration, and with actual combustion flue gas.

Catalyst Scale Up and Reactor Design: The laboratory catalyst test data have been further analyzed with detailed evaluation of transport and reaction steps. A catalyst reaction model was used to interpret the test data and for scaling–up to commercial size reactor with honeycomb catalysts. The following conclusions and observations can be made;

- External mass transfer resistance is negligible for laboratory packed bed tests of granular catalysts; it is also not a significant rate-limiting factor for the commercial reactor with the selected honeycomb configuration.
- Microscopic study of laboratory test samples reveals that active components are concentrated in a thin outer shell, with limited penetration into substrate structure.
- The catalyst model with first order reaction fits well with test data. The data also demonstrated consistent observed activation energy.
- Catalyst effectiveness ç is close to 1.0 for tested catalysts. The catalyst performance was not limited by pore diffusion. Honeycomb catalysts prepared based on the above findings will be able to achieve high activity and effectiveness.

Based on data obtained from bench scale catalyst testing and reaction modeling, conceptual design of a 400 MWe size ammonia-free selective catalytic reactor (AF-SCR) has been developed. The AF-SCR uses honeycomb monolith elements with similar geometry to those used in the conventional ammonia-based SCR, but it uses the activated alumina as substrate and base metal active components developed in this work. The conceptual design provides a basis for cost evaluation of the new NOx control process.

Cost Analysis: Based on the conceptual design and predicted performance data of the ammonia-free selective catalytic reactor (AF-SCR) for a 400 MWe size coal-fired power plant, economic evaluation has been performed for NOx reduction with the AF-SCR system. By eliminating ammonia as reagent and using of low cost catalyst, the AF-SCR system will have significant cost advantages. Compared to the state-of-the-art SCR system, the AF-SCR system is projected to be 17% lower in capital investment, and almost 30% lower in cost of per ton NOx removed. For the 400MWe unit, the present value of total cost savings for NOx control due to the AF-SCR system is approximately 19 million dollars.

Future Research Works: Catalystic process for gas-solid contact can be designed and operated as a packed bed, a fluidized bed (with or without regeneration) or even an injection mode, which depends on the process requirement, and the performance of catalyst, as well as the costs of operation. For commercial scale application, there are still some areas need to be considered and tested for such a process development.

- Better catalyst reactivity test - The microscopic study of laboratory test samples reveals that active components are concentrated in a thin outer shell, with limited penetration into substrate structure. As has been mentioned in the report the catalyst activity increases with metal loadings. Therefore it is very interested and important to enhance catalyst activity and to reduce and extend catalyst operation temperature even lower by increasing the loadings of active components. This can be done by a modified or a better catalyst preparation method or by simply reduced catalyst size.
- Split stream pilot plant scale test - The catalyst needs to be tested under real flue gas from a pilot plant and operation conditions. This will let catalyst to be exposed to the real world with all possible flue gas components and ash from coal combustion.
- Long duration catalyst bench scale test - The formulated catalysts have been tested for hours and days. A long duration test is required for the catalyst to determine any slow transient effects. When such a catalyst is installed in a packed bed, its long life with good resistance to poison gas become a key parameter for its practical application.
- Split stream pilot plant injection option test - Hg capture has been well-known and achieved by injection of active carbon. A patented process by Foster Wheeler was to develop and test a catalyzed active carbon in low cost for the purpose of multi-emission control applicable for the flue gas from boilers, in additional to the Hg capture. This catalyzed active carbon functions as both a catalyst and a sorbent to convert NOx by CO to N_2 and also by active carbon itself, to convert the excess CO on the same catalyst to CO_2, to capture/convert SOx chemically by the sorbent, and to use SOx "poisoned" catalyzed active carbon to capture the Hg in a more effective way. For this purpose, a split stream test with selected catalyst/sorbent injection is suggested.

8.0 REFERENCES

Aarna, I. and Suuberg, E., "A Review of Kinetics of the Nitric Oxide-Carbon Reaction", Fuel, Vol.76, p475, 1997.

Adams, B. R., Cremer, M. A., and Wang, D. H., "Modeling Non-Equilibrium CO Oxidation in Combustion Systems", International Mechanical Engineering Congress and Exposition, November 5-10, 2000.

Dogu, G., "Diffusion Limitations for Reactions in Porous Catalysts", in *Handbook of Heat and Mass Transfer - Volume 2: Mass Transfer and Reactor Design*, edited by Cheremisinoff, N.P., Gulf Publishing Company, 1986.

Foster Wheeler Development Corp., "FW-FIRE, Fossil-fuel Water-walled Furnace Integrated Reaction Emission, Theory and User's Manual", 1999.

Gilliland, E.R., "Diffusion Coefficients in Gaseous Systems ", Ind. Eng. Chem., Vol.26, p.681, 1934.

Holmgren, A., and Andersson, B., " Mass Transfer in Monolith Catalysts – CO oxidation Experiments and Simulations", Chemical Engineering Science, Vol. 53, No.13, p.2285, 1998.

Illan-Gomez, M., Linares-Solano, A., and Salinas-Martinez de Lecea, C. "NO Reduction by Activated Carbon. 6. Catalysis by Transient Metals", Energy & Fuels, Vol.9, p976, 1995

Jurczyk, K., and Drago, R., "Low-Temperature Reduction of NO with CO and n-Hexane Using Metal Oxides on Carbon", Appl. Catal. A: Gen., Vol.173, p145, 1988.

Kunii, D., and Levenspiel, O., *Fluidization Engineering*, 2nd edition, Butterworth-Heinemann, 1991.

Lani, B.; Feeley, T.; Murphy J.; and Green, L.; "A Review of DOE/NETL's Advanced NOx Control Technology R&D Program for Coal-fired Power Plants", DOE/NETL NOx R&D Program Review, March 2005.

Mooney, J., "Emission Control Technology for Light-Duty Vehicles", 2001 Asian Vehicle Emission Control Conference, Bangkok, Thailand, January, 2001

Perry, R. H., and Chilton, C.H., *Chemical Engineers' Handbook*, 5th edition, McGraw-Hill Book Company, 1973.

Randall H., Doepper R., and Renken, A. "Reduction of Nitrogen Oxides by Carbon Monoxide over an Iron Oxide catalyst under dynamic conditions", Appl. Catal. B: Environ. Vol.17, p357, 1998.

White, J.; Price, F.; Walker, J.; Roark, S.; and Sammells, F.; "Catalyst For Direct Decomposition of NOx in Exhaust", NETL 1999 Conf. on SCR/SNCR for NOx Control, Pittsburgh, PA, 1999.